Spring 2011

Identifying groundwater contributions to baseflow in a temperate headwater catchment

Shantar Zuidema
University of New Hampshire, Durham

IDENTIFYING GROUNDWATER CONTRIBUTIONS TO BASEFLOW

IN A TEMPERATE HEADWATER CATCHMENT

BY

SHANTAR ZUIDEMA

B.S. Environmental Earth Science, Eastern Connecticut State University, 2004

THESIS

Submitted to the University of New Hampshire
in Partial Fulfillment of
the Requirements for the Degree of
Master of Science

in

Hydrology

May, 2011

UMI Number: 1498978
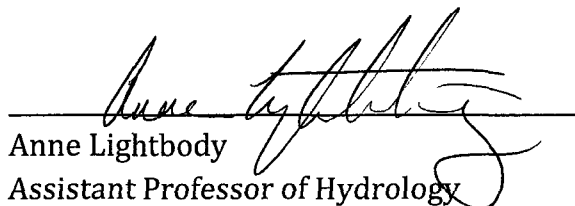
This Thesis has been examined and approved.

Thesis Director, J. Matthew Davis
Associate Professor of Hydrogeology

Julie Bryce
Associate Professor of Geochemistry

Anne Lightbody
Assistant Professor of Hydrology

5/3/11
Date

<u>Acknowledgements</u>

I am indebted to Molly Jankolovits who graciously volunteered her time to instrument the Northwood Study Catchment. My thanks go out to Kathleen Turner and Charles Grant who collected and processed samples, only a small portion of which are analyzed and presented herein. Beyond my citations to his work, I acknowledge Matt Frades whose work motivated the research presented here.

My sincerest thanks go to my advisor, Matt Davis, and members of my advising committee, Anne Lightbody and Julie Bryce for their shared insight and patience. Many throughout the University have greatly improved this project, many quite unwittingly. My thanks go out generally to the faculty and students of the Departments of Earth Sciences, Natural Resources, and Civil Engineering.

I thank my many wonderful friends and family for their thoughts, companionship, and honesty over the years. Though I say it every day, my deepest thanks and love are saved for Abby. My inspiration to better myself, our world, or maybe just our understanding of it, is derived from our wonderful conversations.

List of Tables

List of Figures

Abstract

Identifying Groundwater Contributions to Baseflow

in a Temperate Headwater Catchment

by

Shantar Zuidema

University of New Hampshire, May 2011

Inter-storm streamflow, or baseflow, is commonly assumed to be generated directly from groundwater discharge to the stream network. In moderate-relief terrain of New England, wetlands are important in stream function. The assumption that streamflow is generated from groundwater discharge from a headwater catchment containing 11% wetland or pond area coverage was tested using stable isotopes of water. Binary end-member mixing analysis showed that 18 to 30% of streamflow at the catchment outlet (less than 50% at 95% confidence) was generated from groundwater; the remainder was derived from outflow from an upstream wet meadow. Results from the wet meadow water and isotopic mass balance suggest <27% of meadow outflow was accommodated by groundwater inflows. Increasing isotopic enrichment correlates more strongly with stream length within wetlands ($p = 0.005$) than catchment wetland area ($p = 0.04$); ranking catchments by the same metric also distinguishes catchments by their relative average run-off.

1.   Introduction and Background

Wetlands, or land areas that are saturated or nearly saturated with water for

at least part of the year [Cowardin *et al.*, 1979; Mitsch and Gosselink, 2000], are a

common feature in headwater catchments of many landscapes, including the

temperate forested region of the northeast. Wetlands have been investigated

throughout the region to assess how they influence nutrient [McHale *et al.*, 2004;

Flint, 2008] and other hydrological [O'Brien, 1977; 1980] fluxes. Wetland systems

have been invoked as having the effects of flow regulation and flow maintenance

[Roulet, 1990; Kværner and Kløve, 2006; 2008; Smakhtin and Batchelor, 2005].

After decades of research, the roles that these shallow surface reservoirs have on

maintaining streamflow in temperate catchments in the northeastern U.S.,

particularly during dry conditions, remain poorly defined. Neglecting drainage from

these systems during dry periods may constitute a significant error in analyses

predicated on the assumption that inter-storm streamflow is attributed solely to

groundwater. Potential streamflow generation from groundwater and from

wetlands during dry summer conditions are investigated by volumetric and stable

isotopic measurements in the Northwood Study Catchment in southeastern New

Hampshire, U.S., a temperate headwater catchment of the Lamprey River, to

investigate whether an assumption of groundwater-only baseflow should be

scrutinized in similar terrains.

The following discussion provides a background to the hydrologic fluxes

primarily important to maintaining the water balance throughout headwater

catchments and headwater wetland reservoirs. A brief summary is provided regarding how the water balances of wetland reservoirs have been found to affect the water balances of catchments at a variety of scales. Stable isotopic composition, the abundance of isotopically heavy water molecules, is quantitatively employed in this investigation, and the theoretical background for the method is presented. This chapter concludes with a description of the research objectives.

1.1   Water Balance

The conservation of mass is the fundamental physical principle guiding most hydrologic research. At the land surface where temperature and atmospheric pressure remains within narrow bounds, and when the concentrations of solutes remain low, the density of water is approximately constant and a volumetric balance is approximately equivalent to the mass balance. From the conservation of mass, the sums of water input fluxes ($\sum I$) to and water output fluxes ($\sum O$) from a system must be equivalent to the rate of change in water stored over time (dV/dt) within the system or:

$$\frac{dV}{dt} = \sum I - \sum O \,.$$
(1.1)

The system where equation (1.1) is applied varies depending on the research objectives, and is discussed here in the context of the scales of a headwater catchment, a specific surface reservoir, and a hypothetical reach section.

1.1.1   Catchment Scale

At the catchment scale, water is stored primarily in surface reservoirs such as lakes, ponds, stream channels, wetlands, and snow-pack, or subsurface reservoirs

such as soil moisture and groundwater. A seasonal change in storage is expected throughout the catchment, and is measured as a loss in head or stage within groundwater or surface reservoirs, or as a change in soil moisture, which is beyond the scope of this investigation to characterize. By equation (1.1) volume changes observed at the catchment scale must be associated with specific hydrologic fluxes to balance.

Two primary inputs are considered active in headwater catchments: inter-basin groundwater flow and precipitation. Direct condensation is an example of another possible input for some systems, but is not considered important in the temperate setting of the investigation [Garrat and Segal, 1988]. Inter-basin groundwater flow has been observed in the immediate region [Smith *et al.*, 2007] and may be a significant component of the water budget of some headwater subcatchments. However, the location of groundwater recharge observed in streamflow is not of concern to this study and inter-basin groundwater flow is therefore not quantified herein. Precipitation is the predominant input to headwater catchments; however, its measurement is complicated by the presence of vegetated canopies that intercept precipitation and subject it to evaporation (discussed in §2.3.4). Water passing through the canopy is termed throughfall, and water bypassing run-off at the soil interface may infiltrate and ultimately recharge groundwater. Precipitation varies considerably spatially, but, for the small catchment under investigation, this variability is assumed to be negligible.

Outflow from the catchment occurs via three primary mechanisms: subsurface discharge, streamflow, and evapotranspiration. Groundwater discharge

from headwater catchments is often treated as negligible because most groundwater discharge is directed to the gaining stream network, and the component of groundwater discharge directed downstream near the catchment outlet can be generally neglected as small compared to the component of outflow from the catchment through streamflow [Dingman, 2002]. Additionally, primarily horizontal saturated-flow below the stream bed of a mixture of surface and subsurface water (hyporheic flow) is another mechanism of outflow [Dingman, 2002], but is not explicitly treated here. Streamflow and evapotranspiration are considered here the only non-negligible fluxes out of headwater catchments, with measurements of streamflow being generally much simpler and accurate than measurements of evapotranspiration. In headwater catchments equation (1.1) can often be rearranged to yield an accurate estimate of average annual evapotranspiration by assuming negligible inter-annual changes in storage by:

$$ET = P - Q\,,\tag{1.2}$$

where ET is the total annual evapotranspiration, P is the total annual precipitation, and Q is the total annual surface discharge.

1.1.2   Surface Reservoirs

The water balance of specific surface reservoirs is similar to that of a whole catchment; however, changes in storage are directly measureable as changes in the stage, assuming the bathymetric and storage properties of the reservoir boundary are known [Winter, 1981]. In addition to the fluxes discussed above, surface inflows can be a significant component in the water balance of a surface reservoir. Open-water evaporation, a portion of the total evapotranspiration of an open-water

reservoir or partially vegetated reservoir, is generally greater than catchment

evapotranspiration because of a lower resistance to vertical transport of water

vapor [Dingman, 2002; Drexler *et al.*, 2004]. Groundwater exchange with a surface

reservoir is difficult to measure, and is often estimated as the residual in a

volumetric mass balance with errors typically approaching 100% [Winter, 1981].

1.1.3 Stream Reaches

The mass balance is also evaluated for a specific stream reach. It is assumed

that during inter-storm periods, storage within the reach is constant over time and

the flow is steady [Chow, 1959]. At a downstream cross-section two inputs to the

reach are considered: discharge from upstream reaches measured or estimated at

an upstream location (I_{up}), and riparian groundwater input (I_{rgw}) between the

measurement locations, or:

$$Q_D = I_{up} + I_{rgw} \, , \tag{1.3}$$

where Q_D is the discharge at the downstream sampling point. Equation (1-3) is valid

when other fluxes to or from the reach can be neglecting. Other possible fluxes to

the reach that may complicate the solution of equation (1-3) include unsaturated

soil drainage, deep groundwater sources, or hyporheic flow. Possible fluxes from

the reach include evapotranspiration, or if the reach is losing, streamflow may be

lost to hyporheic or subsurface reservoirs.

1.1.4 Baseflow

Baseflow is the term applied to measureable discharge in stream channels

temporally separated from the short-term elevated discharge due to routing of

precipitation and snowmelt events, or reservoir releases. Most descriptions of

baseflow assume or provide evidence that lumped or spatially distributed sub-surface drainage is the primary input to stream channels and networks during baseflow periods [Brutsaert and Nieber, 1977; Freeze and Cherry, 1979; Mosley and McKerchar, 1993; Mau and Winter, 1997; Brutsaert and Lopez, 1998; Arnold and Allen, 1999; Weiler *et al.*, 1999; Bond *et al.*, 2002; Mosner, 2002; Uhlenbrook *et al.*, 2002; Baillie, 2005; Price and Jackson, 2007; Santhi *et al.*, 2008; Tetzlaff and Soulsby, 2008]. Occasionally, baseflow-generating mechanisms are identified in a general manner, such as the use of the phrase "catchment drainage" by Stewart and others [2007]. Sometimes a more complete description of possible mechanisms is made, such as the attribution by Dingman [2002] of baseflow to the drainage from groundwater, lakes, wetlands, and unsaturated soil. Additional mechanisms at work in the generation of baseflow have been infrequently verified with a notable exception in Hewlett and Hibbert [1963], whose experiments showed the importance of unsaturated soil drainage from an engineered hillslope where simulated rain wetted soil materials drained by gravity for several weeks.

Baseflow is typically investigated in the context of rainfall-runoff studies, in which baseflow is characterized such that it can be distinguished from streamflow generated during precipitation events. Geochemical tracers and geochemical hydrographic separation are often used to identify streamflow attributed to event runoff, as opposed to pre-event water stored within the watershed prior to precipitation [Sklash *et al.*, 1976, 1986; Sklash, 1990; Gibson *et al.*, 1993; Buttle, 1994; Buttle and Peters, 1997; Genereux, 1998; Weiler *et al.*, 1999; Burns *et al.*, 2001; Genereux *et al.*, 2002; Joerin *et al.*, 2002; Uhlenbrook *et al.*, 2002; Baillie,

2005; Stewart *et al.*, 2007]. Typically, these separations are conducted at high frequency, in small catchments, and during storm events to investigate the flow paths generating storm flow. In general, such studies typically find that compositionally stable pre-event water constitutes greater than 50% of streamflow even during large storm events.

Fewer studies investigate the role of the mechanisms generating streamflow during inter-storm baseflow periods. Several studies [Genereux *et al.*, 2002; Uhlenbrook *et al.*, 2002; Baillie, 2005; Hayashi, *et al.*, 2004; St. Amour *et al.*, 2005; Kværner and Kløve, 2006; Stewart *et al.*, 2007; Tetzlaff and Soulsby, 2008; Brooks *et al.*, 2009; Gonzales, 2009] use geochemical tracers to spatially delineate baseflow-generation during longer seasonal timescales, and often outside of the influence of storm events. In seven of the studies over longer durations, baseflow was observed to exhibit geochemical similarities to groundwater, and in only St. Amour and others [2005] and specific catchments in the study of Kværner and Kløve [2006] was baseflow reported as being influenced by surface detention, a signal observed by enrichment of stable isotopes or other geochemical observations. Of the studies listed above, all except for Kværner and Kløve [2006], Brooks and others [2009], and Gonzales and others [2009] the seasonal geochemical tracer investigations listed above are conducted over larger mesoscale study catchments than are the event hydrographic separations discussed in the preceding paragraph, which is indicative of the relatively less effort expended in characterizing baseflow generation processes at the headwater catchment scale. Of the studies listed above, all except for St. Amour and others [2005] and Gonzales and others [2009], which

investigate seasonal streamflow generation in low-relief watersheds in plains of the Canadian shield and coastal margins of the Netherlands, respectively, the geochemical studies of inter-storm baseflow are conducted in mountainous terrain. None of the studies described above are considered directly applicable or representative of the near-coast wetland-rich temperate catchment that is the focus of this study.

Stream discharge during inter-storm baseflow typically decreases exponentially, and is referred to as the recession curve on streamflow hydrographs. The slope and any inflections on the curve are characteristic of a given catchment [Tallaksen, 1995]. The recession curve is often used to inform several estimates of hydrologic fluxes in the catchments water balance. These analyses are conducted by determining manually or via some digital filtering method the point following a storm event when streamflow represents baseflow [Tallaksen, 1995, Arnold and Allen, 1999; Gonzales *et al.*, 2009]. Studies that employ this method typically assume streamflow during the recession is composed of groundwater and neglect evapotranspiration [Tallaksen, 1995]. This assumption facilitates the estimation of groundwater recharge by a recession-curve displacement method [e.g. Rutledge and Mesko, 1996; Rutledge, 2000], or descriptive parameters of contributing riparian aquifers such as aquifer hydraulic conductivity or specific storage [e.g. Brutsaert and Nieber, 1977]. In the context of estimating recharge from recession-curve displacement, these limitations and others are discussed by Rutledge [2000], and pragmatically mitigated in Flynn and Tasker [2004], where their analysis was limited to New England stream networks with minimal impoundments and

evaluations of the master recession curve indices, though not necessarily storm displacements, were limited to fall, winter, and spring months of streamflow data when evapotranspiration losses were less significant.

The study of Gonzales and others [2009] compared geochemical hydrographic separations with hydrograph baseflow separation techniques used in recession analysis in a lowland coastal area and found that commonly used separation methods over-predict the role of event run-off. The important finding of Gonzales and others [2009] illustrates the need to better understand runoff-generation mechanisms to accurately apply convenient volumetric hydrograph analyses, and that the pre-event component of storm run-off can be assumed to be interpretable directly from the hydrograph. This study looks to further investigate another common assumption of baseflow recession analysis, specifically the validity of the groundwater-only assumption of catchment drainage.

1.2   Influence of Wetlands on Baseflow

Wetlands are areas of near or complete saturation throughout part of the year. These systems are widely diverse in ecological and hydrological setting [Cowardin et al., 1979; Mitsch and Gosselink, 2000]. These systems are interpreted in this study to have a specific hydrologic function in that they represent storage of water (reservoir) at the land surface, and surface discharge is controlled by the elevation of stored water relative to an outfall, which may be connected to the stream network. These systems are therefore not hydrologically distinct from ponds or lakes, but vary with regard to average depth and vegetation cover. Throughout this document the term wetland will be used in a hydrologic context to

represent a shallow surface reservoir system, and distinguished from lakes or ponds as having vegetation cover that is not negligible, and further may contain significant soil substrate that remains at or near saturation. This interpretation of the term is considered to be consistent with Cowardin and others [1979] and Mitsch and Gosselink [2000]. The interpretation was applied in review of literature sources that did not otherwise specify or describe their use of the term.

A direct implication of the presence of a shallow surface reservoir within a catchment is the potential for enhanced evapotranspiration relative to what would be expected if water was stored as groundwater, or conveyed out of the catchment directly through a stream channel. It is unclear whether the presence of vegetation within a surface reservoir reduces, increases, or does not materially affect the total evapotranspiration flux of shallow surface systems, though it is likely system dependent [Mitsch and Gosselink, 2000; Goulden et al, 2007].

Applications of baseflow recession-curve analysis are recognized to be limited by the hydrogeomorphic setting of the basin [Rutledge, 2000], or regulation induced by reservoirs [Flynn and Tasker, 2004]. Interception of upstream runoff by natural waterbodies such as wetlands, lakes, or ponds is expected to present a similar challenge during recession analysis. Innovative comparative hydrograph analytical techniques presented by Smakhtin and Batchelor [2005], suggest that wetlands in some watersheds may dampen storm-event response and broaden inter-storm response. The investigators did not attribute these findings to specific functions such as temporary storage and subsequent drainage from the wetlands for storm events, but such interpretations seem reasonable. Estimates of groundwater

recharge from displacement methods would therefore be expected to be biased high if wetlands slowly release a significant volume of direct precipitation from the catchment in a manner characteristic of riparian aquifers. The effect may also reduce baseflow-recession estimates of riparian aquifer hydraulic conductivity. From the review of geochemical studies in section 1.1.4, few generalizations are possible across hydrologic systems regarding the observed role of wetlands on baseflow. In some instances, the presence of wetlands or extensive surface water bodies appears to influence geochemical character of baseflow at catchment [Kværner and Kløve, 2006, 2008] to regional [St. Amour *et al.*, 2005] scales; however, this is not ubiquitous [Tetzlaff and Soulsby, 2008]. Wetlands are diverse systems and the variability observed in the results of these few studies probably reflect this diversity, particularly in the degree of vegetation cover, of the predominate wetlands within these study catchments. Furthermore, though wetland areas of surface detention may or may not impart a geochemical imprint, their volumetric role in a catchment water balance may be more complicated than a simple slowly draining storage reservoir, but may be indicative of locations of enhanced groundwater discharge to the surface [O'Brien, 1977; Roulet, 1990; and McHale *et al.*, 2004]. This diversity of function is highlighted by the review of wetland function by Bullock and Acreman [2003], which dispelled generalizations in hydrologic functions by systematically collating results from 169 studies.

1.3   Stable Isotopes of Water

Geochemically, the influence of surface detention of baseflow within the catchment can be observed through the evaporative fractionation of stable isotopes

of water. During evaporation of open-water surfaces, water molecules containing

the heavy isotopes of hydrogen and oxygen (^{2}H and ^{18}O) are preferentially

discriminated against in the phase transition and their abundances increase in the

evaporating reservoir. This section summarizes some theoretical and practical

developments of previous researchers in the field of stable isotope hydrology

required to present the objectives and methodology employed in this study.

1.3.1 Stable Isotope Abundances

Stable heavy isotopes of oxygen (^{18}O) and hydrogen [^{2}H or deuterium (D)],

exhibit no radioactive decay [Criss, 1999]. Rare abundances found in the water

molecule (H_2O) vary in predictable amounts due to measurable natural processes

and are ideal tracers in natural hydrologic systems [Criss, 1999; Kendall and

Caldwell, 1998; Mook, 2006]. Abundances of stable isotopes of water are reported

as the relative difference in the molar ratios of the heavy isotope to light isotope of a

sample and a standard, currently Vienna standard mean ocean water (VSMOW), for

both isotopes of the water molecule. These differences are presented in the delta

(δ) notation [Coplen, 1996]:

$$\delta^{18}O (‰) = \left[\frac{([^{18}O]/[^{16}O])_{Sample}}{([^{18}O]/[^{16}O])_{VSMOW}} - 1 \right] \times 10^3 \text{, and} \qquad (1.4)$$

$$\delta^{2}H (‰) = \left[\frac{([^{2}H]/[^{1}H])_{Sample}}{([^{2}H]/[^{1}H])_{VSMOW}} - 1 \right] \times 10^3 . \qquad (1.5)$$

Thus, $\delta^{18}O$ and δ^2H of VSMOW are both zero, positive δ-values indicate isotopic

enrichment (greater abundance of heavy isotopes compared to the standard), and

negative δ-values indicate isotopic depletion (lower abundance of heavy isotopes relative to the standard) [Mook, 2006]. Stable isotopic compositions presented in the delta notation are typically expressed in permil (‰) by multiplying their values by 1,000. Consistent with Mook [2006], calculations and derivations presented throughout this document using the δ-notation are not defined in permil. Where delta notation is presented in permil (e.g. tables and figures), the permil (‰) symbol is presented explicitly.

Alternatively, abundances can be presented simply as the ratio of the heavy to light isotope of the element. For example, for hydrogen, the isotope ratio (R_{2_H}) is defined as:

$$R_{2_H} \equiv \frac{{}^2H}{{}^1H},$$
(1.6)

and the isotope ratio for oxygen (R_{18_O}) is:

$$R_{18_O} \equiv \frac{{}^{18}O}{{}^{16}O}.$$
(1.7)

For either element (x), the isotope ratio is related to the δ notation by:

$$R_x = R_{VSMOW}(1 + \delta^x).$$
(1.8)

The absolute isotopic ratios of the standard Vienna standard mean ocean water (R_{std}) are 0.0020052 for ${}^{18}O/{}^{16}O$ and 0.00015575 for ${}^2H/{}^1H$ [Mook, 2006].

Bond energies, which are controlled by the masses of atoms forming the bond, differ between isotopologues (chemically identical molecules with isotopic substitutions) [Criss, 1999]. Several thermodynamic and kinetic physical processes, most notably phase changes and biogenic processes, are responsible for separating or fractionating isotopologues due to these different bond energies [Kendall and Caldwell, 1998; Mook, 2006]. The phase changes of water as it is evaporated into the atmosphere and condensed to form precipitation impart measureable differences in isotopic composition between various compartments of the hydrologic cycle that can be exploited as tracers.

Using samples of individual components of a hydrologic system, estimates of the relative volumes of differing components can be made. The ratio of heavy to light isotopes of either hydrogen or oxygen in a liquid water sample (R_{sample}) is the sum of the ratios of heavy to light isotopes of the n constituent waters multiplied by the respective constituent mole fractions (X) in the sample [Criss, 1999; Kendall and Caldwell, 1998]:

$$R_{sample} = \sum_{i=1}^{n \ constituents} X_i R_i \ . \tag{1.9}$$

In typical surface water systems having constant density and no reactions of either isotope component, the mole fractions of each constituent can be substituted for with volumetric ratios or volumetric-flux ratios. Furthermore, δ-values can be treated as conservative throughout the reservoirs and calculations presented [Mook, 2006; Kendall and Caldwell, 1998]. The mixing of waters of distinct

compositions is utilized in this study to identify fractional contributions from evaporated surface water bodies and groundwater. Where $n = 2$ constituents, equation (1.9) can be expressed as the proportional fraction of either end-member (f_1 or f_2) as a function of representative isotope ratios of the two end-members (R_1 and R_2, respectively), and the isotope ratio of a sample comprised of a mixture of the two end-members (R_S) by [Genereux, 1998]:

$$f_1 = \frac{R_2 - R_S}{R_2 - R_1} \text{, and} \tag{1.10}$$

$$f_2 = \frac{R_S - R_1}{R_2 - R_1}. \tag{1.11}$$

Again, δ-values can be used in place of isotope ratios in equations 1.10 and 1.11.

1.3.2   Isotopic Composition of Precipitation

Fractionation that takes place during evaporation and condensation results in meteoric water (atmospheric water as vapor, clouds, fog, or falling as precipitation) with stable-isotopic composition that varies widely depending on factors such as the temperature where phase transitions occur and the degree of progressive evaporation from source water [Gat, 1980; Ingraham, 1998]. Meteoric waters vary globally in isotopic composition from -500‰ $\leq \delta^2H \leq$ +40‰, and -62‰ $\leq \delta^{18}O \leq$ +4‰ [Criss, 1999]. Fractionating processes operate consistently on isotopologues containing substitutions with ^2H and ^{18}O, when the δ^2H is plotted against $\delta^{18}O$ for samples of meteoric waters, a characteristic line termed the meteoric water line is generated of the general form [Craig, 1961]:

$$\delta\ ^2H\ ‰ \cong\ 8\delta^{18}O\ +\ 10\ ‰\ .\qquad\qquad(1.12)$$

The isotope effect resulting in the non-unity slope in equation (1.12) is primarily

explained by equilibrium (reversible) fractionation between atmospheric water

vapor and cloud forming droplets, which impacts δ^2H more than $\delta^{18}O$ due to the

larger relative mass difference between ^1H and ^2H compared to ^{16}O and ^{18}O [Craig,

1961; Ingraham, 1998; Criss, 1999; Mook, 2006]. The intercept in equation (1.12),

is not explained by this process but is attributed to the irreversible kinetic

fractionating process of evaporation [Dansgaard, 1964]. Dansgaard [1964] outlines

the effects resulting in the coefficients in the meteoric water line:

> *"The [global meteoric water line] may be explained by the condensation of*
>
> *water vapor under conditions close to equilibrium that was evaporated under*
>
> *conditions of nonequilibrium [Dansgaard summarized by Ingraham, 1998]."*

The complete set of processes that create meteoric waters include both equilibrium

or kinetic fractionation are discussed in Gat [1980], Ingraham [1998], Criss [1999],

Gat and others [2000], and Mook [2006], which make reference to the original

research including Craig [1961], Dansgaard [1964], and Craig and Gordon [1965].

Briefly, individual air masses derived from evaporation primarily of oceanic sources

that drop precipitation at a given locality experience unique histories of

temperature-dependent equilibrium fractionation effects (e.g. altitude, latitude,

season) and different rain-out histories [Gat *et al.*, 2000], which result in regional

variation of the coefficients in (1.12) [Dansgaard, 1964]. The unique combinations

of these phenomena result in a site-specific local meteoric water line (LMWL) that

should be characterized using the complete annual record of data at a locality [Ingraham, 1998]. The annual depth-averaged mean isotopic composition of precipitation generally closely reflects the isotopic composition of groundwater at a given locality [Mook, 2006].

1.3.3 Craig-Gordon Model of Evaporative Enrichment

Fractionation during evaporation is governed by both the temperature-dependent equilibrium fractionation and by irreversible kinetic fractionation [Craig and Gordon, 1965; Gat et al., 2000; Horita et al., 2008]. The kinetic effect in evaporative enrichment is dependent on the characteristic humidity of the evaporating system and the specific geometry of the evaporating surface (e.g. flat surface or droplets) [Craig and Gordon, 1965; Stewart, 1975; Horita et al., 2008]. Surface water experiencing evaporation exhibits an isotopic composition that departs from the local meteoric water line at a shallower slope than the meteoric water line (which has a slope of about 8; cf. equation 1.12). A slope between 4 and 5 in plots of δ^2H against $\delta^{18}O$ and is said to form an evaporative water line [Mook, 2006]. Figure 1 depicts a sample relation between the meteoric and evaporative water lines in a plot of δ^2H versus $\delta^{18}O$, and indicates characteristic isotopic composition for samples of groundwater and evaporated surface water.

Evaporation and evaporative fractionation depend on the degree of saturation of water vapor in the atmosphere. The degree of saturation of the atmosphere is expressed as the normalized humidity (h_N), which approaches zero when water vapor is virtually absent, and equals one when the actual water vapor

pressure equals the saturation vapor pressure at the temperature and pressure of

the water surface. The normalized humidity at any elevation (z) within the vapor

column above the reservoir ($h_{N,z}$) is:

$$h_{N,z} = \frac{e_{a,z}}{e_s^*},$$ (1.13)

where $e_{a,z}$ is the actual water vapor pressure at elevation z, and e_s^* is the saturated

vapor pressure at the temperature of the surface [Craig and Gordon, 1965; Gat *et al.*,

2000; Horita *et al.*, 2008].
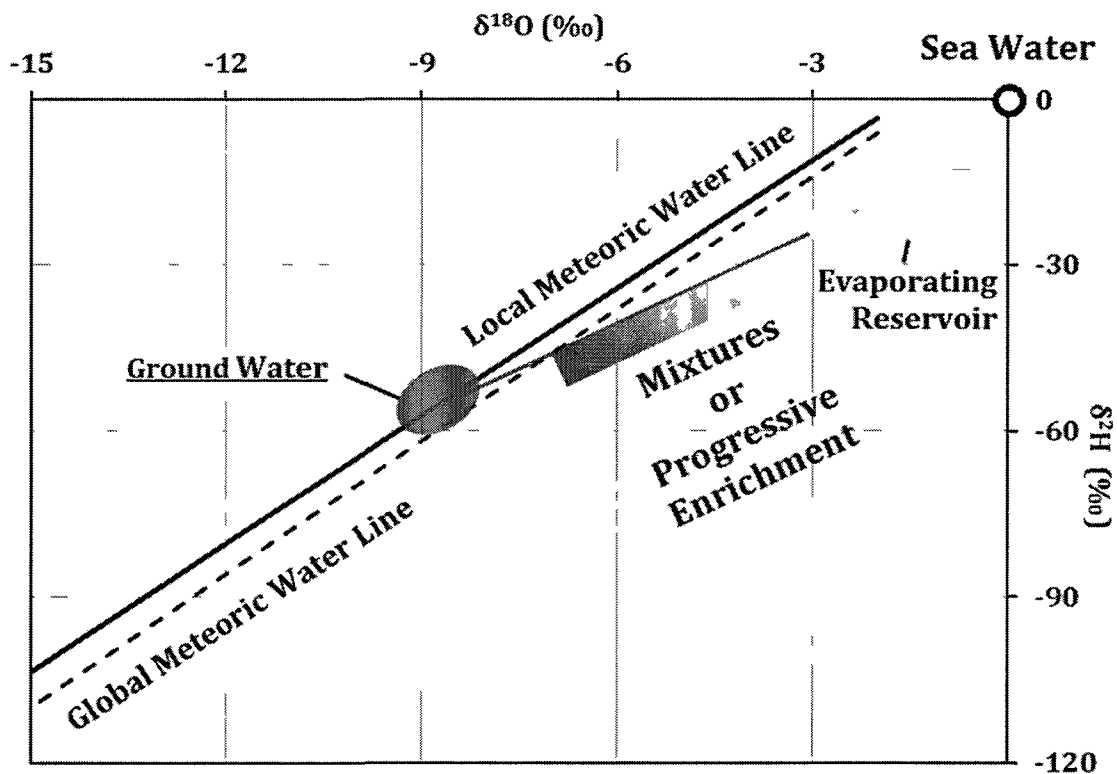
Figure 1: Sample plot of δ^2H versus $\delta^{18}O$ for terrestrial waters. Includes groundwater
(assumed to represent average precipitation), and evaporating surface water. Mixing
between evaporating reservoir and groundwater sources is exploited in the study to
investigate the relative contribution of sources, and the progressive evaporative enrichment
is accounted for in an isotopic mass balance.

The Craig-Gordon [1965] model of evaporative enrichment is derived for a one-dimensional evaporating surface where the evaporation rate is controlled by a humidity gradient and resistances to upward molecular transport. Evaporation is controlled by a gradient in humidity between a water-vapor saturated surface (where the relative humidity is equal to unity) and a free atmosphere of humidity $h_{N,A}$ not affected by the flux of water vapor from the water body.

The model assumes that the evaporation process occurs over three layers: an interface layer at the water surface, an overlying laminar layer where upward transport of water molecules is controlled by diffusion, and a turbulent atmospheric boundary layer [Craig and Gordon, 1965; Gat *et al.*, 2000; Horita *et al.*, 2008] as shown schematically in Figure 2. Resistances (ρ) limit the rate of upward transport of water vapor composed of the heavy (indicated by *) and light isotopologues, with the heavier isotopologue experiencing greater resistance. During transient evaporation, an instantaneous steady state in the isotopic composition through the atmosphere is assumed such that the relative rates of upward transport through the interface, laminar layer, and turbulent layer, are controlled only by the evaporation rate at the surface [Craig and Gordon, 1965].

If the net transport of water molecules from the surface is described as a Rayleigh process (where the removal of molecules can be described by a constant reaction factor, but once removed molecules cannot re-enter the system) the net removal of water can be described by the ratio of the amount of water remaining in the reservoir at any instant (N) to the initial amount in the reservoir (N_0) to define the reaction progress variable f [Craig and Gordon, 1965]:
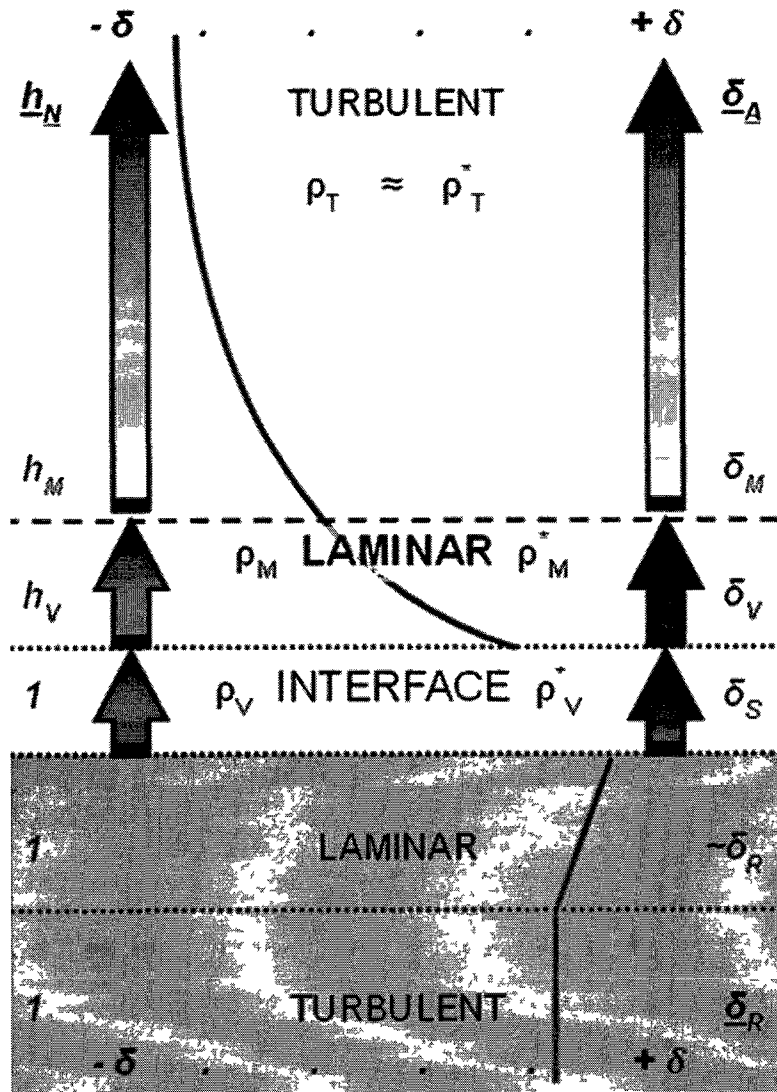
Figure 2: Diagram illustrating the Craig-Gordon Model of evaporative enrichment (after Craig and Gordon, 1965, Figure 13). Symbols to the left indicate the degree of saturation of the bulk water vapor through the evaporating column: normalized humidity of the free atmosphere (h_N), top of the laminar atmospheric layer (h_M), top of the vapor-liquid interface (h_V), and saturation at the interface and within the liquid (*1*). Symbols to the right indicate the relative abundance of the heavy isotope in the free atmosphere (δ_A), within the liquid (δ_R), or evaporating vapor at: top of the laminar atmospheric layer (δ_M), top of the vapor-liquid interface (δ_V), and vapor-liquid interface (δ_S). Here, the isotopic composition of the laminar liquid layer is assumed to be well-mixed with the turbulent liquid reservoir below. Symbols at center indicate resistances to vertical transport for light isotopologues ρ, and heavy isotopologues ρ^*: in the turbulent atmospheric layer $\rho_T \approx \rho_T^*$, in the laminar atmospheric layer $\rho_M \neq \rho_M^*$, and at the vapor-liquid interface $\rho_V \neq \rho_V^*$. δ symbols at top and bottom suggest the relative isotopic composition of the liquid or vapor at the given indication of the red line (δ-values decrease through the atmosphere).

$$f = \frac{N}{N_0}. \qquad (1.14)$$

The Craig-Gordon model states that the isotopic composition of an evaporating

reservoir (δ_R) can be described as a function of the remaining volume f as:

$$\frac{d\ln(1 + \delta_R)}{d\ln f} = \frac{\left(\frac{h_{N,A}(\delta_R - \delta_A)}{1 + \delta_R}\right) - \varepsilon}{1 - h_{N,A} + \varepsilon_K}, \qquad (1.15)$$

where δ_A is the isotopic composition of water vapor in the free atmosphere that

condenses and exchanges with water in the reservoir, and ε and ε_K are the total and

kinetic isotopic enrichment factors, respectively, that describe the fractionation

effect at any instant. ε and ε_K are discussed shortly.

Craig and Gordon [1965] and Ehalt and Knott [1965], solved equation (1.15)

to obtain an instantaneous estimate of the isotopic composition of the net

evaporative flux leaving the reservoir (δ_E):

$$\delta_E = \frac{\alpha_{V/L}\delta_R - h_{N,A}\delta_A - \varepsilon}{\left(1 - h_{N,A}\right) + \varepsilon_K}. \qquad (1.16)$$

where $\alpha_{V/L}$ is the equilibrium fractionation factor described shortly. In equation

(1.16), an additional resistance to the isotopic flux leaving the reservoir is neglected

that accounts for an enrichment of heavy isotopes within the laminar layer of liquid

near the water surface (cf. caption of Figure 2). The additional resistance, and the

imparted effect, is small compared to the total resistances imparted by the

evaporative flux [Gat *et al.*, 2000], and defining its exact magnitude is beyond the scope of the present study.

1.3.4   Fractionation and Enrichment Factors

Isotopic fractionation is described by two related variables, the fractionation factor (α) and the enrichment factor (ε). Both can be used to represent equilibrium or kinetic fractionation. The enrichment factor (ε), related to α by

$$\varepsilon = 1 - \alpha, \qquad (1.17)$$

is a small value expressing the additive enrichment effect of a process, and is typically expressed in permil. The fractionation factor (α) is a number close to unity and is defined identically to an equilibrium rate constant.

The fractionation factor (α) can be defined in two ways relative to the reservoir of interest. For the ratio of the isotopic composition of a liquid reservoir with an overlying saturated atmosphere, the fractionation factor is defined by the liquid-vapor transition ($\alpha_{eq,V/L}$) such that it is less than unity, meaning that heavy isotopologues have a lower probability than light to transition to the vapor medium during the process of evaporation. The equilibrium fractionation factor is directly measureable under equilibrium conditions system by:

$$\alpha_{eq,V/L} = \frac{R_{vapor}}{R_{liquid}} < 1. \qquad (1.18)$$

The equilibrium fractionation factor is temperature dependent and has been well characterized from 0°C to 100°C [Majoube, 1971] and to 374.1°C [Horita and Wesolowski, 1994]. Polynomial regression equations for the temperature

dependence of the fractionation factors defined for the vapor-liquid transition $(\alpha_{eq,L/V})$ from Horita and Wesolowski [1994] are:

$$10^3 \ln \alpha_{eq,\,^2H,L/V} = \left[1158.8\left(T^3/10^9\right) - 1620.1\left(T^2/10^6\right)\right.$$
$$\left. + 794.84\left(T/10^3\right) - 161.04 + 2.992\left(10^9/T^3\right)\right] \pm 1.2 \qquad (1.19)$$

$$10^3 \ln \alpha_{eq,^{18}O,L/V} = \left[-7.685 + 6.7123\left(10^3/T\right) - 1.6664\left(10^6/T^2\right)\right.$$
$$\left. + 0.3504\left(10^9/T^3\right)\right] \pm 0.11 \qquad (1.20)$$

where T is temperature (K) and errors indicate 68% confidence intervals on $10^3 \ln \alpha_{eq}$. The equilibrium fractionation factors from equations (1.19) and (1.20) are related to the fractionation factors needed by $\alpha_{eq,V/L} = \alpha_{eq,L/V}^{-1}$. Typical values of $\alpha_{eq,V/L}$ for this study range from 0.988 to 0.991 for $\delta^{18}O$ and from 0.899 to 0.940 for δ^2H. The equilibrium enrichment factor is defined as $\varepsilon_{eq} = 1 - \alpha_{eq,V/L}$ and as defined is positive. The total enrichment factor (ε) found in equation (1.16) is the sum of the equilibrium enrichment (ε_{eq}) and the kinetic enrichment (ε_K), or:

$$\varepsilon = \varepsilon_{eq} + \varepsilon_K. \qquad (1.21)$$

The kinetic isotope effect is most easily described by the enrichment factor (ε_K) and is parameterized based on the Craig-Gordon model. The kinetic enrichment factor describes an overall isotope effect observed from evaporating reservoirs and is ultimately dependent on the humidity of the free atmosphere. The effect is explained by either kinetic [Criss, 1999] or diffusive theory [Craig and Gordon, 1965; Ehalt and Knott, 1965]. Both theories use identical definitions of the equilibrium fractionation factor and kinetic enrichment factor. It should be noted at

the outset that although significant effort has been expended [Craig and Gordon, 1965; Ehalt and Knott, 1965; Merlivat, 1978; Cappa, 2003; Luz *et al.*, 2009], no description of the kinetic isotope effect completely satisfies physical theory of gases [Horita *et al.*, 2008; Luz *et al.*, 2009].

In the Craig-Gordon model, the kinetic fractionation that occurs by diffusion in the laminar boundary layer appears to explain the kinetic isotope effect [Craig and Gordon, 1965; Horita *et al.*, 2008]. The kinetic effect is assumed to be proportional to a diffusional concentration gradient of water vapor described by (1-h_N), the ratio (θ) of the resistance to upward transport of water vapor from molecular diffusion (ρ_M) to the total resistance (ρ), and the relative differences in the resistance to upward transport of water vapor from molecular transport for the heavy (ρ^*_M) and light (ρ_M) isotopologues, so that the kinetic enrichment factor is [Craig and Gordon, 1965; Gat *et al.*, 2000; Horita *et al.*, 2008]:

$$\varepsilon_K = (1 - h_N)\frac{\rho_M}{\rho}\left(1 - \frac{\rho^*_M}{\rho_M}\right) = (1 - h_N)\theta\left(1 - \frac{\rho^*_M}{\rho_M}\right). \qquad (1.22)$$

The ratio in the resistances due to molecular diffusion for the heavy and light isotopes (ρ^*_M / ρ_M) is proportional to the ratio of inverses of the isotopologue's molecular diffusivities in air (D^*_M and D_M for the heavy and light isotopologues, respectively), each raised to the geometric factor n, such that [Craig and Gordon, 1965; Gat *et al.*, 2000; Horita *et al.*, 2008]:

$$\varepsilon_K = (1 - h_N)\,\theta\left[1 - \left(\frac{D_M}{D^*_M}\right)^n\right] \cong (1 - h_N)\,\theta\, n\left(1 - \frac{D_M}{D^*_M}\right). \qquad (1.23)$$

The geometric factor n varies by the geometry under which the evaporation is occurring and ranges from 0.5 (plane) to 1 (sphere) [Craig and Gordon, 1965; Ehalt and Knott, 1965; Stewart, 1975; Barnes and Allison, 1988; Horita et al., 2008]. The ratio of resistance in the laminar layer to the overall resistance appears to be about 1 under most circumstances of open water bodies unless the water body is large enough to affect the overlying atmosphere [Gat et al., 2000; Horita et al., 2008].

Merlivat [1978] presented results of measurements of the ratio of molecular diffusivities for the $^1H_2^{16}O/^1H_2^{18}O$ and $^1H^2H^{16}O/^1H_2^{18}O$ isotopologue pairs, though they are not explained by the mass differences of the isotopes alone [Merlivat, 1978; Cappa, 2003; Horita, 2008; Luz, 2009]. For a geometric factor n of 0.5 and diffusivity ratios from Merlivat [1978], kinetic enrichment factors are expressed as:

$$\varepsilon_{K,\,^2H} = 0.0125(1 - h_N), \text{and} \tag{1.24}$$

$$\varepsilon_{K,\,^{18}O} = 0.0142(1 - h_N). \tag{1.25}$$

Typical values for the kinetic enrichment used in this study range from 0.1‰ to 8.9‰ for $\delta^{18}O$ and from 0.1‰ to 7.8‰ for δ^2H.

It should be noted that the transpiration flux is typically not distinctly parameterized from the evaporation flux, and the total latent heat of the surface layer is attributed to the lumped processes and termed evapotranspiration [Monteith, 1965; Shuttleworth and Wallace, 1993; Dingman, 2002]. Transpiration has not been found to impart a fractionation effect on the pool of soil water that plants draw from [White et al., 1985], though enrichment is present within the leaf

[Flanagan and Ehleringher, 1991; Dawson and Ehleringher, 1998]. Stable isotopes of water show utility in segregating components of the total evapotranspirative flux through eddy covariance techniques [Wang and Yakir, 2000]. Little is known about whether enriched waters within leaves of emergent plants can be reintroduced to the surface reservoir in significant volumes as to bias studies of open-water isotopic enrichment due to evaporation. If such a mechanism is significant, this may be a source of error for the current investigation that is beyond the scope of this study to characterize.

1.3.5   *Isotopic Composition of an Evaporating Reservoir*

Evaporative fractionation influenced by realistic ranges of humidity and temperature results in surface water samples that plot below the LMWL along a slope of between 4 and 5, which forms an evaporative water line [Mook, 2006]. Stable isotopes have been used in many lake studies [Dinçer, 1968; Welhan and Fritz, 1977; Gibson *et al.*, 1993, 1996, 1999, 2002; Benson and White, 1994; Hostetler and Benson, 1994], to estimate some component of the lake water balance such as evaporation or net groundwater fluxes.

The volumetric water balance and isotopic mass balance for a reservoir are described by Dinçer [1968] and Gonfiantini [1986]:

$$\frac{dV}{dt} = I - Q - E \text{ , and} \tag{1.26}$$

$$\frac{d(V\delta_R)}{dt} = \frac{Vd\delta_R + \delta_R dV}{dt} = I\delta_I - Q\,\delta_R - E\delta_E \qquad (1.27)$$

where reservoir volume, non-fractionating inflows, non-fractionating outflows, and fractionating evaporation are represented by V, I, Q, and E, respectively, and time is denoted by t. The isotopic composition (δ) of the reservoir, inflows, and evaporative flux are denoted by subscripts R, I, and E, respectively. Isotopic compositions representing fluxes (I and E) are flux-weighted averages [Gonfiantini, 1986; Horita *et al.*, 2008]. If storage within the lake changes, both equations (1.26) and (1.27) are solved simultaneously. However, when changes in lake volume are generally unidirectional and smooth, the effect of the volume change can be described by the residual fraction of reservoir volume ($f = N/N_0 = V/V_0$ for constant density). A well-mixed natural reservoir receiving and/or losing water from/to both ground and surface water sources or other non-fractionating processes (e.g. transpiration, abstraction) while undergoing evaporative fractionation, has an average isotopic composition that can be described analytically by [Gonfiantini, 1986, p 134]:

$$\delta_R = \left(\delta_0 - \frac{\delta_I + Ax}{1 + Bx}\right) f^{-(1+Bx)/(1-x-y)} + \left(\frac{\delta_I + Ax}{1 + Bx}\right),$$

where δ_0 is the isotopic composition of the reservoir at the start of the evaluation period, δ_I is the cumulative flux-weighted average isotopic composition of all inputs since the beginning of the evaluation period, x is the fraction of inflowing water lost to fractionating evaporation ($x = E / I$), y is the fraction of in-flowing water lost to non-fractionating processes ($y = Q / I$), and A and B are defined as:

$$A = \frac{h_{N,A}\delta_A - \varepsilon}{1 - h - \varepsilon_K} \text{ , and,} \qquad\qquad (1.29)$$

$$B = \frac{h_{N,A} + \varepsilon}{1 - h_{N,A} - \varepsilon_K} . \qquad\qquad (1.30)$$

Humidity ($h_{N,A}$) and temperature used to estimate the enrichment factors in A and B are the cumulative evaporative flux-weighted averages over the period of evaluation [Gonfiantini, 1986; Horita *et al.*, 2008].

1.3.6   Isotopic Composition of Catchment Compartments

To evaluate the contribution from constituent hydrologic sources to any reservoir within a catchment, the challenge in solving the mixing equation (1.9) for the fraction of any given component is adequately sampling the resulting mixture and the contributing components, as well as accounting for any additional fractionation effects. For a two end-member mixing scenario where there are no additional fractionating effects, equations (1.10) and (1.11) estimate the contributing fractions of the two end-members. A unique solution also requires the components to have unique isotopic compositions. Contributing components of interest typically include precipitation, which may be the most straightforward to sample, groundwater, and surface water as both event run-off and baseflow.

Groundwater often maintains the annual flux-weighted average composition of precipitation for a given catchment that defines a LMWL [Mook, 2006], as has been observed by Frades [2008] in the Lamprey River Headwaters watershed. This is despite of the fact that infiltration is often unequally represented by precipitation

events to those that create nearly saturated soils, create ponding, and include throughfall that undergoes evaporation during interception on vegetation canopies [Kendal and Caldwell, 1998]. Infiltrated water that bypasses storage in soil typically undergoes negligible fractionation [Gonfiantini et al., 1998]. However, shallow riparian aquifer systems often reflect a seasonal variation in isotopic composition that is dampened relative to precipitation, and is often exploited to estimate residence time of the aquifer system [Gonfiantini, et al., 1998; Frades, 2008]. Deeper groundwater sources further dampen seasonal variation.

Surface-runoff from precipitation events results in mixing of waters derived from sources such as precipitation, throughfall, interflow, and saturation overflow of soil water and catchment storage. Because precipitation from individual events often maintains distinct stable isotopic compositions compared to other sources of streamflow, their use has led to important insights into the temporal and spatial distribution of run-off generating mechanisms. Several studies have shown that pre-event water, or water flowing in a channel prior to runoff from a precipitation event, represents a large fraction of event runoff, and that few generalizations can be made regarding the soil horizon (e.g. capillary fringe) or structure (e.g. macropore) most responsible for storm hydrographs [Sklash et al., 1976, 1986; Sklash, 1990; McDonnell, 1990; Buttle and Peters, 1997; Genereux and Hooper, 1998]. In many of the above studies, stable isotopes were found to be well suited to temporal hydrograph separation during storms; however, insights as to where in the catchment flow generation has occurred have been more difficult to obtain [Genereux and Hooper, 1998].

Surface-runoff between events has a less well characterized isotopic composition. One study looked at spatial contributions from a variety of subcatchments of the River Dee watershed (1,850 km²) in Scotland [Tetzlaff and Soulsby, 2008]. Inorganic and isotope tracers showed that groundwater from headwater catchments played an important role in sustaining baseflow within downstream reaches of the river's mainstem. The magnitude of diel fluctuations in discharge were correlated with peat soil coverage, and were attributed to either an evapotranspirative flux from the stream and riparian vegetation or by a reduction in seepage from soil distributed throughout the catchments exhibiting the response. No apparent enrichment from consistent groundwater compositions were observed at these catchments suggesting either a reduction in seepage or that a transpiration-dominated evapotranspiration flux caused the diel fluctuations.

St. Amour and others [2005] used stable isotopes to identify flow paths and to perform component hydrograph separations for seasonal meltwater in a series of multiple watersheds in the sub-arctic. Winter stream baseflow exhibited the closest isotopic signature to groundwater of any surface water sample. Evaporative enrichment was observed downstream of wetlands throughout the summer.

Isotopic enrichment of baseflow was observed during both winter and summer inter-storm periods from the 90 km² moderate relief Headwaters Lamprey River (HWLR) in southeastern New Hampshire [Frades, 2008, Frades *et al.*, In Prep]. Between 2006 and 2007, weekly samples were collected and analyzed for stable isotopes of water at the UNH Stable Isotope Laboratory [Frades, 2008]. Sampling

included Lamprey River discharge at the Headwaters Lamprey River (HWLR)

catchment outlet, groundwater from a monitoring well set within glacial deposits

central to the catchment, precipitation, and infiltration from a site immediately east

of the study catchment in Pawtuckaway State Park. A local meteoric water line

(LWML) was established for the HWLR as [Frades *et al.*, In Prep]:

$$\delta \,^2H \ = \ 7.71\delta^{18}O \ + \ 12.1\%o\,, \tag{1.31}$$

and is similar to other LMWLs in the region based on precipitation samples [Abbot

et al., 2000; Burnett *et al.*, 2004; Frades *et al.*, In Prep]. Moreover, it was found that

isotopic composition of groundwater was well represented by isotopic composition

of average annual flux-weighted precipitation. Infiltrated water was generally

similar in composition to precipitation on sampling dates.

The observation that streamflow during periods of baseflow was consistently

isotopically enriched relative to groundwater was explained by the presence of a

very shallow groundwater source assumed to be riparian groundwater that

experienced evaporative enrichment. The source had an apparent mean residence

of 46 days, and an enriched composition was suspected to be imparted during

evaporation residing at or near the surface, possibly within headwater wetlands.

1.4   Research Objectives

The work of Frades [2008] has motivated this investigation to further refine

the potential sources of the imparted enrichment on summer baseflow. Specifically,

this study investigates if headwater wetlands may represent a significant, poorly

defined role in baseflow generation. The topography, geological character, and

ecology of the Lamprey River watershed are similar to other watersheds throughout the region, and results of this study are expected to be adequately extended regionally.

1.4.1 Project Overview

As discussed above, from review of studies evaluating the geochemical composition of stream water, no simple generalizations regarding the role of wetlands in generating baseflow are apparent across studies or climates, as is observed for their hydrologic function volumetrically [Bullock and Acreman, 2003]. The study is intended to investigate baseflow-generating mechanisms in a wetland-rich moderate-relief temperate headwater catchment and to determine whether an assumption that baseflow from the catchment was derived from a groundwater reservoir would be justified.

The Northwood Study Catchment, which contains a series of riparian wet meadows, was chosen and instrumented for this study. The catchment, which is described in Chapter 2, is considered to be an ideal area to investigate the role of wetlands in catchment processes in moderate-relief near-coast temperate catchments because of the presence of a narrow complex of riparian wet meadows where wetland processes can be studied in a longitudinal manner. A broad goal of this study was to characterize the major hydrologic fluxes throughout the catchment during summer-time low-flow conditions through both volumetric measurement and isotopic methods.

In discussing the role of groundwater in the Northwood Study Catchment, a distinction is made between riparian groundwater sources and deeper aquifer groundwater. As discussed further in Chapter 2, unconsolidated sediments were observed as a thin veneer adjacent to streams throughout the catchment overlying bedrock, and were often unsaturated several meters away from stream channels. Therefore, deeper aquifer groundwater would imply a fractured bedrock aquifer source. The bedrock aquifer was characterized by samples of bedrock groundwater collected by Frades [2008] in 2006 and 2007 at a well located approximately 5 km south of the study catchment, which exhibited negligible seasonal variation.

1.4.1   Study Hypotheses

A possible explanation for the isotopic enrichment of streamflow compared to groundwater in the Lamprey River during inter-storm periods observed by Frades [2008] was hypothesized to be the result of temporary storage within headwater wetlands. The study therefore aims to refute a possible explanation of the observed isotopic enrichment in baseflow as reflecting the isotopic composition of shallow riparian groundwater, which has not been characterized in the catchment prior to this investigation.

To investigate the applicability of the groundwater-only assumption of baseflow generally, the study aimed to test whether groundwater discharge (shallow riparian or deep bedrock) to the stream network could accommodate observed streamflow, either through direct discharge to the stream, or by accommodating outflow from upstream surface reservoirs. To this end, stable

isotopes of water are used to partition the groundwater component of streamflow hydrograph, and to calibrate a mass balance of an upstream wetland. Specific hypotheses directing this research are presented below.

- Shallow riparian groundwater, in contrast to bedrock groundwater, was expected to exhibit seasonal variation resulting from seasonal changes in the isotopic composition of precipitation. Seasonal variation in the isotopic composition of riparian groundwater, coupled with any evaporative enrichment experienced preceding infiltration, was not expected to reflect the isotopically enriched composition of streamflow. The observation would reject a possible explanation of baseflow enrichment as being attributed to shallow riparian groundwater discharge.
    - A series of near-stream groundwater wells were installed in floodplain deposits adjacent to streams throughout the catchment. Groundwater and streamflow isotopic composition was compared during periods of baseflow.
- Isotopic enrichment compared to groundwater was hypothesized to occur within the wet meadow complex, confirming this wetland system as a possible source of baseflow enrichment observed by Frades [2008].
    - Isotopic composition of the wet meadow complex was compared to groundwater, precipitation, and surface inputs.
- Streamflow at the catchment outlet was expected to represent a mixture of the isotopic composition of groundwater (shallow riparian or deep bedrock) and evaporated water from the wet meadow complex as is depicted on Figure 2. It

was hypothesized that any recession from wetland sources would occur faster than groundwater sources, and that an increase in the contribution from groundwater to streamflow would occur throughout the summer.

- o End-member mixing fractions (equations 1.10 and 1.11) quantitatively distinguishing between the two sources were calculated through the study period and inspected.

- The role of groundwater in baseflow generation is not limited to stream reaches, but is investigated as potentially supporting surface outflow from an upstream surface reservoir.

- o A calculated isotopic mass balance and water balance estimate is developed for a large wet meadow upstream of the catchment outlet. The system is solved for a range of conditions and compared to the observed isotopic composition. The influence of groundwater inflows on the system were estimated for well calibrated system descriptions. The system descriptions were varied within known constraints to assess the fraction of outflow from the wetland potentially supported by direct groundwater inflows to the wetland.

The support of groundwater to surface discharge of the upstream reservoir, combined with observed downstream inflows, defines the total influence of groundwater on discharge within the stream network. The sum is compared to the groundwater-only assumption that catchment baseflow should be entirely comprised of, or accommodated by groundwater discharge to the stream network. If the total influence of groundwater is determined to be less than the total

streamflow throughout an extended period of baseflow, the groundwater-only assumption would be challenged for this wetland-rich headwater catchment.

1.4.3   Study Goals

The role of wetlands on the hydrology of the study catchment is explored more broadly. The catchment was established for this project, and a general assessment of its response to both low-flow and storm events is of interest. Specifically, several hypotheses regarding the roles of wetlands in the catchment hydrology are considered.

- Streams within the study catchment were expected to exhibit isotopic composition that could be related to the coverage of wetland and pond areas of their respective subcatchments.
    - Composition of streamflow from streams throughout the catchment was compared to measures of wetland coverage.
- Wetlands were also expected influence the nature of the baseflow recession. Throughout the summer it is expected that the baseflow recession curve will be more gradual downstream of individual wetlands, or in catchments with a greater proportion of wetlands and ponds.
    - Discharge was estimated continuously by developing rating curves at three streams whose sub-catchments reflect different proportions of coverage by wetlands, and records of run-off are compared.

1.4.2   Outline of the Document

The remainder of the document describes the study conducted in four additional chapters. Chapter 2 focuses on characterizing the Northwood Study Catchment. The chapter begins with a description of the setting and study duration, and is followed by a discussion of the methodology used to measure and estimate the hydrologic fluxes and their isotopic character. Chapter 3 describes the analytical methodology employed to estimate mixing fractions and their error and the development of the isotopic mass balance estimate for the Lower Wet Meadow. Chapter 4 describes the results of the investigation including a description of the observed hydrologic fluxes throughout the catchment, the results of mixing analyses, and the results of sensitivity analyses performed on the water balance. Finally, Chapter 5 concludes with a discussion of the major findings of the study, the applicability of the results, how they relate to other studies, and what data would be most beneficial to further refinements to this study, or similar studies.

2.   Study Catchment and Methods

The Lamprey River drains approximately 500 km² to the Great Bay Estuary in southeastern New Hampshire. The stream network starts in moderate-relief terrain towards the northern and western portions of the catchment, with the highest peaks at elevations of approximately 430 meters above mean sea level (m asl). Towards the eastern portions of the catchment, topography is of lower relief, and it drains to the Great Bay Estuary in Durham, New Hampshire at an elevation of approximately 1 m asl. The catchment is predominately forested with increasing suburbanization [Daley *et al.*, 2010].

The Lamprey River watershed has been the focus of a decade of hydrologic and biogeochemical study by investigators at the University of New Hampshire [Daley *et al.*, 2010]. Throughout the decade of study, several projects have focused on discrete subcatchments or sections of the Lamprey River and its watershed, notably the Headwaters Lamprey River watershed [Frades, 2008]. Additional studies have focused on the relationship between land-use/land-cover and water quality throughout the Lamprey River watershed [e.g. Daley, 2000; Flint, 2007].

Synthesis of data from long term sampling campaigns for nutrient and water quality parameters throughout the Lamprey River to evaluate the nitrogen balance demonstrate upwards of 90% dissolved inorganic nitrogen retention throughout the watershed [Daley *et al.*, 2010]. Flint [2007] found generally that 10 wetlands in or near the Lamprey River watershed resulted in lower downstream nitrate and

total dissolved nitrogen (TDN) concentrations than upstream inputs, suggesting these systems may be important to the high overall N retention observed.

The following sections reference previous research, public domain geospatial information, and field observations to describe an upstream catchment of the Lamprey River chosen for the investigation. Subsequently, a discussion is presented of the methodology used to establish estimates of the hydrologic fluxes through the catchment, and their representative isotopic compositions. Analysis methodology applied to these data will be discussed in the following chapter, and are chosen to estimate the fractions of water leaving the catchment characteristic of water stored in wetlands and in groundwater. Combined with isotopic measurements and the fractionation effects described in Chapter 1, the estimates of the hydrologic fluxes developed below are used to create an isotopic mass balance model to explore possible baseflow generating mechanisms from the meadow and to investigate further research priorities.

2.1   Northwood Study Catchment

The 7.40 km² Northwood Study Catchment (NWSC) centered at 43°12' N, 71°12' includes the most upstream reaches of the Lamprey River, which discharges to the Great Bay in Newmarket, New Hampshire 74 km downstream (Figure 3). The forested, undeveloped catchment occupies land managed by the N.H. Department of Resources and Economic Development as the Northwood Meadows State Park and Forest Peters Wildlife Management Area and is bounded on the east and south by Saddleback Mountain. The catchment includes several small ponds, Meadow Lake

impounded in 1975, and a series of linear wet meadows transecting the majority of the catchment from northeast to southwest that are maintained by a beaver dam at the southwestern terminus (Figure 4). The descriptions of the NWSC presented herein follow place names of Burtt [2010], who held large portions of the NWSC in private ownership for decades and self-published a journal of his research of the natural history and his development activities.

The linear wet meadows are divided between the upper and lower meadows by a former logging road (Old Mountain Road), which creates a hydrologic barrier so that discharge from the upper to lower meadows can be measured. Both meadows are described in the Snyder [2009] ecological assessment, where reference was made to an ecological assessment by Sperduto and Sperduto [1996], as being occupied by combinations of emergent vegetation described as sweetgale – meadowsweet - tussock sedge fen bordered by isolated red maple swamp and other tall shrub thickets. The U.S. Fish and Wildlife Service NWI [2001, and 2010 update] map the series of wet meadows as a combination of palustrine forested, shrub, and emergent vegetated wetlands. The NWI identifies only the Upper Wet Meadow as beaver affected; however, the Lower Wet Meadow was impounded by a beaver dam throughout the duration of this study, whereas the Upper Wet Meadow was impounded by a beaver dam only intermittently from July 2009 through March 2010.
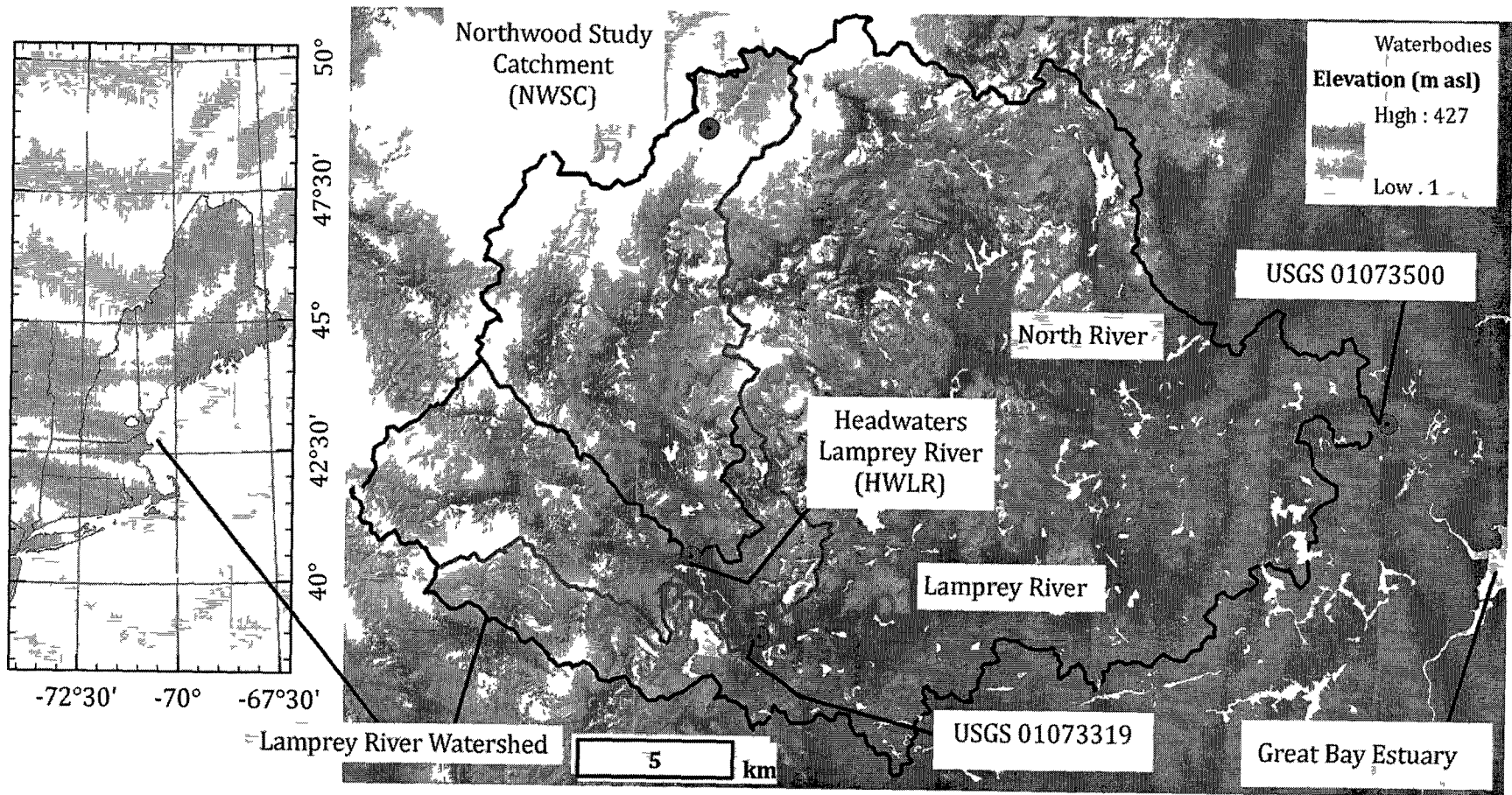
Figure 3: Digital Elevation Model (DEM) of the Lamprey River watershed. Location of Lamprey River watershed at left. Catchment outlines are shown for U.S. Geological Survey gages 01073500 in Durham near Newmarket, and 01073319 in Raymond, and for the New Hampshire 1:24,000 National Hydrographic Dataset Headwaters Lamprey River subwatershed. North is vertical.
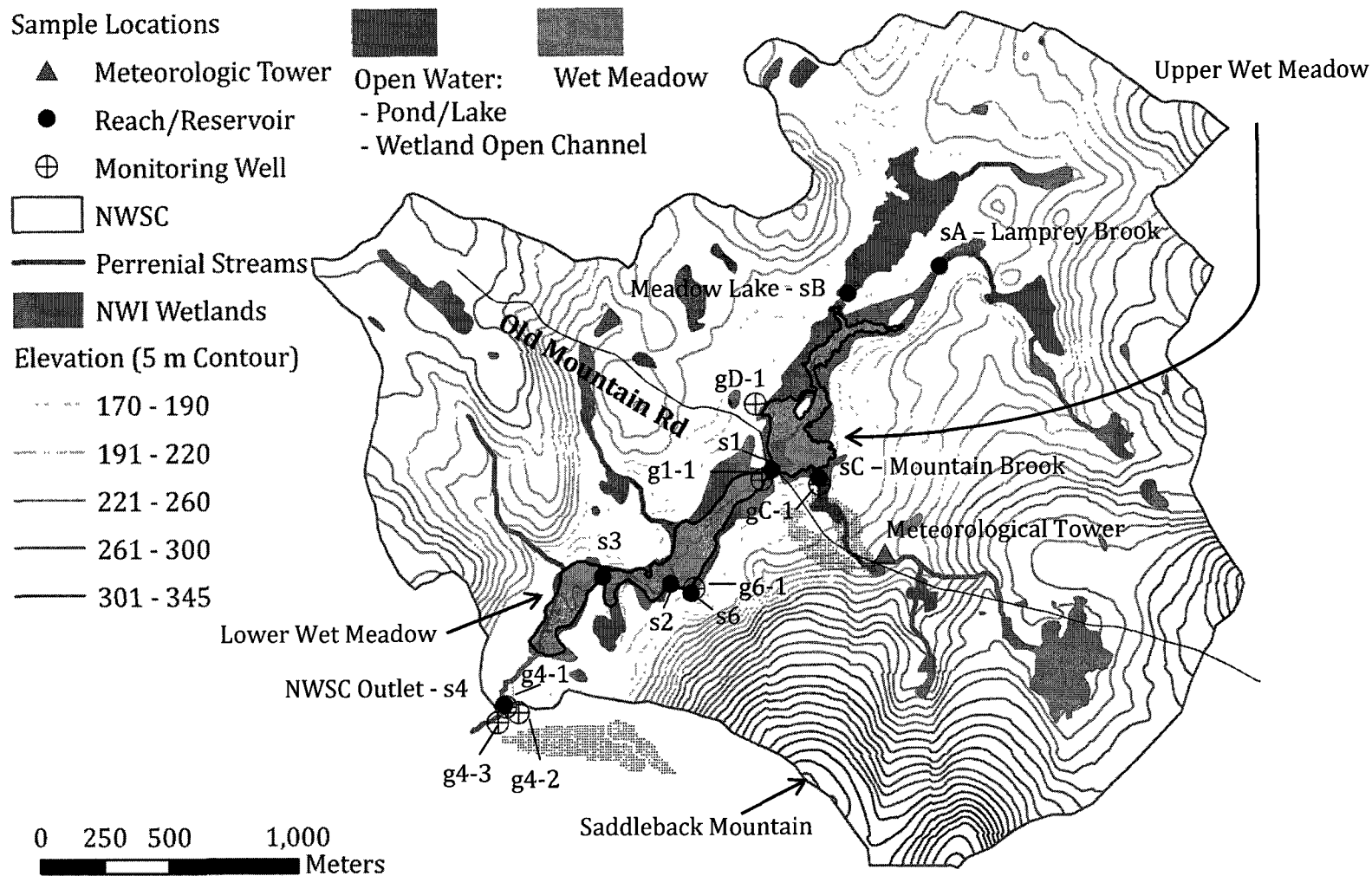
Figure 4: Northwood Study Catchment. Depicts suface topography as 5-m contours and drainage and water bodies as indicated. Sample locations are indicated for surface waters [*sX*] and ground water monitoring wells [*gX*]. Gray areas near the catchment outlet and between sC and s1 are locations of DEM modification described in Section 2.1.1. North is vertical.
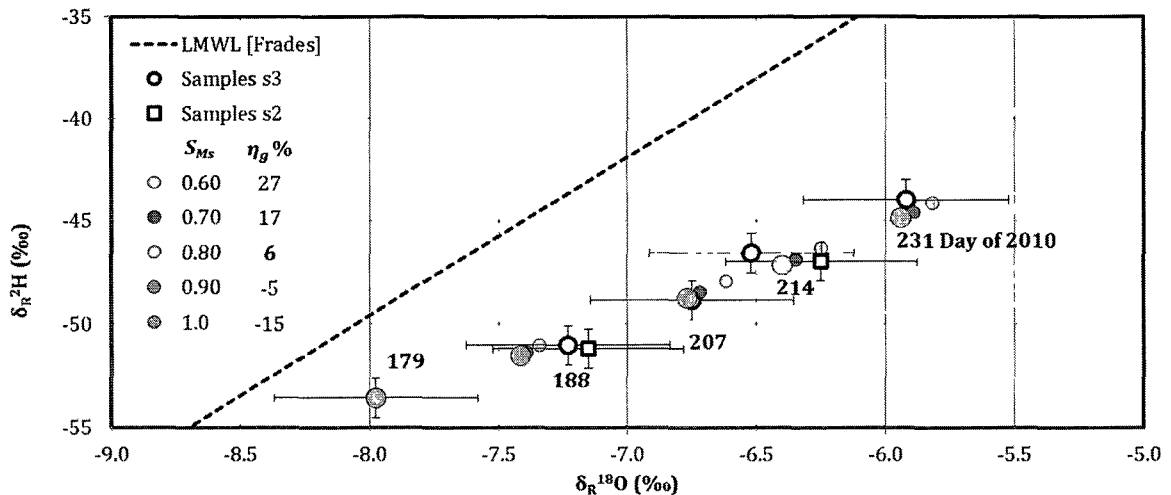
Figure 33: Predictions of Lower Wet Meadow isotopic composition for five system states. 99% confidence intervals of sample analytical results are presented as error bars. Larger orange markers indicate results from the bolded parameter combinations in Table 8 that result in an optimized model efficiency (E > 0.95) for both $\delta_R^{18}O$ and δ_R^2H.

the system demanded by the water balance provided by the groundwater flux are

more depleted than the isotopic composition of water within storage, the reduction

in volume that requires enrichment easily compensates for the differences in

isotopic composition. The value S_{Ms} = 0.80 provides the best predictive capacity by

optimizing the NSE for both $\delta_R^{18}O$ and δ_R^2H to values greater than 0.95. The

prediction from this parameter combination is bolded on Table 8, and highlighted

on Figure 33. The optimized parameter S_{Ms} predicts that only about 6% of outflow

from the Lower Wet Meadow during the evaluation period could be accommodated

by direct groundwater inflow. The parameter combinations presented on Table 8

and Figure 33 result in predictions within analytical uncertainty of wet meadow

composition, so optimization between the parameter combinations is not a

conclusive identification of the role of groundwater in the Lower Wet Meadow

water balance. However, for the range of values tested for S_{Ms}, which are considered

2.1.1 Geospatial Data

A geographic information system (GIS) of the study area was generated using data available through *NH GRANIT* including LANDSAT-derived land use and land cover [LANDSAT, Complex Systems Research Center, 2001], National Wetland Inventory [U.S. Fish and Wildlife Service, 2001, 2010], the New Hampshire 1:24,000 National Hydrographic Dataset [U.S. Geological Survey, U.S. Environmental Protection Agency, Complex Systems Research Center, and N.H. Department of Environmental Services, 2006], and 0.3-meter resolution orthoimagery flown in 2005 [N.H. Department of Transportation, 2007].

Elevation data were obtained through a field survey and the New Hampshire Geological Survey [2007], which produced a 10-meter resolution, hydrologically filled digital elevation model (DEM) derived from USGS digital line graph data of the region encompassing the Lamprey River watershed and is shown in Figure 3. In August 2010, a series of cross-sectional topographic surveys of the Meadow Lake dam and stream reaches from the outlet of the Lower Wet Meadow downstream to the NWSC catchment outlet were conducted. A Sokkia SET5A Total Station was used to estimate true relief in the areas, which was underestimated by the 10-meter NHGS DEM. Topography was measured at about 5-meter spacing between cross-sections at the Meadow Lake dam. Relief of the beaver dam forming the outlet of the Lower Wet Meadow was surveyed at about a 3-meter grid spacing to about 15 meters downstream. The channel and valley cross-sectional geometry between the

Lower Wet Meadow and catchment outlet was surveyed at about 1-meter resolution within the channel, and 5-meter resolution above the channel every 25 to 50 meters.

These data were combined with a 5-meter resampling of the 10-meter NHGS DEM to produce a revised DEM of the NWSC. A stream network was derived using the hydrology tools in ArcGIS version 9.1 (Environmental Systems Research Institute, Inc.). The stream network defined by the resampled and corrected DEM resulted in hydrographic inconsistencies with observations. The DEM incorrectly predicted the confluence of Lamprey Brook and Mountain Brook (near sC on Figure 4) to be south of Old Mountain Road, and the confluence of another unnamed brook with the Lamprey River within the NWSC upstream of s4. The DEM was manually altered to force observed drainage at these two locations while maintaining consistent drainage throughout the remainder of the catchment. Individual grid cells in the areas depicted on Figure 4 were modified less than 1 meter vertically. The modified DEM is presented as topographic contours of the NWSC in Figure 4. The catchment has a relief of 175-meters from the top of Saddleback Mountain to the wet meadows. The steepest slopes in the catchment are 35% from horizontal along the western side of Saddleback Mountain and average about 5% throughout the catchment. The water surface across a 280 meter down-channel section of the southern terminus of the Lower Wet Meadow indicated no hydraulic gradient at the time of the survey in August 2010, and the NHGS DEM represents the meadows at a constant elevation.

Both the upper and Lower Wet Meadows contain defined channels surrounded by saturated riparian areas covered with emergent vegetation. The

meadow and channel areas were traced from 30-centimeter resolution orthoimagery [New Hampshire Department of Transportation, 2007] and are depicted in Figure 4. The meadows delineated from orthoimagery occupy a combined area of 0.18 km²; delineation was conducted to approximate areas that were observed in the field that remained at or nearly at saturation at the surface throughout the summer months. The NWI dataset indicates the meadows, ponds, palustrine, and riparian wetlands occupy approximately 0.8 km² (10.8%) of the catchment surface area. NWI wetlands encompass the wet meadows and ponds delineated using orthoimagery, as well as other areas on hillslopes that are less apparent from the orthoimagery. The NHD and NHD Plus datasets identify 0.45 km² (6.1%) and 0.13 km² (1.8%) of waterbodies, respectively. The NHD dataset includes the upper and Lower Wet Meadows and headwater ponds, whereas the NHD Plus dataset includes only the headwater ponds, and both datasets omit other smaller wet meadows and wetlands on the hillslopes. The Natural Resources Conservation Service (NRCS) reports soils (other than mucks and other ponded soils associated with saturated areas) on the hillslopes within the NWSC are predominately tilled derived sandy loams, many are well drained and typical depths to bedrock are less than 2 meters [Soil Survey Staff, 2011].

2.1.2   Stream Network and Sampling Locations

Eight locations (Figure 4) within the NWSC were selected for surface water sampling and discharge measurements. Lamprey Brook (sA) drains two successive ponds before discharging to the Upper Wet Meadow, which also receives surface discharge from the outlet of Meadow Lake (sB). Mountain Brook (sC) begins at a

small pond along the northern slope of Saddleback Mountain and drains to the Upper Wet Meadow immediately northeast of Old Mountain Road. The Lower Wet Meadow (s1) spills across Old Mountain Road to the Lower Wet Meadow. One-half kilometer southwest of Old Mountain Road a stream emanates from a small sphagnum covered fen (s6) and drains to the Lower Wet Meadow about 100 meters northeast of an established sampling point of an open channel reach of the meadow (s2). Two small streams drain the western slopes of the catchment to the Lower Wet Meadow and were not sampled or otherwise characterized in this study. A sampling point was established in an open channel of the meadow at the northern end of a bedrock peninsula (s3). A beaver dam forms the downstream terminus of the Lower Wet Meadow about 280 meters southwest of s3. The Lamprey River continues southwest of the impoundment along a series of reaches deeply incised within intact foliated gneiss and phyllite and then grades to more shallowly incised reaches set amongst hummocky glacial topography at the outlet of the study catchment (s4) located at the first measureable section downstream of the meadow outlet just upstream of a clearing of riparian meadow.

2.2   Study Period / Evaluation Period

The study focuses on hydrologic conditions at the NWSC during the summer of 2010. For several months between May and August inter-event baseflow was predominant throughout the watershed, making the investigation period ideal for the study. Baseflow sampling events were conducted at a weekly frequency throughout the summer beginning on 25 May (d=144) and continuing through 20

August (d=231). Results from an additional sampling event conducted on 12 October (d=284) are included in characterizing trends in isotopic composition. The period from 29 June (d=179) to 20 August (d=231) 2010 was selected for the isotopic mass balance study of the Lower Wet Meadow in the NWSC because a) isotopic composition was well characterized in advance and throughout this period, b) continuous periods of inter-event baseflow permitted a consistent record of isotopic samples, and c) from qualitative review of hydrographs and isotopic composition of surface waters, the major influence of stored spring rainfall and snowmelt appeared to have passed.

In presenting results (Chapter 4) a distinction is made between the *study period* 25 May (d=144) and continuing through 27 August (d=238), which is discussed in the context of hydrologic fluxes and isotopic sampling throughout the catchment, and the *evaluation period* 29 June (d=179) to 20 August (d=231) 2010, when the water balance was evaluated.

The study period and evaluation period are further distinguished from the *period of record*, which spanned from June 2009 through November 2010. Installation of field equipment at the NWSC described in the following sections began in June 2009. Activities used in to characterize hydrologic fluxes and their isotopic composition began at that time and continued through the period of record. Some of the data presented (such as gauging measurements and samples for the isotopic composition of rainfall) were used in the general characterization of the study catchment.

2.3   Meteorological Measurements and Processes

Meteorological data was collected within the NWSC for estimation of local evapotranspiration by physically based mass-transfer / energy balance combination methods. On 8 July 2009, tower-mounted sensors were deployed on a small meteorological tower (Figure 5) in a clearing at the location indicated on Figure 4 to measure wind speed, incoming short-wave solar radiation, temperature, relative humidity, barometric pressure, and bulk precipitation. The accuracies for the instruments presented below are reported in instrument documentation.

Wind speed was measured with a spinning-cup anemometer calibrated in the UNH Mechanical Engineering wind tunnel against results of an anemometer of known calibration. Incoming solar radiation was measured with a level factory-calibrated Apogee silicon shortwave radiation precision pyranometer (PYR-P) with an absolute accuracy of ±5%. Temperature and relative humidity was measured with a Campbell Scientific HMP45C Temperature and Relative Humidity Sensor mounted at approximately 2 meters above the ground surface within a passive (non-aspirating) radiation shield. Temperature measurements collected by the probe have accuracies of ±0.2°C at 20°C increasing to ±0.4°C at -20°C and 60°C. Relative humidity measurements, which use a Vaisala HUMICAP capacitive polymer H chip, have an accuracy of ±2% for values up to 90%, and ±3% from 90 – 100% humidity. A Texas Electronics TE525WS tipping bucket rain gauge logged bulk precipitation at 0.254-millimeter intervals on a Hobo Event datalogger. The device underestimates precipitation rates greater than 25.4-millimeters; however, rainfall rates this high were not observed throughout the period of record. The accuracy of

the calculated rainfall rate from the tip logging is reported as ±1% for rates up to 25.4-millimeters per hour. The funnel and assembly of a second TE525WS gauge was deployed without the tipping bucket and recorder and tubing directed falling bulk precipitation to a high-density polyethylene (HDPE) 2-L plastic bladder housed within a pail on the ground for collection.

Barometric pressure was recorded at the meteorological tower with a Solinst BaroLogger Gold after 6 August 2010. A Solinst BaroLogger LT had been deployed since August 2009 but, due to spurious fluctuations in barometric response, the hourly record from October 2009 to removal in August 2010 was not consistently reliable. However, correlation between hourly average barometric pressure between the NWSC and the Thompson Farm AIRMAP station in Durham, New Hampshire was strong throughout the devices deployment (r^2 = 0.95 for all data, and improves to r^2 = 0.99 for data collected between August and September 2009 when the device was functioning consistently). Therefore, the Thompson Farm AIRMAP data are used for barometric pressure measurements between September 2009 and August 2010.

2.3.2   Estimating Evapotranspiration

Open-water evaporation (e_W [m_{water} h^{-1}]) and plant transpiration (e_T [m_{water} h^{-1}]) were estimated by the Kohler-Parmele refinement of the Penman combination equation (KP-PCE) and the Penman-Monteith combination equation (PMCE), respectively [Penman, 1948; Monteith, 1965; Kohler and Parmele, 1967;

Shuttleworth and Wallace, 1985; Wessel and Rouse, 1994; Allen *et al.*, 2000;

Dingman, 2002]:

$$e_W = \frac{\Delta \cdot (K + L') + \rho_a \cdot c_a \cdot C_{at} \cdot e_a^*(1 - h_a)}{\rho_w \cdot \lambda_v \cdot (\Delta + \gamma')} \tag{2.1}$$

$$e_T = 2 * \text{LAI} * \frac{\Delta \cdot (K + L') + \rho_a \cdot c_a \cdot C_{at} \cdot e_a^*(1 - h_a)}{\rho_w \cdot \lambda_v[\Delta + \gamma' \cdot (1 + C_{at}/C_{can})]} \tag{2.2}$$

where the terms in the above equations are explained in Table 1 below.

Figure 5: Meteorological tower installed at NWSC. Location depicted on Figure 4. See text for sensor description.

Table 1: Definitions of terms used in evapotranspiration calculation. Compiled by Dingman [2002] unless stated otherwise.

Term	Units	Description	Formulation
Δ	$kPa\ K^{-1}$	slope of the ratio between saturation vapor pressure and air temperature (in K)	$\dfrac{2508.3}{[T_a + 237.3]^2}\ exp\left(\dfrac{17.3 \cdot T_a}{T_a + 237.3}\right)$
T_a	$°C$	mean air temperature in degrees centigrade	Measured
K	$MJ\ m^{-2}\ h^{-1}$	Net incoming solar radiation	Measured
L'	$MJ\ m^{-2}\ h^{-1}$	Kohler and Parmele [1967] corrected net longwave radiation	$\varepsilon_w[\varepsilon_a \cdot \sigma \cdot (T_a + 273.2)^4] - \varepsilon_w \cdot \sigma \cdot (T_a + 273.2)^4$
ε_w	-	emissivity of water	0.95
ε_a	-	emissivity of the atmosphere	$day:\ 1.72 \cdot \left(\dfrac{e_a}{T_a + 273.2}\right)^{1/7} \cdot \left[1 + 0.22 \cdot \left(1 - \dfrac{K}{K_{cs}}\right)^2\right]$ $night:\ 0$
σ	$MJ\ K^{-4}\ h^{-1}$	Stefan-Boltzman constant	$1.177 \times 10^{-7}\ MJ\ K^{-4}\ h^{-1}$
e_a	kPa	actual water vapor pressure	$e_a = h_a \cdot e_a^*$
K_{cs}	$MJ\ m^{-2}\ h^{-1}$	clear sky radiation	Estimated from extraterrestrial solar radiation
h_a	-	relative humidity (fraction)	Measured: relative humidity / 100
e_a^*	kPa	saturation water vapor pressure	$0.6108 \cdot exp\left(\dfrac{17.27 \cdot T_a}{T_a + 237.3}\right)$

Table 1 (Continued): Definitions of terms used in evapotranspiration calculation. Compiled by Dingman [2002] unless stated otherwise.

Term	Units	Description	Formulation
γ'	kPa K^{-1}	Kohler and Parmele (1967) corrected psychrometric constant	$\dfrac{c_a \cdot P_a}{0.622 \cdot \lambda_v} + \dfrac{4 \cdot \varepsilon_w \cdot \sigma \cdot (T_a + 273.2)^3}{K_E \cdot \rho_w \cdot \lambda_v \cdot v_a}$
c_a	MJ kg^{-1} K^{-1}	heat capacity of air	$1.00 \times 10^{-3} MJ\ kg^{-1}\ K^{-1}$
P_a	kPa	barometric air pressure	measured
λ_v	MJ kg^{-1}	latent heat of vaporation of water	$2.50 - 2.36 \times 10^{-3} \cdot T_a$
K_E	m hr^2 kg^{-1}	efficiency of vertical transport of water vapor	$\dfrac{0.622 \cdot \rho_a}{P_a \cdot \rho_w} \cdot \dfrac{k^2}{\left[ln \left(\frac{z_m - z_d}{z_0} \right) \right]^2}$
ρ_a	kg m^{-3}	density of air	$\dfrac{P_a}{T_a R_a}$
ρ_w	kg m^{-3}	density of water	1000 kg m^{-3}
k	-	Von Karmon's constant	0.4
$z_{[x]}$	m	m: height of v_a measurement, d: zero-plane displacement, 0: roughness height	$z_d = 0.7 \cdot$ height of vegetation (z_{veg}), $z_0 = 0.1 \cdot z_{veg}$ open-water: $z_d = 0$, $z_0 = 2.3 \times 10^{-4}$
v_a	M hr^{-1}	average wind speed (at z_m)	measured
R_a	kJ kg^{-1} K^{-1}	gas constant	0.288

Table 1 (Continued): Definitions of terms used in evapotranspiration calculation. Compiled by Dingman [2002] unless stated otherwise.

Term	Units	Description	Formulation
C_{at}	$m\ h^{-1}$	atmospheric conductance	$v_a k^2 / \left[ln\left(\frac{z_m - z_d}{z_0}\right) \right]^2$
C_{can}	$m\ h^{-1}$	canopy conductance	$0.5 \cdot C_{leaf}$
LAI	-	leaf area index	assigned value from Federer and others [1996] based on landcover (3.0)
C_{leaf}	$m\ h^{-1}$	Stewart's [1988] estimate of stomatal leaf conductance	$C^*_{leaf} \cdot f_K(K_{in}) \cdot f_\rho(\Delta\rho_v) \cdot f_T(T_a)$
C^*_{leaf}	$m\ h^{-1}$	maximum stomatal conductance	assigned value from Federer et al. (1996) based on landcover (40)
$f_{[x]}$	-	Stewart's [1988] functions describing stomatal conductance due to environmental factors	Stewart [1988], Dingman [2002] Table 7-6
$\Delta\rho_v$	$kg\ m^{-3}$	humidity deficit	$\frac{e}{T_a R_a} - \frac{e^*}{T_a R_a}$
α	-	albedo	Water: $0.127 \cdot exp(-0.0258 \cdot K_{in})$ [Dingman, 7-27, p 282] 0.20 (Grass/Meadow), 0.22 (Crops)

The open water evaporation (e_w) represents an estimate of a thin film of water where all latent-heat energy is utilized in water evaporation but does not account for energy storage in a real water column. Vegetation transpiration (e_T) is an estimate of the rate of water lost through the transpiration process of plants and needs to be distinguished from (e_w) when applied to emergent vegetation in a wetland because the process imparts no apparent fractionation of the reservoir [White et al., 1985]. The vegetation transpiration rate is defined as zero for those times when the canopy is storing water. Note the distinction between the variable names distinguishing the depth rate of evaporation (e_x) from the common variable definition of water vapor pressure from Table 1, which is italicized (e_a) and the volume rate flux counterparts (E_x m^3 d^{-1}) discussed later.

The estimation of net longwave radiation was performed in accordance with Kohler and Parmele [1967] where the atmospheric emissivity is estimated from cloud fraction related to the ratio of measured incoming solar radiation and expected clear-sky solar radiation for each hourly observation (1- K/K_{cs}). Clear-sky solar radiation is given by Dingman [2002] and Allen and others [2000] and is estimated from the proportion of extraterrestrial solar radiation expected to reach the Earth's surface at a given latitude at a specific time of day. In the current work, estimates of the ground heat-flux, water-stored energy, and advected energy are not incorporated into the KP-PCE or PMCE estimates. The effects of ground heat-flux and advected energy are expected to be negligible for the wetland system; however, neglecting water-stored energy is expected to result in an overestimation of day-time evaporation [Dingman, 2002] as the water body is warming through the

summer months. Furthermore, the estimate assumes neutral stability conditions and does not account for convective water vapor loss from buoyant mixing of a warm air mass developed immediately above a radiatively heated ground surface.

In a review of lake water balance studies Winter [1981] found that errors in estimating seasonal evaporation from energy balance methods using measurements of meteorological parameters above the lake are on the order of 13% when compared to other methods, and these errors increase for shorter averaging periods. Drexler [2004] summarizes several applications of the PCE and PCME to wetland evapotranspiration and the root mean square error of these methods compared to more direct estimates were typical of morning and afternoon evaporation rates (<0.1 mm hr⁻¹) when using measurements from immediately above the wetland surface.

2.3.3   Estimating Temperature at the Evaporating Surface

Isotopic fractionation is governed by a number of factors that require characterization of meteorological conditions including the temperature of the evaporating surface and the ambient humidity normalized to the temperature of the evaporating surface. Furthermore, the isotopic composition of atmospheric water vapor can be related to other measures of atmospheric water vapor content.

Water surface temperature is back-calculated from the Penman combination equation in accordance with the direct substitution method of Tracy and others [1984], and further discussed by Bristow [1987]. Estimation of surface temperature from air temperature and the latent heat flux is complicated by non-linearity (fourth

order polynomial) in the emitted long-wave radiation, and in the relation between saturated vapor pressure and air temperature (Δ). Following Tracy and others [1984], the surface temperature of a saturated surface experiencing evaporation and exposed to shortwave radiation can be initially estimated from air temperature (in Kelvin) as:

$$T_{s,j=1} = T_a + \frac{(K + L' + Q) - \lambda_V e_w - \varepsilon \sigma T_a^4}{0.036 + \lambda_V e_w \left(\frac{\Delta}{e_a^* - e_a}\right) + 4\varepsilon \sigma T_a^3} \tag{2.3}$$

and can be further refined by an iterative direct substitution method. The iteration number is given by j, and the method converges to negligible differences between $T_{s,j}$ and $T_{s,j-1}$ within five iterations (j = 5) by refinement according to [Tracy et al., 1984]:

$$T_{s,j} = T_a + \frac{(K + L' + Q) - \lambda_V e_w - \varepsilon \sigma \left(T_a^4 + 4T_a^3(T_{s,j-1} - T_a)\right)}{0.036 + \lambda_V e_w \left(\frac{\Delta_{j-1}^*}{e_a^* - e_a}\right) + 4\varepsilon \sigma T_{s,j-1}^3} \tag{2.4}$$

where $T_{s,j}$ is the surface temperature (K) estimated by the current iteration, Δ^*_{j-1} is the slope of the vapor pressure saturation curve at a temperature intermediate between the air temperature and the surface temperature estimated by the previous iteration, and other variables are defined in Table 1. The estimate of surface temperature is used to calculate the normalized relative humidity h_N (equation 1.13).

56

2.3.4 Rainfall, Interception, and Throughfall

Measured rainfall was totaled on an hourly interval yielding rainfall intensities in millimeters per hour. A continuous record of estimated effective rainfall that accounted for interception loss was calculated in accordance with an adaptation of the exponential canopy wetting formulation of Liu [1997 and 2001] similar to that of Carlyle-Moses and Price [2007]. In contrast to more common models of the interception process based on the Rutter model [Rutter *et al.*, 1971], which characterizes the forest canopy as a storage reservoir that must fill to saturation prior to canopy drainage, the Liu model characterizes the canopy as exponentially reducing the amount of precipitation that reaches the ground based on the dryness of the canopy. The Liu formulation results in virtually all precipitation events producing some amount of throughfall, which is supported by field observations [Carlyle-Moses and Price, 2007; Carlyle-Moses *et al.*, 2010], whereas the Rutter model can result in no throughfall for brief and light showers. Furthermore, the Rutter model is more heavily parameterized with necessary input from field measurements. The few parameters used in the Liu model are easily estimated; however, the accuracy of the model has been shown to be greatly increased with an accounting of the sparseness of the canopy [Carlyle-Moses and Price, 2007] and with the inclusion of measured response of stem flow [Carlyle-Moses *et al.*, 2010]. The following derivation presents a continuous formulation of the Liu model that, like the formulation of Carlyle-Moses and Price, incorporates the sparseness of the canopy structure.

The following treatment of the interception process called the continuous Liu model is not explicitly tested in the literature. The formulation is unique to this study; however, the original work of Liu [1997] identifies a continuous form as possible. This investigation did not measure throughflow (or stem flow) directly so estimating it from a theoretically derived method is a suitable alternative. Cited studies testing the Liu interception model focus on event-scale processes and require assumptions regarding the dryness of the canopy prior to storm events, and the method works well empirically under storm-integrated conditions. The long-term continuous record of interception required in the present study required a formulation that accounts for drying of the canopy.

Following Liu [1997], a volume of rain falling is reduced by passage through the canopy by an amount ΔP. The magnitude of this change is proportional to the rainfall intensity (R), the canopy dryness index (D), and the time interval (Δt):

$$\Delta V_P = kRD\Delta t \qquad (2.5)$$

where k is proportionality constant shown to be equivalent to the canopy cover fraction (c) [Liu, 1997; 2001]. D is a factor ranging from 0 to 1 that describes the relative dryness of the canopy by:

$$D = 1 - \frac{C}{C_M} \qquad (2.6)$$

where C is a measure of the water in storage under the set of conditions (millimeters), and C_M is the maximum canopy storage capacity (millimeters). The canopy cover fraction is assumed to be related to the canopy gap fraction (g) by:

58

$$c = 1 - g. \tag{2.7}$$

A dryness index less than 1 implies canopy storage of water and forces the vegetation transpiration flux to zero (Section 2.3.2).

As rainfall passes through the canopy a change in the water stored in the canopy over a given time period (ΔC in millimeters) is realized equal in magnitude to the change volume of precipitation falling through the canopy, and is related to a commensurate change in the dryness index (ΔD, dimensionless). From the definition of the dryness index, ΔD will be negative and is related to ΔC by:

$$\Delta D = -\frac{\Delta C}{C_M} \tag{2.8}$$

From the equality of ΔC and ΔV_P, equations (2.5) and (2.8) are combined and integrated with respect to time by treating the canopy as a linear reservoir. Setting the initial value for the dryness index to D_i, noting that the rainfall intensity multiplied by the time period of integration gives p_i (the total rainfall depth of the time step), and neglecting evaporation yields the following relation for the dryness index for any time step i during precipitation [Liu, 1997]:

$$D_i = D_{i-1} \exp\left(-\frac{(1-g)p_i}{C_M}\right). \tag{2.9}$$

Evaporation from canopy storage at a rate estimated as the open-water evaporation rate (e_w) and the increase in canopy storage due to incoming precipitation occur

simultaneously. The two processes act in additive manner to impart the total

interception over the timestep (N_i) [Liu, 1997]:

$$N_i = C_m(1 - g)D_{i-1}\left[1 - \exp\left(-\frac{p_i}{C_m}\right)\right]$$

$$+ e_W \Delta t(1 - g)\left[(1 - D_{i-1})\exp\left(-\frac{p_i}{C_m}\right)\right].$$

(2.10)

In accordance with Carlyle-Moses and Price [2007], both canopy wetting and

evaporation from the canopy are distributed to the fraction of the area occupied by

the canopy $(1 - g) = c$.

During periods without precipitation, the change in storage of water on the

canopy is related to the rate of open-water evaporation (e_w):

$$\Delta C = e_w \Delta t,$$

(2.11)

and for simplicity here is not treated as a function of the wetness ($1-D$) as originally

proposed by Liu [1997, equation (27)]. Open-water evaporation is considered a

slight underestimation of the actual evaporation rate from a saturated canopy;

however, for the comparatively low values of C_m, the canopy can be dried after only

a few hours. From the definition of the dryness index we have:

$$\Delta C = \Delta D \; C_M = e_w \Delta t$$

(2.12)

For timestep i, the dryness index, when less than unity, and when no precipitation is

occurring, is given as:

$$D_i = D_{i-1} + \frac{e_w \Delta t}{C_M},$$ (2.13)

until a value of unity is reached. It should be noted that in application neither Liu [2001] nor Carlyle-Moses and Price [2007] estimated the drying of the canopy from evaporation, but assumed that the canopy was dry (D = 1) after a sufficient amount of time passed between storms. The above formulation differs from that of Carlyle-Moses and Price only in that this is formulated in a continuous form and simplistically accounts for drying due to evaporation between rainfall events, which were measured at hourly resolution in this study.

Inherent in the assumptions of the model are that interception is only applicable during periods of incoming precipitation, therefore, interception is 0 for those timesteps that do not meet this criteria. To calculate throughfall ($p_{tf,i}$), the fraction of the area covered by canopy (c) is treated with the above canopy treatments, whereas the gap fraction (g) experiences the bulk precipitation rate:

$$\text{For } p_i = 0 \ ... \ p_{tf,i} = 0$$

(2.14)

$$\text{For } p_i > 0 \ ... \ p_{tf,i} = (1 - g) \cdot (p_i - N_i) + g \cdot p_i.$$

To illustrate how the dryness index and calculated throughfall from this formulation of the Liu model respond to rainfall and evaporation, Figure 6 presents a simulated 72-hour period where the model is forced by hypothetical conditions. The simulation assumes an initial relative dryness of 1. Rainfall begins at simulation hour 3 and continues through hour 25 at a constant rate (0.9 mm hr^{-1}, total storm

rainfall of 20.7 mm, total predicted throughfall of 19.0 mm). From hour 31 to 42, the

canopy experiences moderate evaporation at a constant rate (0.35 mm hr^{-1}, total

day 2 evaporation of 4.2 mm), and the canopy dryness index rapidly approaches 1

as expected. A second lower intensity storm begins on hour 45 and continues

through hour 60 at a constant rate (0.5 mm hr^{-1}, total storm rainfall of 8.0 mm, total

storm throughfall of 7.2 mm) and is immediately followed by moderate evaporation.

Note the inflections in predicted throughfall resulting from changes in the

evaporation rate as evaporation increases (hours 7 and 55) and decreases at hour

19. After hour 19 when the evaporation rate decreases to an overnight minimum of

0.001 mm hr^{-1}, the throughfall rate virtually equals the precipitation rate (N_{19} to N_{25}

$\cong$ 0).
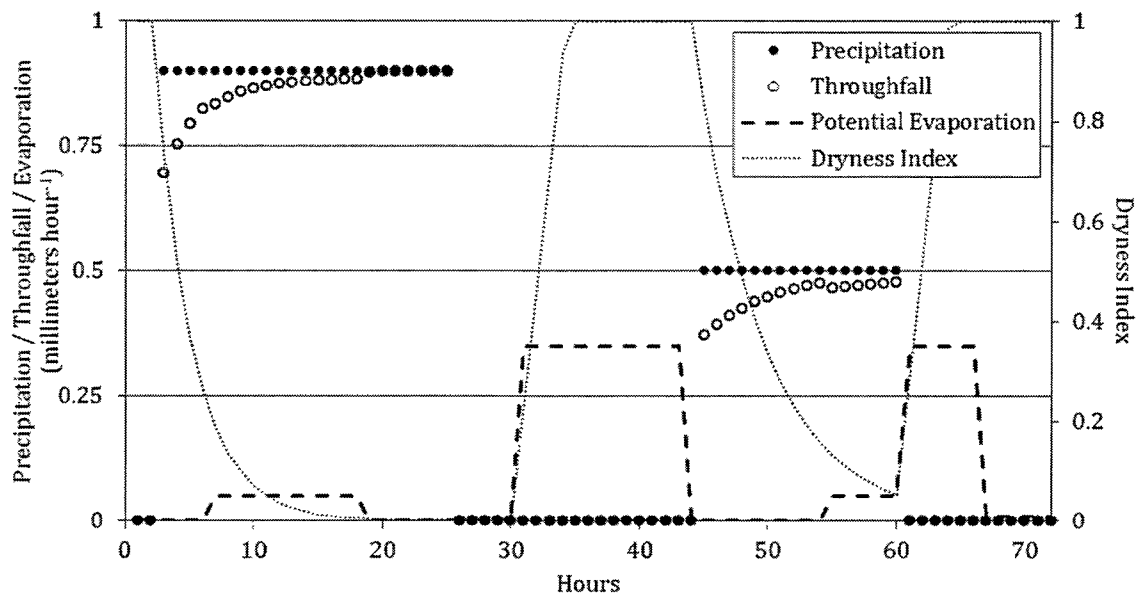
Figure 6: Sample simulation of continuous Liu interception model. Shows effects of two continuous rate storms under varying evaporation conditions (see text for explanation) over a 72 hour period. Canopy gap fraction g is set equal to 0.45, and the canopy storage C_m is set equal to 1.5 millimeters.

Liu published a table of the parameters used to compare his and other interception models on 30 datasets (2001). Representative values for the canopy gap fraction and the canopy storage were chosen from studies summarized by Liu with similar vegetative communities as those found within the NWSC. Within the Lower Wet Meadow, canopy storage (C_m) was assigned a value of 1.5-millimeters and the canopy gap fraction (p) was assigned a value of 0.45. These parameters are used in the creation of Figure 6.

2.4   Streamflow

Stage/discharge relationships were developed and maintained at the Northwood Study Catchment (NWSC) at five locations (sA, sB, sC, s1, and s4) between July 2009 and November 2010. The stage discharge relationship for the outlet of Meadow Lake (sB) was problematic because intermittent entrapment of debris at the culvert restricted outflow while raising stage, introducing inconsistencies in the stage/discharge relationship. Furthermore, the stage/discharge relationship at the outlet of the Upper Wet Meadow at s1 was problematic from July 2009 through March 2010. During March 2010 several weeks of heavy precipitation removed woody debris presumed to be an incomplete beaver dam. After removal, the dam was not replaced throughout the remainder of 2010. Only discharge measurements collected at s1 in June 2009 and between March and September 2010 were utilized in developing the stage discharge relationship. The following sections describe stage and discharge measurements, and how these are used to estimate continuous records of discharge throughout the NWSC.

2.4.1 Stage Measurement

In June 2009, Style C staff plates demarcated in feet were installed at five sampling locations (sA, sB, sC, s1, and s4). Four stilling wells were installed at three of the locations with staff gages (sC, s1, and s4) and at s3. Stilling wells were constructed using 32-millimeter diameter Water Source LLC stainless steel well points extending above the streambed and 32-millimeter 316 stainless steel riser pipe at s3 and s4. At sC and s1 stilling wells consisted of capped, perforated 25-millimeter diameter polyvinyl chloride (PVC) piping mounted to the staff gages.

Stage was measured both visually at staff plates and with Solinst LeveLogger Junior or Solinst LeveLogger Gold data-logging pressure transducers, which, in addition to logging pressure, record temperature of the water. Staff gauges are demarcated to 0.01-feet and measured to 0.005-foot (1.5-millimeters) accuracy. Pressure transducers have manufacturer-reported accuracies of 1.5 or 3.0 centimeters for the Gold and Junior models, respectively. Pressure transducers were lab-calibrated to visual measurements of stage throughout the range of observed transducer submersions. Lab-calibration was performed at the University of New Hampshire Hydrology Laboratory by submerging the transducers within a clear plastic cylinder with a stadia rod, adjusting the height of the water column, and comparing the average (n=10) recorded change in transducer response with the change calculated from the visual reading. The error attributed to the calibration consists of the variance in measured values for each measured water column height and the uncertainty in measurement from the stadia rod. The root mean square error of repeated measures from each logger was assumed to provide an unbiased

estimate of the error, and the uncertainty in visual readings is estimated at ±0.8 mm. Both sources of error are propagated to provide an estimate of the error in the calibration response coefficient $C = \left(\frac{\text{Measured depth of displacement}}{\text{Depth of transducer response}}\right)$ at 95% confidence. The deviation of the calibration response coefficient from unity (17 to 20 mm per meter of response) exceeds the error associated with the calibration for each logger (about 4 mm), therefore the calibration response coefficients are considered not to be associated with error in the calibration and were employed in estimating stage.

Continuous records of stage were maintained at the catchment outlet (s4) and in the Lower Wet Meadow (s3) from 21 March 2010 and at the outlets of Mountain Brook (sC) and the Upper Wet Meadow from 25 May 2010. No continuous records of stage were maintained at the first order sA or sB catchments. However, a frequent record of manual measurements provides a record of discharge during periods of baseflow. Table 2 summarizes transducer field installation date and each device's calibration response. The response from each transducer measurement was adjusted using a calibrated response coefficient.

Table 2: Transducer deployment and expected measurement error. Transducers were continuously deployed after the indicated date through November 2010.

Transducer S/N	Location	Deployed	C	Error (m) at 95% CI
0-1042144	sC	26 May 2010	1.0195	0.00436
0-1042423	s1	26 May 2010	1.0184	0.00414
0-1051069	s3	21 March 2010	1.0169	0.00438
0-1051060	s4	21 March 2010	1.0173	0.00378

Transducer logs were kept at 6-minute intervals, and smoothed using a 9-point (54-minute) moving median to minimize the influence of occasional spurious readings. Hourly average stage was calculated from the smoothed record and compensated for changes in barometric pressure. At s1 and s4, calibrated, smoothed, averaged and barometrically compensated (hereafter "corrected") transducer stage records were regressed against manual staff plate measurements collected between May and November 2010, when the loggers were deployed. Rating curves, discussed shortly, were developed from discharge measurements and stage measurements from visual reading of staff plates collected throughout the period of record from June 2009 through November 2010. The measurements used to develop the rating curves are all considered representative for the study period; there were no observed changes in channel morphology throughout the period of record. Measurements collected outside the study period included the highest discharge measurements. The regressions were carried out so that transducer measurements could be related directly to staff plate measurements, instead of defining new rating curves from data collected only during the study period.

At s4, the transducer was deployed within a stilling well upstream within the same pool as the staff plate. Comparison of corrected transducer response to verticality corrected staff plate measurements did not yield a linear response, which is attributed to differing hydraulic responses at the two locations. Figure 7 presents staff plate measurements for s4 from 21 May to 12 November 2010 and the corrected transducer response at the time of measurement. A power function is used to estimate stage and appears to adequately reflect the observed relationship

($r^2 = 0.98$). At s1, continuously declining stage required the stilling well to be

lowered on the staff plate twice, on 9 July and again on 13 August, 2010. Figure 8

presents staff plate measurements for s4 from 25 May to 12 November 2010 and

the corrected transducer response at the time of measurement. Linear functions are

used to estimate stage during the three time periods (r^2=0.990 for 25 May to 9 July,

r^2=0.988, for 9 July to 13 August, and r^2=0.999 for 13 August to 16 November,

2010). The deviation from one of the slope of the response to the staff plate

measurements is greater than measurement error observed during lab calibration,

but is unsystematic. Furthermore, other functions, such as the power function used

at s4, did not result in better representation of the data. Therefore, the functions

presented on Figure 8 were used to estimate a continuous record of stage. The

slope coefficient between transducer estimates and visual measurements at the

installation on 13 August differ from coefficients describing previous installations.

The 13 August installation was at a second staff plate located approximately 2

meters from the staff plate. Is is unclear why the coefficient would change from less

than to greater than one due to the translocation.

At sC, the transducer was mounted directly to the staff plate. Because the

period of record of representative discharge measurements coincided with

transducer deployment at sC, the corrected transducer responses were used to

develop rating curves. Hourly average stage was estimated relative to the stilling

well top of casing at s3 in the Lower Wet Meadow because no staff plate was

installed at this location, and converted to estimates of wetland stage from periodic

measurements of height of the top of casing from the peat surface.
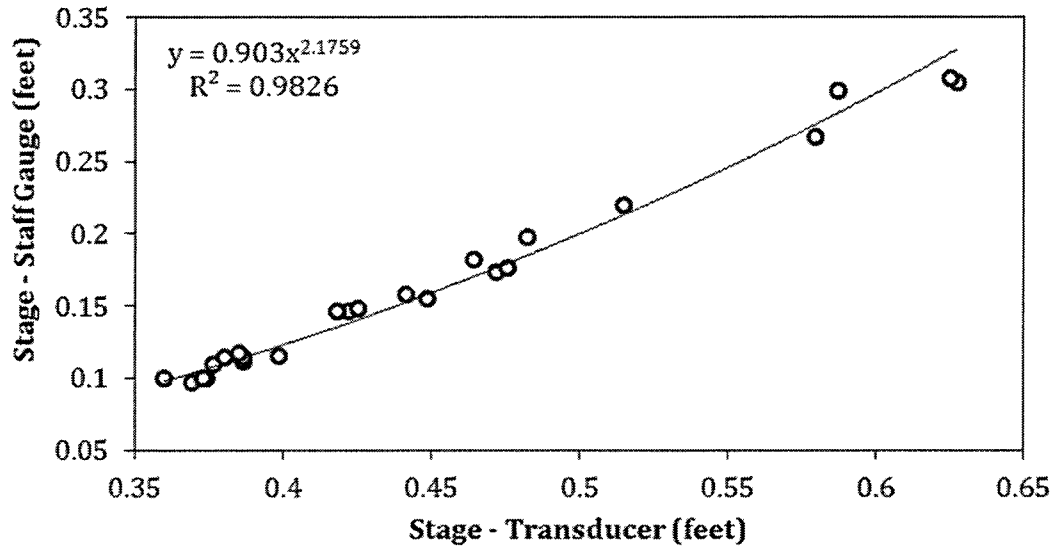
Figure 7: Corrected transducer responses with staff plate measured stage at NWSC outlet. Staff plate measurements have been corrected for non-verticality.
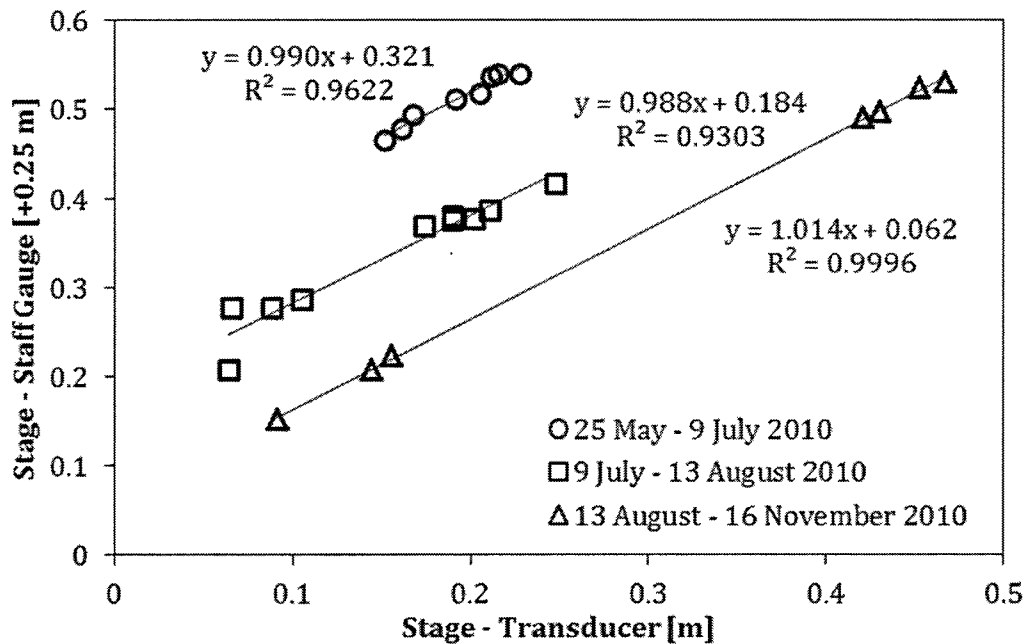
Figure 8: Corrected transducer responses with measured stage at Upper Wet Meadow outfall. Results for three different deployments of the transducer.

2.4.2 Discharge Measurements

Estimates of stream discharge throughout the NWSC were made using the equal-width cross-sectional flow velocity method [Buchanan and Somers, 1969; Dingman, 2002]. Stream velocity measurements were collected at equal or near-equal intervals at sections perpendicular to streamflow at locations in immediate proximity to stream gages at the five gaged locations (sA, sB, sC, s1, and s4). Channel width and intermediate intervals were measured using a tape measure and channel depth at each interval was measured using a US standard wading rod (measurements in feet). Average velocity at 60% of channel depth at each interval section was measured using a Marsh McBirney, Inc. Model 410B electromagnetic velocity profiler mounted on a US standard wading rod. The velocity profiler has not to date been calibrated to known fluid velocities and therefore any systematic bias in stream measured discharge is not evaluated. Manipulation of the channel cross sections was required at the beginning of the study (June 2009) at sA, sC, and s4 in attempt to create uniform flow conditions at each cross section. Manipulations included the movement of channel bed boulders upstream or downstream of the measurement section. Manipulations were again required at sC in May 2010 after spring runoff repopulated the measurement section with boulders creating highly turbulent flow paths. Measurements at sB and s1 were conducted where pond effluent was locally channelized. At sB, outflow was channelized for approximately 50-centimeters at the Meadow Lake outlet culvert (Figure 9) and periodically required adjustment of channel bed materials to allow velocity measurements. At

s1, outflow was channelized for approximately 1.5-meters immediately upstream of the Old Mountain Road crossing (Figure 10).

2.4.3 Rating Curves

Rating curves were established against stage measurements from staff gages at each of the measurement sections. Rating curves were calculated using a power function of stage [Dingman, 2002]. Figure 11 depicts rating curves for Lamprey Brook (sA), Mountain Brook (sC), the outlet of the Upper Wet Meadow (s1), and the Lamprey River at the catchment outlet (s4). Discharge measurements were not well correlated with measurements of stage at the outfall of Meadow Lake (sB) due to intermittent debris at the culvert, and no rating curve could be developed. The rating curve for Mountain Brook (sC) is limited to six measurements in the summer of 2010. This curve does not describe conditions during 2009, likely due to scour of the channel in the spring of 2010 and subsequent re-manipulation of channel bed sediments. The rating curve for the Lamprey River at the outlet of the Upper Wet Meadow was similarly limited to only six measurements due to beaver impoundments between July 2009 and March 2010 and the disconnection between the upper and Lower Wet Meadows after June 2010. The rating curve for the outflow from the Upper Wet Meadow outlet is extended below the lowest discharge measurements. A result of the geometry of the flow from the upper to Lower Wet Meadows is that velocities at the broad shallow channel became too low to quantify. In lieu of another measurement strategy, the extrapolation of rating curve is the only available means of estimating discharge at low stage. Estimates of error on the
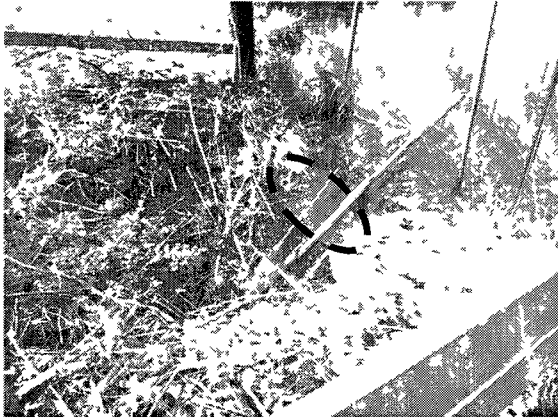
Figure 9: Outlet of Meadow Lake (sB) during episode of heavy woody debris emplacement. Measurements at ellipse.

Figure 10: Outlet of Upper Wet Meadow (s1) at crossing of Old Mountain Road. Measurements at ellipse.

rating curves include an estimate of error from reading staff measurements at s1 and s4, and the transducer error estimated from the lab calibration for the transducer installed at sC. Table 3 summarizes the coefficients for each rating curve, and the associated standard error on each coefficient. Extrapolation of rating curves above measured values was necessary for peak run-off events. It is expected that peak run-off resulted in flow retained within channels and evaluation of overbank discharge was not conducted as part of this investigation. Flow remained channelized throughout the water balance evaluation period. In applying the rating curves to estimate discharge, error associated with measuring the staff plate at sA, the transducer error at sC, and the RMSE of the regressions relating transducer to staff plate measurements (Figures 7 and 8), is propagated into the estimate of error of the discharge.

Table 3: Rating curves and estimates of error for the measured sections. Discharge is calculated from these ratings as Q =antilog($m \log(s) + b$).

Section	$m \pm SE$	$b \pm SE$	r^2	Dates
sA	5.522±0.438	1.473±0.290	0.946	7/09 – 11/10
sC	5.021±0.583	1.38±0.532	0.949	5 -11/10
s1	5.509±0.768	-0.309±0.172	0.930	6/09; 5-11/10
s4	3.931±0.111	1.050±0.087	0.991	7/09 – 11/10

2.4.4   U.S. Geological Survey Data

A continuous record of estimated discharge is maintained by the USGS at the Raymond gage (01073319) using a discharge/stage relation between a continuous log of stream stage and periodic measurements of river discharge. The record of discharge was obtained from the USGS web-site for the study period (http://waterdata.usgs.gov/nh/nwis/uv/?site_no=01073319&PARAmeter_cd=000 65,00060). The data used in this investigation did not undergo final quality control evaluation by the USGS prior to use.

2.5   Groundwater Depth

Soil and geologic conditions permitted the installation of shallow groundwater monitoring wells adjacent to four of the stream sampling locations (sC, s1, s6, and s4) and at one location adjacent to the Upper Wet Meadow. Wells were installed during June and July 2009. Locations were piloted and soil conditions observed using a stainless steel solid-stem hand auger. At stream sampling locations s2 and s3, soils were unsaturated above the refusal depth, where compact till or more likely intact bedrock was encountered. Generally soils were brown to
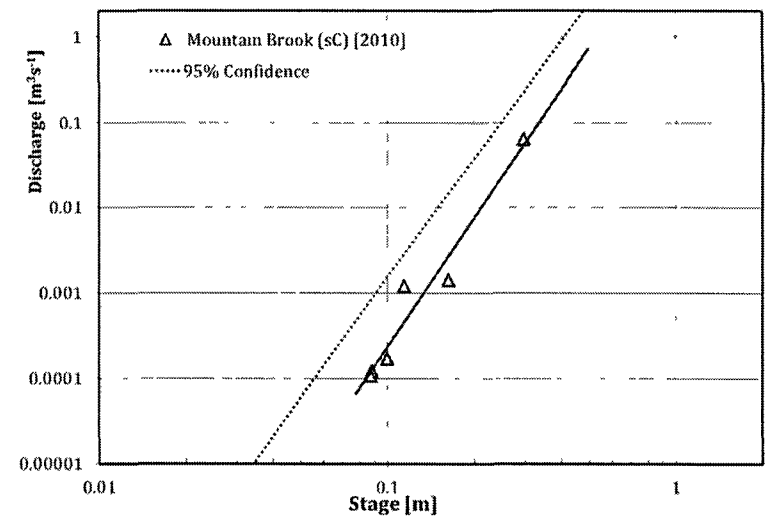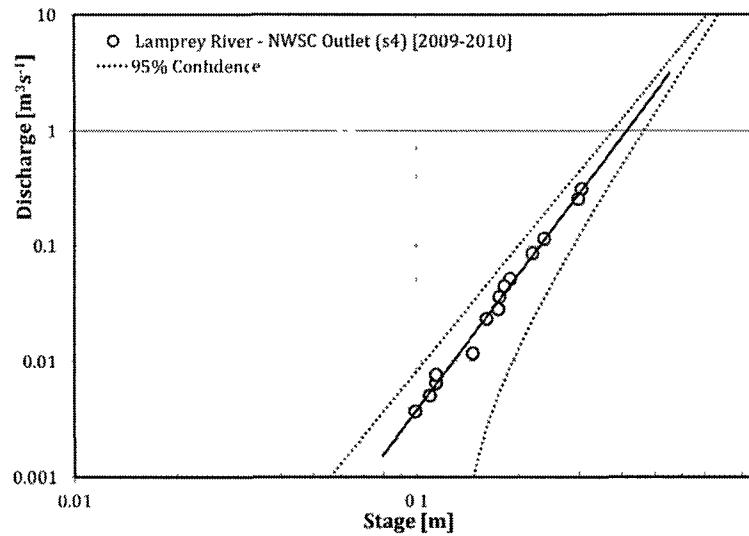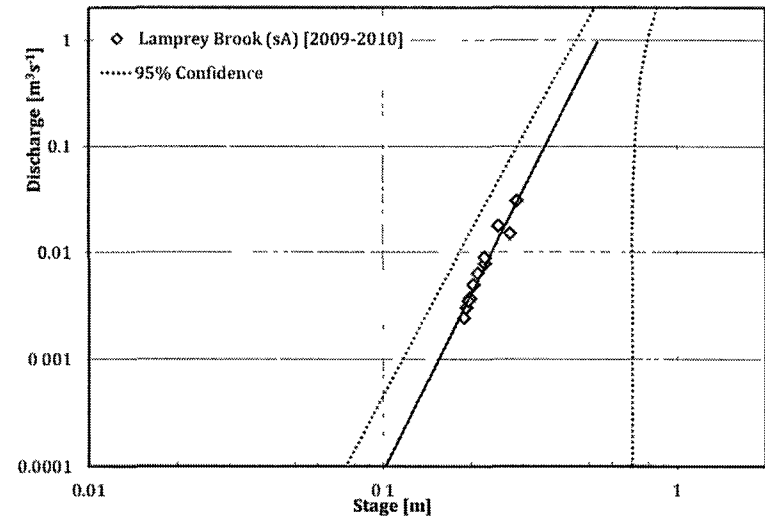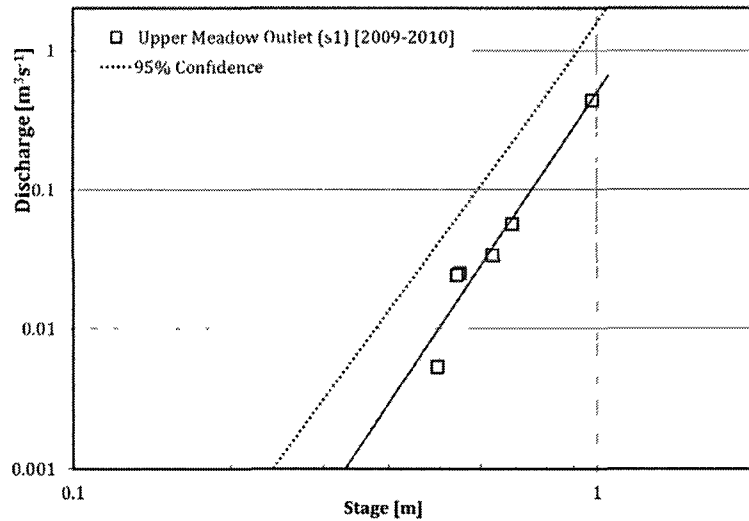
Figure 11: Stage/Discharge rating curves with 95% confidence as the dotted lines. Rating curves at sC and s1 are not resolved greater than zero at 95% confidence. Ratings are representative for the timeframes indicate on each plot.

reddish-brown sands and gravels with variable quantities of fines. Soil depths were typically less than 50 cm away several meters from the stream channels.

Monitoring wells were constructed with 32-millimeter diameter Water Source LLC stainless steel well points and 32-millimeter diameter 316 stainless steel riser pipe. Wetted bentonite chips were placed 15 centimeters around the well points to depths of about 30 centimeters to seal the wells from surface infiltration. Wells were driven by hand, and developed by alternating bailer surging and over-pumping in June and July 2009. Screen lengths ranged from 760 to 910 millimeters. Depth to water was measured with a tape measure plunker to the top of casing, and is expected to be accurate within 3 millimeters for the shallow well installations. Top of casing was periodically measured relative to the ground surface. Figure 12 depicts a sample a sample well installation (well g4-1).

Figure 12: Example monitoring well installation. Well g4-1 installed immediately downstream of the catchment outlet at s4 approximately 5-m from Lamprey River (at left). Well extends 51.51-cm above grade and extends to 137-cm below grade.

2.6   Tracer Sampling and Analysis

Stable isotopes of water are the primary tracer used in this investigation; however, dissolved silica and non-particulate organic carbon (NPOC) were sampled on select dates and used to complement findings from the isotopes.

2.6.1   Sample Collection

Samples collected for stable isotopic measurements were collected in clean and oven-dried 30 or 60 milliliter HDPE bottles, and stored at 4°C within 12 hours of collection. Field samples were collected with minimal or no headspace by overfilling and compressing the container during capping, or capping while the container was submerged. Within 7 days of collection HDPE syringes and disposable 0.45-μm polytetrafluoroethylene (PTFE) membrane syringe filters or 0.45-μm silica fiber filters housed in polycarbonate (PC) canisters were used to filter samples. Samples were then returned to 4°C storage. Filtered samples were transferred to borosilicate vials and filled to minimize, but not eliminate, headspace to reduce potential exchange of entrained atmospheric water vapor with sample water but allow water expansion without rupturing vials during sample transport.

Precipitation samples were collected directly from the collection bladder into a HDPE sample bottle. Groundwater samples were collected through HDPE and silica tubing using a field-deployable peristaltic pump [Montana Drill Pump – Woessner, 2007] after adequate well purging. The pump was laboratory calibrated to operate at pumping rates between 100 mL to 160 mL per minute. Well purging was conducted immediately prior to sampling until 3 volumes were purged, until

immediately prior to well pump out, or for 5 minutes, whichever criterion was met first. Replicate samples collected at the beginning and end of well purge activities were found to be within analytical error suggesting that 5 minutes was adequate for typical purge duration. Samples of surface water were collected by grabbing samples across representative sections of flow below the immediate water surface to minimize bias associated with a potentially enriched boundary layer.

During collection of water for analysis of dissolved silica and NPOC, similar sampling procedures were utilized. Samples were collected into acid-washed (10% hydrochloric) and oven-dried 125-mL HDPE bottles with minimal headspace. No precipitation samples were collected for dissolved silica or NPOC. Groundwater samples were collected using dedicated acid-washed tubing for each well. Quality assurance samples included field replicates and collecting laboratory deionized water (transported in acid-washed HDPE) through dedicated peristaltic pump tubing.

Samples collected during campaigns that included sampling for dissolved silica and NPOC were filtered in the field or in the laboratory typically within 24 hours (always within 30 hours) of collection. Aliquots for silica analysis were filtered using 0.45-µm PTFE disposable syringe filters into acid-washed 30-mL HDPE bottles and stored at 4°C. Aliquots for NPOC analysis were filtered using 0.45-µm silica fiber filters housed in acid washed PC canisters into acid-washed 30-mL HDPE bottles and frozen. Aliquots for analysis of stable isotopes of water during these sampling campaigns were treated as discussed above.

2.6.2 Laboratory Analysis

Stable isotopes were analyzed at the Colorado Plateau Stable Isotope Laboratory (CPSIL) at Northern Arizona University in three batches on a Los Gatos Research Liquid Water Isotope Analyzer (LGR-LWIA), which employs off-axis cavity ring-down spectroscopy to analyze isotopic ratios of hydrogen and oxygen simultaneously [Lis *et al.*, 2007]. Each batch of sample analyses contained replicate UNH Stable Isotope Laboratory internal standards, and blind duplicate samples used for quality assurance. Each batch of samples was provided with results of repeated analytical results of CPSIL internal reference standards. In addition, multiple blind duplicates or triplicates of samples were analyzed.

Analytical uncertainty at 99% confidence was determined as 2.58 times the root mean square error of three measurements: replicate measurements of laboratory internal reference standards compared to their accepted compositions (n = 192), blind duplicate analyses of the same field sample (n = 19), and measurement of field duplicate samples (n = 5). Variances of duplicate measurements were calculated from their means for both the laboratory and field duplicate treatments. Table 4 summarizes the 99% confidence interval for the three treatments. Replicate measurements of reference standards provide the best estimate of laboratory analytical uncertainty, and represent the most conservative measure of uncertainty for $\delta^{18}O$. The 99% confidence interval calculated on blind duplicates for δ^2H exceeds the laboratory replicate analysis and is therefore chosen as the conservative estimate. The 99% confidence calculated on field duplicates is less than analytical uncertainty. The analytical uncertainties for stable isotopic measurements in this

study exceed those reported by Frades [2008] ($\pm$0.240‰ for $\delta^{18}O$ and $\pm$0.587‰ for δ^2H), where different instrumentation and more replicate sample analyses were performed.

Dissolved silica and NPOC were analyzed at the University of New Hampshire Water Quality Analytical Laboratory. Silica was analyzed via automated colorimetric analysis on a SmartChem Discrete Analyzer in accordance with United States Environmental Protection Agency (U.S. EPA) 370.1 Method No. 440-100A. NPOC was analyzed by high temperature catalytic oxidation on a Shimadzu TOC 5000 in accordance with U.S. EPA 415.1. Replicate analytical uncertainty for both dissolved silica and non-particulate organic carbon were reported as 3%.

Table 4: Summary of analytical error in stable isotopic measurements at CPSIL.

Treatment	99% Confidence $\delta^{18}O$ (‰)	δ^2H (‰)	n
Replicates of Standards	**0.370**	0.874	192
Lab Duplicates	0.340	**0.933**	19
Field Duplicates	0.346	0.765	5

3. __Analysis Methodology__

Data collected from the NWSC by the methods outlined in Chapter 2 are used to determine whether riparian groundwater may be the primary generating source of baseflow, or if wetlands, specifically the Lower Wet Meadow, are an identifiable source of baseflow within the catchment. Isotopic tracers are suitably utilized to estimate the contributing fractions of sources, typically event and pre-event water during rainfall-runoff events [Sklash *et al.*, 1976, 1986; Sklash, 1990; Gibson *et al.*, 1993; Buttle, 1994; Buttle and Peters, 1997; Genereux, 1998; Weiler *et al.*, 1999; Burns *et al.*, 2001; Genereux *et al.*, 2002; Joerin *et al.*, 2002; Uhlenbrook *et al.*, 2002; Baillie, 2005; Stewart *et al.*, 2009]. The application of those methods is extended here by attempting to quantify sources of baseflow from distinct locations, which is done less frequently [Uhlenbrook *et al.*, 2002; Baillie, 2005; St. Amour *et al.*, 2005; Tetzlaff and Soulsby, 2008; Brooks *et al.*, 2009; Gonzales *et al.*, 2009]. Mixing calculations are used to estimate the proportional contribution from isotopically distinct sources, including groundwater and enriched surface water. Then, the isotopic composition of several fluxes are utilized to constrain a water balance for the Lower Wet Meadow as an example of what role specific wetlands play in maintaining baseflow.

3.1   Calculating Component Fractions

Riparian groundwater and evaporated water detained within the Lower Wet Meadow were evaluated to determine if they represented distinct isotopic compositions. After this determination, they were chosen as the distinct end-

members contributing to streamflow during periods of baseflow at the outlet of NWSC. Stable isotopes were then used to calculate the fraction of water in NWSC outflow derived from the Lower Wet Meadow.

The composition of streamflow at the outlet was estimated by assuming a binary mixture of water represented by isotopic composition of the Lower Wet Meadow and riparian groundwater, which assumes a steady flow (Section 1.1.3). The fraction of water derived from the Lower Wet Meadow (f_{lwm}) from sample results collected at time i was calculated by:

$$f_{lwm,i} = \frac{\delta_{s4,i} - \delta_{gw,i}}{\delta_{lwm,i} - \delta_{gw,i}}.$$ (3.1)

and the fraction of water derived from groundwater sources (shallow riparian or deep bedrock) were calculated as:

$$f_{gw,i} = \frac{\delta_{lwm,i} - \delta_{s4,i}}{\delta_{lwm,i} - \delta_{gw,i}}.$$ (3.2)

where, δ_x are the average isotopic compositions of the outlet (s4), shallow riparian or deep bedrock groundwater (gw), and Lower Wet Meadow (lwm) at time i [after Genereux, 1998]. Uncertainty in f_{lwm} or f_{gw} is calculated in accordance with Genereux [1998]:

$$u\{f_{lwm}\} = \left[\left(\frac{\delta_{lwm} - \delta_{s4}}{(\delta_{lwm} - \delta_{gw})^2} 2u\{\delta_{gw}\}\right)^2 + \left(\frac{\delta_{s4} - \delta_{gw}}{(\delta_{lwm} - \delta_{gw})^2} 2u\{\delta_{lwm}\}\right)^2\right.$$

$$\left. + \left(\frac{-1}{(\delta_{lwm} - \delta_{gw})^2} 2u\{\delta_{s4}\}\right)^2\right]^{\frac{1}{2}} = u\{f_{gw}\},$$

(3.3)

where $u\{\delta_{s4}\}$ is the uncertainty in the streamflow sample and is represented by the uncertainty of the analytical measurement and $u\{\delta_x\}$ represents the uncertainty of the isotopic composition estimate of the indicated reservoir. The isotopic composition uncertainties for the Lower Wet Meadow and for riparian groundwater are considered to be constant throughout the summer and are given by the combined analytical uncertainty and the mean square error of reservoir measurements. The mean square error is calculated as the square root of average variance in estimates of the mean of the reservoir r (Lower Wet Meadow or riparian groundwater) from n_s samples, on the n_t sampling dates, and is multiplied by two to yield uncertainty in the reservoir estimate at 95% confidence. The combined uncertainty for reservoir r was calculated as

$$u\{\delta_r\} = \left[\left(2 * \sqrt{\left(\frac{1}{n_t}\sum^{n_t}\left(\frac{1}{n_s}\sum^{n_s}(\delta_r - \overline{\delta_r})^2\right)\right)}\right)^2 + (u\{\delta_{an}\})^2\right]^{1/2},$$

and because the analytical uncertainty here is at a confidence of 99%, the above calculation yields a confidence of greater than 95% if the spatial variability of the reservoir is well characterized.

3.2   Volumetric Fluxes to the Lower Wet Meadow

Results of natural tracer sampling, particularly stable isotopes are used to estimate the role of groundwater discharge to the Lower Wet Meadow on the generation of surface runoff from the Lower Wet Meadow. A water balance for the Lower Wet Meadow is developed for a defined period during the summer of 2010 where fluxes into and out of the meadow reservoir are associated with estimates of their isotopic composition. Isotopic composition of the meadow (δ_{lwm}) throughout the summer is used to calibrate the mass balance. Parameters were developed to describe unconstrained aspects of the system (described below) and were varied over a range of values that in combination define plausible system states for the volumetric water balance. System states were identified that adequately describe the isotopic composition of the meadow. The mass balance was calculated on a daily timestep.

The role of groundwater inflows to the Lower Wet Meadow are investigated for system states that result in reasonable calibrations to observed isotopic composition of the reservoir (δ_{lwm}). Volumetric net inflows are reported as average rates as well as proportions of surface discharge from the meadow; however, confidence intervals are not attributed to these estimates for several reasons. The dataset used in developing the water balance does not characterize a sufficient amount of the spatial variability to result in a meaningful analysis of the error involved in component fluxes (evapotranspiration or precipitation), isotopic compositions (e.g. un-sampled surface inflow), and important variables used in estimation of fluxes or fractionation conditions (e.g. humidity and temperature).

Spatial variability is cited as being an important, yet largely neglected, source of error in lake balance studies [Winter, 1981] and in stable isotopic mass balance of lakes [Benson and White, 1994], but was beyond the scope of this study to evaluate. Furthermore, the simple single reservoir approach used in developing the analysis is poorly suited to interpreting the influence of spatial error.

Instead of reporting confidence intervals about the estimates of groundwater inflows, ranges of plausible values are presented that result from well-calibrated system states. Additionally, error associated with individual inputs to the mass balance that are well characterized are investigated for their influence on the resulting predictions to 1) provide an indication of the degree of error expected from the mass balance estimate, and 2) to investigate which data present the largest relative sources of error to the estimate. By attributing the residual of the water balance of a reservoir to a flux of interest when other fluxes are characterized as is done in this study, errors in that estimate approaching 100% can be expected [Winter, 1981]. The incorporation of stable isotopic mass balance is expected to provide additional constraint on roles of evaporation and groundwater inflows, which is expected to provide a significant improvement over an estimate relying solely on volumetric water balance.

3.2.1   Volumetric Surface Inflows and Outflows

Surface outflow from the Lower Wet Meadow was not directly measured. Reaches immediately downstream of the Lower Wet Meadow impoundment are incised in bedrock, highly turbulent, and diverge around numerous boulders within

the channel. Discharge measurements in these conditions would accordingly be unreliable. Therefore, discharge from the Lower Wet Meadow (Q_{lwm}) was estimated by multiplying the estimated fraction of wetland contribution (f_{lwm}) and discharge at s4 (Q_{s4}), the first downstream location suitable for continuous measurement as

$$Q_{lwm,i} = Q_{s4,i} \cdot f_{lwm,i} \ . \tag{3.4}$$

Surface inflows to the Lower Wet Meadow on day i include discharge from the Upper Wet Meadow measured at s1 ($I_{s1,i}$) with a drainage area of 485 ha and discharge from 248 ungauged hectares ($I_{u,i}$). Daily run-off from sC (Q_{sC}), a second order tributary to the Upper Wet Meadow, was used to estimate discharge from the ungauged area as catchment area scaled runoff calculated by:

$$I_{u,i} = A_u \cdot \frac{Q_{sC}}{A_{sC}} \ , \tag{3.5}$$

where A_u and A_{sC} are the total area of ungauged catchments and the area of the Mountain Brook catchment upstream of sC, respectively.

3.2.2   Volumetric Evapotranspiration Fluxes

Lake evaporation and emergent vegetative transpiration were calculated using the Kohler-Parmele adaptation of the Penman combination equation (KP-PCE) and Penman-Monteith equation (PMCE), respectively (equations 2.1 and 2.2). In the water balance analysis, channel areas experience fractionating open-water evaporation described by the KP-PCE, and the meadow areas experience a combination of open-water evaporation and non-fractionating vegetative

transpiration. Grasses and vegetation in the meadow areas remove water from the reservoir by transpiration, considered not to impart any fractionation to the reservoir, but reduces the potential for lake evaporation by shading the water surface between emergent stems. In the water balance calculation the daily flux of E_L and E_T in meadow areas is partitioned by a fraction of open water (f_w) that lumps the effect on the water balance from transpiration and the reduction in area available for lake evaporation. Because the evaluation period is limited to a mid-summer time period when vegetation appeared to exhibit little additional growth, and when the stage of the meadow only dropped approximately 25 cm with no appreciable changes in the saturated meadow area, the value of f_w is considered constant throughout. The meadow is considered to be covered in greater than 50% plants based on the classification of the Lower Wet Meadow as "dominated by vegetation cover" [Tiner, 2010]. The fractionating lake evaporation flux ($E_{lwm,i}$), and non-fractionating transpiration flux ($T_{lwm,i}$) from the meadow surface for day i are calculated as:

$$E_{lwm,i}[m^3 d^{-1}] = (A_C + f_w \cdot A_M)e_{L,i} \text{ , and} \tag{3.6}$$

$$T_{lwm,i}[m^3 d^{-1}] = (1 - f_w) \cdot A_M \cdot e_{T,i} \text{ ,} \tag{3.7}$$

where A_C and A_M are the areas of the channels and meadows respectively traced from orthoimagery and $e_{L,i}$ and $e_{T,i}$ are the sum of hourly lake evaporation and transpiration rates on day i. Considering the observation that vegetation appeared to have exhibited little additional growth during the evaluation period, parameters describing transpiration rates including the leaf conductance, leaf area index, and

the sheltering factor were assumed constant over the evaluation period. Values appropriate for well watered grasses or crops were assigned [from Dingman, 2002]. A result of this approach is that the total evapotranspiration flux from the Lower Wet Meadow is less than would be estimated for a completely open comparably sized water body. There is considerable debate as to whether this is an accurate representation of the effects of wetland vegetation on the evapotranspiration flux [Mitsch and Gosselink, 2000; Goulden *et al.*, 2007].

The partitioning treatment is simplistic, but similar to an approach employed by Wessel and Rouse [1994] who described the evapotranspiration from boreal wetlands by partitioning the flux between vegetation, bare soil, and open water. No bare soil contributions were included in this approach because of negligible coverage. The method is also to that of Wessel and Rouse [1994] in that the evaporative flux from the canopy was scaled by an assumed LAI of 3. The LAI was not used in developing the big leaf approximation from the stomatal conductance functions of Stewart [1988]. The way in which net radiation is treated between coverages, where albedo and emissivity are dependent on the cover, is expected to be similar to the method of Wessel and Rouse [1994] though their details were not provided. The method differs from that of Shuttleworth and Wallace [1985] who calculated the extinction of radiation through a canopy by Beer's Law to estimate the energy budget at the soil surface; their method was not formulated to predict evaporation from an open-water surface but could be adapted to do so.

3.2.3 Volumetric Precipitation Flux

The open water fraction (f_w) is also used to estimate the direct precipitation flux to the wet meadow. Gross precipitation rate is introduced across the area of the channel and the open-water fraction of the meadow, whereas the fraction of the meadow occupied by vegetation ($1-f_w$) experiences throughfall that undergoes interception modeled using the adaptation of the Liu model [1997 and 2001] discussed in Section 2.3.4. The total daily precipitation flux ($P_{lwm,i}$) to the Lower Wet Meadow is calculated as the sum of the direct precipitation flux ($D_{lwm,i}$) and throughfall flux ($Tf_{lwm,i}$). $D_{lwm,i}$ and $Tf_{lwm,i}$ are calculated similarly to the evaporation and transpiration fluxes:

$$D_{lwm,i}[m^3 d^{-1}] = (A_C + f_w \cdot A_M)p_i \text{, and} \tag{3.8}$$

$$Tf_{lwm,i}[m^3 d^{-1}] = (1 - f_w) \cdot A_M \cdot p_{tf,i} \text{, with} \tag{3.9}$$

$$P_{lwm,i}[m^3 d^{-1}] = Tf_{lwm,i} + D_{lwm,i} \text{,} \tag{3.10}$$

where here, p_i and $p_{tf,i}$ are the sum of hourly gross precipitation and throughfall rates on day i. Note that the f_w is defined separately from the gap fraction (g) used in the Liu interception model which is assigned a value of 0.45.

3.2.4 Volumetric Groundwater Inflows and Outflows

Groundwater (gw) exchange with the Lower Wet Meadow was the primary unknown term in the water balance and the daily net flux was determined as the residual (R_i). To attribute the daily net residual with the appropriate isotopic flux, the residual was distinguished between a net input or net output on a given day, or:

$$I_{gw,i} = \begin{cases} I_{gw,i} = -R_i & \text{For } R_i \leq 0 \\ I_{gw,i} = 0 & \text{For } R_i > 0 \end{cases}, \quad \text{and} \tag{3.11}$$

$$Q_{gw,i} = \begin{cases} Q_{gw,i} = 0 & \text{For } R_i < 0 \\ Q_{gw,i} = R_i & \text{For } R_i \geq 0 \end{cases}, \tag{3.12}$$

where $I_{gw,I}$ is the net groundwater inflow on day i, and $Q_{gw,I}$ is the net groundwater

outflow on day i.

3.2.5   Lower Wet Meadow Storage

As described in Chapter 1, the Lower Wet Meadow consists of saturated

hummocky grass and shrub meadow areas and a defined channel approximately 1.5

to 2 meters deep. The bathymetry of the meadow and channel, and the proportion

of the meadow occupied by hummocks has not been surveyed rigorously. However,

the area of the channel and meadow were accurately determined from 0.3-meter

resolution aerial imagery flown in 2005 [N.H. Department of Transportation, 2007].

Stage was measured at s3 in a stilling well set immediately adjacent to the channel

in an abnormally deep portion of the meadow. Water column height at this portion

of the meadow ranged from 0.8- to 1.2-meters throughout the evaluation period.

Two specific yield parameters describe the volumetric storage of the

vegetated areas of the Lower Wet Meadow. The shallow specific yield (S_{Ms})

represents the change in water volume stored within the vegetated areas for a given

change in stage and is defined with regard to units of area $\left(\frac{m^2}{m^2}\right)$. The shallow

specific yield is bounded by low values of the drainable porosity of fibric materials

and sediments deposited on the meadow surface, which were assigned to be

consistent with values presented by Boelter [1968], Letts and others [2000] and Sumner [2007]. Specific yield values for surface flow wetlands are typically assumed to be at unity or near unity, with a few percentage of the area occupied by vegetation stems [Sumner, 2007]. The Lower Wet Meadow is considered to have microtopographic variations from larger hummocks and areas of higher vegetated ground which may reduce values considerably from unity [Sumner, 2007]. Therefore, a sensitivity analysis was conducted that varied the values of this parameter from a lower bound of 0.6 to 1. A deeper specific yield (S_{Md}) represents meadow sediment yield and accounts for microtopographic hollows. The parameter is used to estimate the total volume of water stored within the reservoir, which is assumed to be well mixed, and is used in the predictions of the isotopic composition of the reservoir. Appropriate values were taken from Boelter [1968], which range from 0.15 to 0.45. A median value of 0.25 is often assumed [Letts *et al.*, 2000].

An effective water column height (d_e) equal to the average meadow bed surface elevation defines the portions of the water column at which the yield parameters operate. The effective water column height that defines the transition between S_{Ms} near the surface and S_{Md} below is chosen as 0.7 meters above the meadow bed surface at the stilling well (s3). Over the evaluation period, the total saturated area of the meadow appeared to be fairly constant for the change in depth of 25 cm. The effective water column height was chosen as below the lowest measured stage during the evaluation period.

The total volume of water in the Lower Wet Meadow reservoir on day *i* ($V_{lwm,i}$) is calculated as:

$$V_{lwm,i}[m^3] = s_{lwm,i} \cdot A_C + d_e \cdot S_{Md} \cdot A_M + (s_{lwm,i} - d_e) \cdot S_{Ms} \cdot A_M , \tag{3.13}$$

where $s_{lwm,I}$ is the average daily water column height recorded as stage at s3. In contrast the change in volume introduced or discharged from the Lower Wet Meadow on day I $(dV_{lwm,I} / dt)$ is calculated as:

$$\frac{dV_{lwm,i}}{dt}[m^3 d^{-1}] = (s_{lwm,i} - s_{lwm,i-1}) \cdot A_C + (s_{lwm,i} - s_{lwm,i-1}) \cdot S_{Ms} \cdot A_M , \tag{3.14}$$

and is used to estimate the residual to the water balance assigned to the net groundwater flux on day i.

3.2.6 Lower Wet Meadow Water Balance

The water balance for a surface reservoir is discussed generally in §1.1.2. The water balance for the Lower Wet Meadow on day i $\left(\frac{\Delta V_{s3}}{\Delta t}\right)_i$ is calculated on a daily timestep from a form of equation (1.1) that includes the fluxes considered relevant to the conceptualization of the system:

$$\left(\frac{\Delta V_{s3}}{\Delta t}\right)_i = \Sigma I_i - \Sigma Q_i \pm R_i \tag{3.15}$$

where,

$$\Sigma I_i = I_{s1,i} + I_{u,i} + P_{lwm,i} + I_{gw,i} , \text{and} \tag{3.16}$$

$$\Sigma Q_i = f_{lwm,i} \cdot Q_{s4,i} - E_{lwm,i} - T_{lwm,i} - Q_{gw,i}. \tag{3.17}$$

From the definition of the riparian groundwater terms (section 3.2.4) the residual (R_i) in equation (3.13) is 0; however is retained in the above definition for completeness.

3.3   Isotopic Composition of Hydrologic Fluxes

The hydrologic fluxes discussed in section 3.2 were attributed representative isotopic compositions. For measureable water (i.e. streamflow, groundwater, and precipitation) these fluxes were characterized by sample results as discussed in the following sections. Consistent and linear changes in isotopic composition of riparian groundwater and streamflow entering the wet meadow throughout the evaluation period were exploited so that estimates of daily isotopic composition associated with individual fluxes could be included in the mass balance.

3.3.1   Isotopic Composition of Surface Inflows

Daily isotopic composition (in δ-values) of inflow to the Lower Wet Meadow from the upstream outfall of the Upper Wet Meadow at s1 ($\delta_{s1,i}$) was estimated from regression of isotopic composition measured throughout the summer versus day of the year. Surface water input associated with the ungauged portion of the catchment was estimated from a regression of the isotopic composition of the four first- or second-order streams draining to the wet meadows (sA, sB, sC, and s6). δ-values were regressed against day of the year to yield daily estimates for the isotopic composition of the ungauged portion of the catchment.

3.3.2 Isotopic Effects of Evaporation Flux

The analytical approach of Gonfiantini [1986] (equation 1.28) accounts for the evaporative fractionation and the flux of isotopes leaving the reservoir. The solution requires an estimate of the isotopic composition of atmospheric water vapor (δ_A) to which the reservoir is evaporating. A typical assumption in stable isotope hydrology is that isotopic composition atmospheric water vapor (δ_A) is in equilibrium with the composition of average precipitation composition (δ_P) over a time period of investigation (e.g., annual, seasonal, monthly), which has been shown to be valid in New England during precipitation events [Lee *et al.*, 2006]:

$$\delta_A \cong \delta_{V,*} = \frac{\delta_P}{\alpha_{V/L}}, \tag{3.18}$$

where $\delta_{V,*}$ is the composition of water vapor in equilibrium with measured precipitation of composition δ_P and $\alpha_{V/L}$ is the equilibrium fractionation factor discussed in § 1.3.4. Between precipitation events, this approximation is expected to misrepresent atmospheric composition, as evaporative fluxes from terrestrial waterbodies will provide a volume of water vapor from upwind and nearby areas that is difficult to quantify.

Several investigators have compared and regressed measurements of the isotopic composition of atmospheric water vapor with other meteorological measurements including precipitation equilibrated moisture ($\delta_{V,*}$), and two measures of humidity [White and Gedzelman, 1984; Jacob and Sonntag, 1991; Lee *et al.*, 2005; Lee *et al.*, 2006]. These regressions capture broad-scale variation within

the climatic system that may be applicable over long timescales though they may fail to represent short-term fluctuations due to the movement and histories of individual weather systems. These estimates are expected to improve upon any assumptions of complete equilibrium with average precipitation. Formulas used to estimate the isotopic compositions of atmospheric water vapor are summarized in Table 5 below.

The two measures of humidity used in regressions include the molar mixing ratio (w [mmol mol^{-1}]) and specific humidity (h_s [g kg^{-1}]) and are calculated by [Dingman, 2002]:

$$w_i = \frac{e_{a,i}}{P_{a,i}} * 1000 \text{ , and} \tag{3.19}$$

$$h_{s,i} = 0.622 \, w_i \text{ .} \tag{3.20}$$

The estimation of the isotopic composition of the evaporating reservoir is also dependent on the estimated temperature of the evaporating surface ($T_{s,i}$) and the surface temperature normalized relative humidity ($h_{N,i}$) to calculate values of $\alpha_{V/L}$ and ε_K. The parameters on which the solution for the fractionating evaporation is dependent, namely $T_{s,i}$, $h_{N,i}$, $\delta_{V,*}$, w, and h_s (the latter three are precedents to estimates of δ_A) are calculated as cumulative open-water evaporation flux-weighted averages for the period of evaluation [Gonfiantini, 1986; Horita et al., 2008] by:

$$N_i = \sum_{j=a}^{i}\left(\sum_{k=0}^{23} N_k \mathrm{e}_k\right)_j \bigg/ \sum_{j=a}^{i}\left(\sum_{k=0}^{23} \mathrm{e}_k\right)_j. \qquad (3.21)$$

where N_i is the cumulative flux weighted average of parameter N (e.g. T_s, h_N, $\delta_{V,*}$, w, and h_s) on day i, e_k is the open-water evaporation rate for hour k of day j of the evaluation period. The beginning of the evaluation period is identified by day a, and the averaging is conducted from the beginning of the evaluation period to day i.

3.3.3 Isotopic Composition of the Precipitation Flux

Precipitation samples were collected continuously throughout the summer in expandable bladders (Section 2.3.1). All precipitation collected between sample dates was assigned the measured composition, therefore the isotopic composition of precipitation introduced to the Lower Wet Meadow water balance was constant between sampling dates. The isotopic composition of throughfall was also assigned the measured value of precipitation (i.e. evaporative enrichment of temporarily intercepted water was neglected).

Table 5: Regressions used to estimate atmospheric isotopic composition. Composition of water vapor compared to meteorological parameters or isotopic composition to precipitation equilibrated atmospheric moisture. Measurements are hourly average values except in White and Gedzelman (1984) where they are four hour averages.

Relation	R^2	Study Location	Source
$\delta_V{}^2H = 3.6\,h_S - 141\ ‰$	0.84	Palisades, New York	White and Gedzelman (1984)
$\delta_V{}^{18}O = 1.11\,\delta^{18}O_{V,*} + 1.56\ ‰$	0.84	Heidelberg, Germany	Jacob and Sonntag (1991)
$\delta_V{}^2H = 1.0\,\delta^2H_{V,*} + 2.0\ ‰$	0.89	Heidelberg, Germany	Jacob and Sonntag (1991)
$\delta_V{}^{18}O = 0.467w - 24.3\ ‰$	--	Logan, Utah	Lee and others (2005)
$\delta_V{}^{18}O = 1.20\,\delta^{18}O_{V,*} + 1.41\ ‰$	0.64	New Haven, Connecticut	Lee and others (2006)
$\delta_V{}^{18}O = -35.02 + \ln(w)\ ‰$	0.78	New Haven, Connecticut	Lee and others (2006)

3.3.4 Groundwater Inflows

Net groundwater inflows ($I_{gw,i}$) calculated from positive residuals of the water balance are attributed two sources of groundwater. The mass balance was calculated separately assuming that all groundwater inflows were attributed the isotopic composition of riparian groundwater measured as part of this study and assuming that all groundwater inflows were attributed the isotopic composition of bedrock groundwater reported by Frades [2008] and Frades and others [In Prep]. The daily composition of riparian groundwater was estimated from a regression of sample results from four wells (gD-1, g6-1, g4-1, and g4-3). The daily composition of deep bedrock groundwater was considered constant. No mixing of groundwater sources was considered; the implications of this will be discussed later. Net groundwater outflows on day i, calculated from negative residuals of the water balance, result in a reduction of lake volume available for mixing with inputs on day i, or damping the effects of evaporative fractionation on day i, but are not directly attributed an isotopic composition.

3.3.5 Lower Wet Meadow Storage

Isotopic composition of the meadow water was measured at s2 and s3, and is evaluated by the Gonfiantini [1986] model of isotopic fractionation discussed below. Measurements at the two locations are considered to represent the isotopic composition of the assumed well mixed reservoir δ_R.

3.4 Estimating the Isotopic Fractionation

The analytical solution presented by Gonfiantini [1986] was implemented to predict the isotopic composition of the Lower Wet Meadow reservoir from estimated water balance flux terms and representative compositions or fractionating effects of the evaporation flux. Predicted compositions for both $\delta_R{}^2H$, and $\delta_R{}^{18}O$ were compared to samples collected on 8 and 27 July, 3 and 20 August collected at the Lower Wet Meadow.

Calibration of the mass balance estimate was needed to match observations. The parameters characterizing the yield (S_M) and the fraction of open water (F_w) of meadow portions of the reservoir were varied across a wide range of values, as these values are not constrained by field measurements. S_M was the critical parameter influencing the role of the groundwater in the mass balance. Calibration of conditions describing the evaporation was performed by varying four input measurements of hourly meteorological data forcing the KP-PCE and PCME $(v_a, K_{in}, T_a,$ and $e_a)$ by less than 10%. Sensitivity of the variation of the parameter values on the KP-PCE estimates is discussed in Section 4.1.3, and the calibration results to the isotopic mass balance model are discussed in Section 4.3.1.

3.4.1 Gonfiantini Solution

The analytical formulation for the isotopic composition of the reservoir water presented by Gonfiantini [1986] (equation 1.28) is evaluated using cumulative volumes of all fractionating and non-fractionating fluxes. The terms x and y which represent the ratios of the average rates of fractionating evaporation to

inflow (E/I) and average rates of non-fractionating outflows to inflow (Q/I). The values x and y are estimated for each day i as the ratios of the total cumulative volumes of each flux during the evaluation period starting on day $i = 0$ (d= 179, 29 June, 2010). Groundwater inflows and outflows from the residual of the water balance are included in the calculation of x and y. Furthermore, the parameters that describe the evaporative fractionation, namely the temperature dependent equilibrium enrichment factor (ε^*), the humidity dependent kinetic enrichment factor (ε_K), the surface normalized humidity (h_N), and the isotopic composition of atmospheric vapor (δ_A^2H and $\delta_A^{18}O$) are cumulatively weighted in proportion to the evaporative flux throughout the evaluation period in accordance with equation (3.19).

3.4.2 Model Performance

Prediction quality was assessed using the Nash-Sutcliffe efficiency (NSE) to describe the model's ability to predict δ_R^2H and $\delta_R^{18}O$ compositions for the average of s2 and s3 on four sampling dates. The NSE is given by:

$$NSE = 1 - \frac{\Sigma(\delta_{obs} - \delta_{calc})^2}{\Sigma(\delta_{obs} - \overline{\delta_{obs}})^2},$$

(3.22)

and expresses the efficiency to which the model predicts observations better than the mean of the observations [Moriasi *et al.*, 2007, Nash and Sutcliffe, 1970]. An efficiency of unity signifies a perfectly efficient model, and large negative numbers indicate that the mean of the observations are a better predictor of individual observations than the model [Moriasi *et al.*, 2007].

4.   Results and Analysis

Meteorological conditions during the summer of 2010 were ideal to investigate the contribution of wetlands and areas of surface detention to summer baseflow in the Lamprey River. Moderate to below normal precipitation resulted in runoff predominately supported by baseflow permitting weekly sampling events of baseflow conditions for eight weeks. This chapter presents results of the evaluation of hydrologic fluxes and meteorologic conditions throughout the NWSC, as well as the characterization of the evaporating surface of the wet meadows during the summer of 2010. Subsequently, results from isotopic tracer analyses are presented to assess whether riparian groundwater was similar in composition to streamflow, and whether wetlands or other ponds are likely sources of streamflow throughout the headwater catchment. The final portion of the chapter then focuses on results of the isotopic mass balance of the Lower Wet Meadow and the sensitivity of parameters used in the calculation.

4.1   Hydrologic Fluxes and Meteorologic Conditions

Hourly estimates of discharge, stage, groundwater depth, and precipitation are presented in Figure 13 for the study period. Runoff from each catchment and the backwards difference derivative of runoff from three catchments with continuous records of discharge are presented in Figures 14 and 15, respectively. Hourly estimates of several meteorological parameters and estimates of the evapotranpiration fluxes are presented for the study period in Figure 16.

4.1.1 Observed Streamflow and Error

Figure 13 presents hourly discharge for sC, s1, s4 and point estimates of discharge at sA with hourly total precipitation for the period between 25 May and 26 August 2010 with 95% confidence intervals. Lower confidence intervals were positive only for sA and s4 during higher flow in June and late August, and are not shown on Figure 13 to enhance readability; the lower confidence level for the remainder of discharge measured was not greater than zero flow. These estimates of error include error associated with the respective rating curve (all points), error associated with the transducer measurement (sC), and error associated with the regressions relating transducer measurements to staff plate measurements facilitating extension of the rating curve to measurements collected prior to May 2010 (s1 and s4). The hydrographs represent flow conditions throughout the majority of baseflow tracer sampling.

Estimated discharge at the catchment outlet was consistently greater than at other locations throughout the catchment as expected, except at the onset of heavy precipitation on 25 August when discharge at Mountain Brook momentarily exceeded discharge at other locations within the catchment. Recession is apparent throughout the catchment throughout June, until July when a series of small storms resulted in apparent event flow at the outlet of the Upper Wet Meadow, Mountain Brook, and U.S. Geological Survey gage 01073319 in Raymond. A much subdued or negligible response is apparent at the catchment outlet (s4) or stage within the wet meadow. Towards the end of July recession continued throughout the catchment with event flow apparent on 10 August in the NWSC. Several days prior (7-8

August) event flow is suggested at Mountain Brook and the Upper Wet Meadow; however, no precipitation was recorded and only subtle evidence of a response was observed in the Lower Wet Meadow or the catchment outlet. A distinct response at the U.S. Geological Survey around this time is also observed, and is considered to be the result of rainfall in a different portion of the catchment or due to a managed reservoir release. Discharge and stage throughout the watershed responded to a 75-mm storm on 25 and 26 August.

Catchment-area normalized runoff varies throughout the catchments and may result from wetland drainage. Table 6 presents several measures of wetland and waterbody area as fractions of catchment area, and stream length distances within wetlands or waterbodies. Wetland area fractions, and stream length through wetlands are consistent at the Upper Wet Meadow, the catchment upstream of the Lower Wet Meadow outlet, and the catchment outlet. The wetland area fraction for the Mountain Brook catchment is greater than the wetland area fraction for Lamprey Brook; however, the wetland stream length fraction is greater in Lamprey Brook than elsewhere throughout the NWSC. Figure 14 shows daily area-average runoff for the four measured catchments. Lamprey Brook maintains the highest average runoff throughout the summer; whereas, Mountain Brook maintains the lowest average runoff through much of the summer. The relative wetland stream length fractions throughout the subcatchments appear to distinguish the relative magnitude of the average runoff between sA and sC; sA exhibits greater runoff and stream-length fraction in wetlands, sC the least. Downstream locations at s1 and s4 exhibit intermediate run-off and wetland stream length fraction comparable to sA.
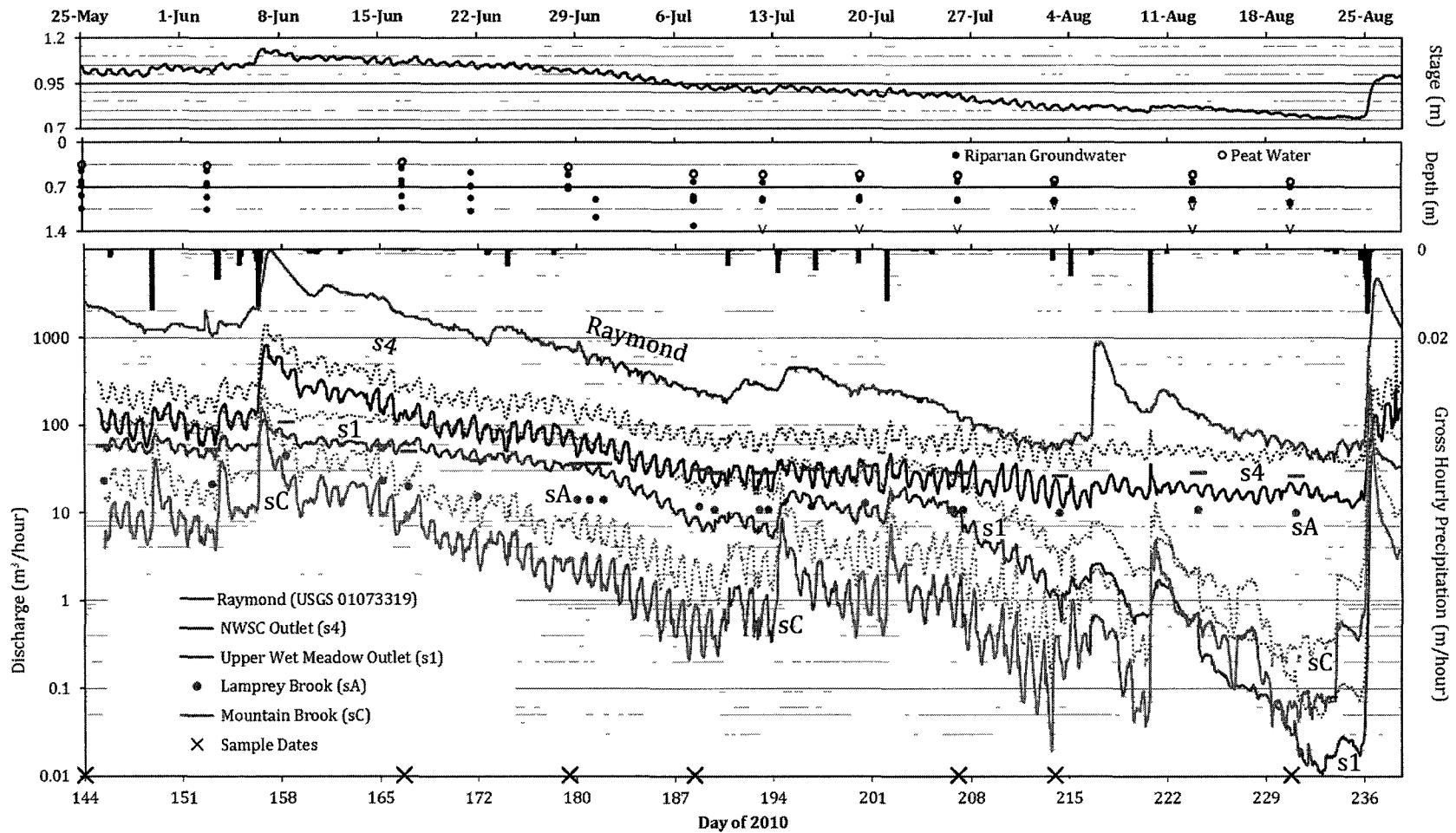
Figure 13: Stage at the lower wet meadow, groundwater depth throughout the NWSC, and hourly discharge hydrographs of the Lamprey River at Raymond and four stream sections within the NWSC. Gross precipitation hyetograph along the top axis of hydrographs. Isotope sampling events are indicated on the bottom axis. Dotted lines (for s4, s1, and sC) and horizontal bars above circles (for sA) indicate 95% confidence intervals on discharge and are not resolved above zero for the majority of the study period. Downward arrows (v) indicate depth of dry monitoring wells.

Table 6: Wetland and waterbody coverage in subcatchments of the NWSC. Coverages expressed as fractional areas and fractional stream course lengths within each subcatchment. Catchment statistics for s3 represent the outlet of the Lower Wet Meadow and are not distinguished separately for s2.

Sampling Station ID	Catchment Area	Wetland (NWI) Area	Waterbody (NHD) Area	Stream Length	Wetland (NWI) Length*	Waterbody (NHD) Length*
Units	km²	% of Catchment Area		km	% of Stream Length	
sA	1.0	7%	3%	1.3	60%	31%
sB	1.1	12%	7%	1.0	75%	55%
sC	1.5	8%	4%	2.1	38%	15%
s1	4.8	11%	6%	6.3	65%	40%
s3	7.3	11%	6%	9.4	63%	42%
s4	7.4	11%	6%	9.8	60%	40%
s6	0.12	0.03%	0%	~0.0	~0%	0%

* - Stream courses are derived from the 5-meter resampled NHGS DEM. Streams through horizontal wetlands and waterbodies are estimated as straight line paths from the inlet to the outlet and not through defined channels when present. Stream courses were not derived for the s6 catchment; the first surface flow within the catchment was sampled.

From Figures 13 and 14, the baseflow recession at Mountain Brook (sC) and the outlet of the Upper Wet Meadow (s1) appear markedly different from the recession observed on Lamprey Brook (sA) or at the NWSC outlet (s4). Inflections in the recession curves occur around 29 June, 27 July, and immediately after a precipitation event on 10 August. After these points, the recession rate appears to increase; however, these inflections are not as clear on a plot of the derivative of runoff over time. Figure 15 presents the backward difference derivative of runoff

versus time for the three stream sections with continuous records of discharge. Apparent from Figure 15, no subcatchment is consistently exhibiting greater or lower recession rates, therefore it does not appear that either the Lower Wet Meadow between s1 and s4, or differences in the wetland or waterbodies cover throughout the catchments are influencing the rates of recession.
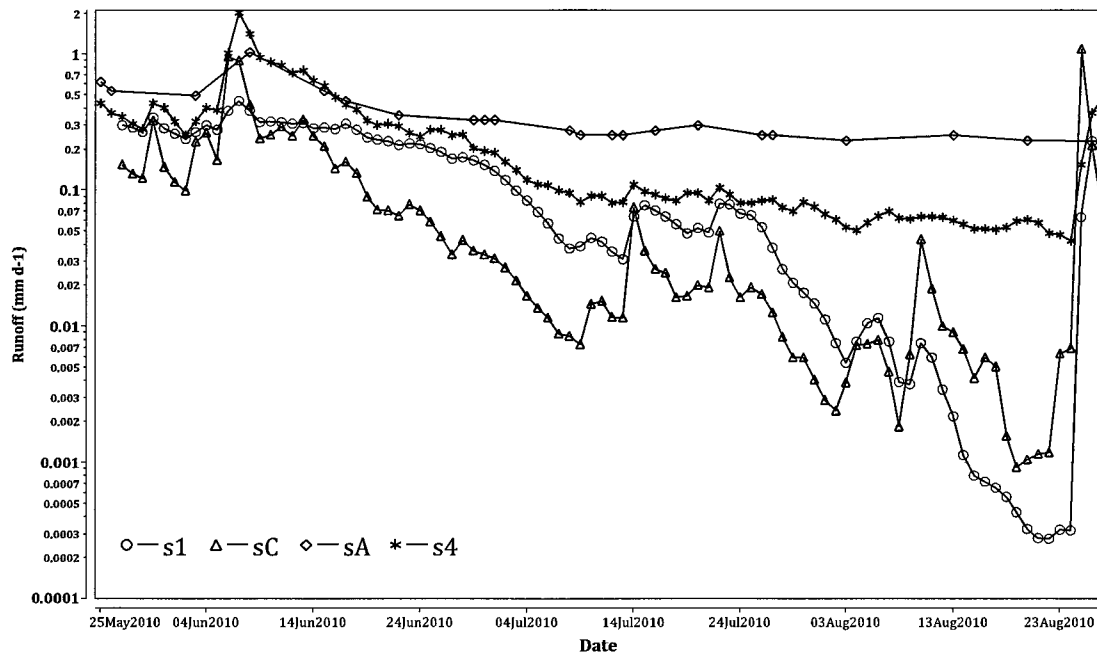
Figure 14: Daily area-average runoff for four subcatchments.

Generally, storm flow response at the catchment outlet (s4) associated with precipitation events (e.g. days 173, 190, 193, 197, 201, 215) appears dampened compared to upstream hourly discharge measurements (Figures 13 and 14). The upstream sampling points at Mountain Brook (sC) and the Upper Wet Meadow outlet (s1) exhibit a flashier response to rainfall events. Figure 15 shows the change in daily-average runoff for small storm events in mid- and late-July and again in mid-

August is smaller at the catchment outlet than for the other sub-catchments. The Lower Wet Meadow in particular appears to be dampening the effect of runoff observed at the Upper Wet Meadow and Mountain Brook; few of these events result in appreciable inflections in the steadily decreasing daily-average stage of the Lower Wet Meadow (Figure 13). The absence of inflections in stage in the Lower Wet Meadow propagate downstream as dampened storm responses at the catchment outlet. Low wetland coverage and distal downstream proximity from wetlands at the gauging point at sC correlates with a flashy response, but high wetland coverage and response from the outfall of the Upper Wet Meadow results in an intermediate flashiness in run-off response compared with Mountain Brook and the downstream response at the catchment outlet (Figure 15). Therefore, wetland coverage or proximity to wetland systems alone doesn't appear to correlate with the dampening of storm-events observed, which suggests that either wetlands or waterbodies are not primarily responsible for controlling the observed dampening effects or the Lower Wet Meadow specifically is controlling the dampening observed at the catchment outlet.

The dampening of the storm response is likely the result of storage within the meadow system and subsequent increased evapotranspiration within the meadow than throughout the surrounding catchments. The mechanism is likely also responsible for lower observed runoff after 8 August, and consistently lower discharge after 14 August at the outfall of the Upper Wet Meadow than Mountain Brook. Continued inflows from Lamprey Brook and Mountain Brook to the Upper Wet Meadow are easily accommodated by relatively minor changes in stage and

continued evapotranspiration from the meadow surface. From mid- to late-August,

the Upper Wet Meadow was acting as an evapotranspirative sink to streamflow

from Lamprey and Mountain Brooks.
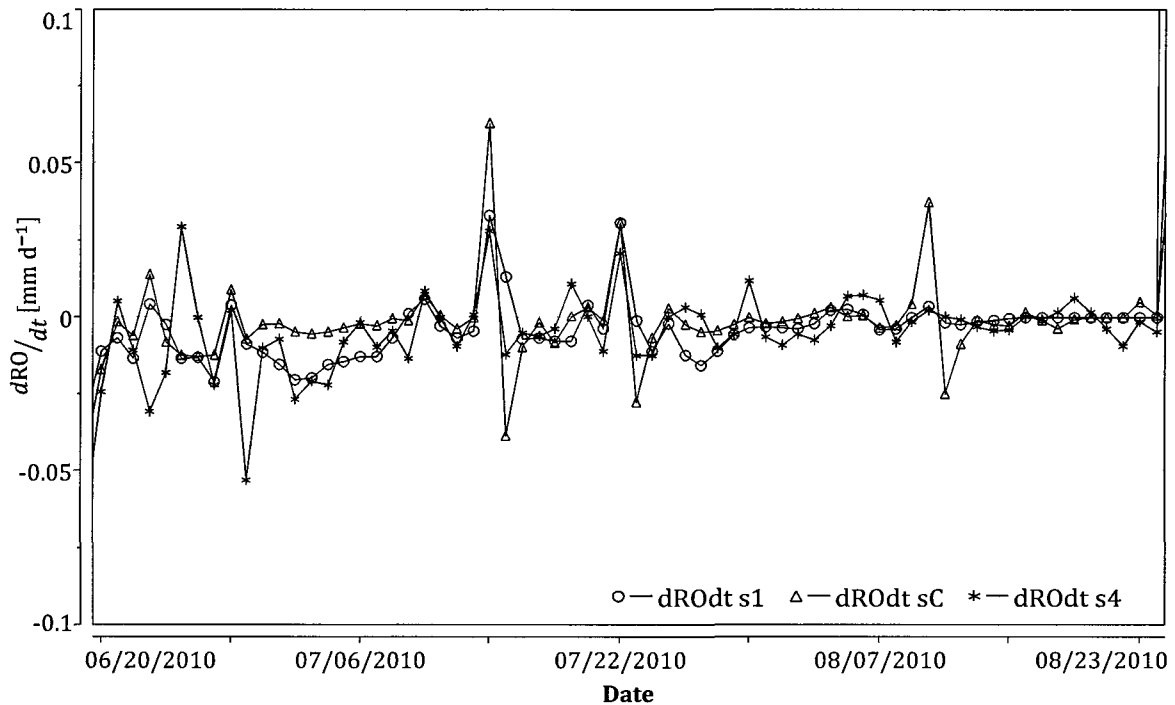
Figure 15: Backwards difference derivative in daily runoff. Change in runoff with respect to time is calculated for the three stream with continuous discharge records. Scale is isolated to |0.1 mm d⁻¹| to facilitate inspection of recession period from 20 June through 24 August. Derivative values before and after this period greatly exceed |0.1 mm d⁻¹|.

Diel fluctuations (Figure 13) that reflect the daily evapotranspiration are

observed at the continuously gaged points within the catchment. Fluctuations in

stage with amplitudes of about 5 cm are observed at the Lower Wet Meadow.

Fluctuations in the expected discharge at the catchment outlet are on the order of

about 20 m³ h⁻¹ throughout each day. Diel fluctuations are observed at the outlet of

Mountain Brook and are in sync with those observed within the wet meadows and

at the outlet suggesting a response to an evapotranspiration flux. Throughout late

June and early July, as well as periods near the beginning and middle of August, diel fluctuations are observed at the outlet of the headwaters Lamprey River at U.S. Geological Survey gage 01073319.

4.1.2   Observed Groundwater Depth

Groundwater surface elevations throughout the catchment were observed to decline throughout the summer, depicted as the central scatterplot in Figure 13. Water was measured during every gauging event in three wells (gC-1, g4-1, and g4-3). Groundwater in the vicinity of wells gD-1 and g6-1 receded below the bottom of the monitoring points by 13 July and 3 August, respectively, and the respective depths of the wells are indicated by the symbol (v) on Figure 13 to indicate groundwater was below that depth in the vicinity of the well. The average recession in the groundwater table for the five wells between the observed shallowest water table on 17 June and deepest water table on 20 August was 27 cm. This average includes the maximum measured change in depth at g6-1 and gD-1 and underestimates the total change in depth at those locations over the time period. This recession in groundwater compares closely to an observed recession in the stage of the Lower Wet Meadow of 30 cm over the same time period. It should be noted that the Lower Wet Meadow was only immediately adjacent to one of the wells (g6-1), so the comparable recession is not likely a reflection of the Lower Wet Meadow operating as a direct control on the elevation of groundwater.

4.1.3   Observed Meteorological Conditions

Meteorological measurements are summarized in Figure 16, including calculated estimates of evaporation, evapotranspiration, as well as throughfall estimated from the adaptation of Liu interception model. Stipled dots associated with direct atmospheric measurements indicate 95% confidence on hourly measurements calculated using the standard deviation of sub-hourly measurements. Larger uncertainty in hourly barometric pressure measurements starting on day 195 are associated with reported calibration activities at the Thompson Farm meteorological station; the hourly uncertainty in barometric pressure measurements essentially disappear with the installation of the new BaroLogger at the NWSC on day 217. Expected diel fluctuations were observed in incoming short-wave solar radiation (K_{in}), wind-speed (v_a), air temperature (T_a), and relative humidity (h_a). The effects or measured parameters on the evapotranspiration estimates are immediately observable. For instance, the week between 8 June and 15 June, as well as 10 and 11 July, correspond with high humidity, low temperatures, and reduced wind-speed and incoming radiation, which act to reduce the evaporation. Rain falling on 20 July and 10 August fell during overnight hours and did not substantially affect estimated evapotranspiration on these days.

Open-water evaporation for the duration of the study period from 25 May to 27 August 2010 totaled 411 mm. The highest open-water evaporation rate was estimated for the afternoon of 26 July at 1.94 mm hour^{-1}; the total estimated evaporation for that day was 15.1 mm. Meadow evapotranspiration was
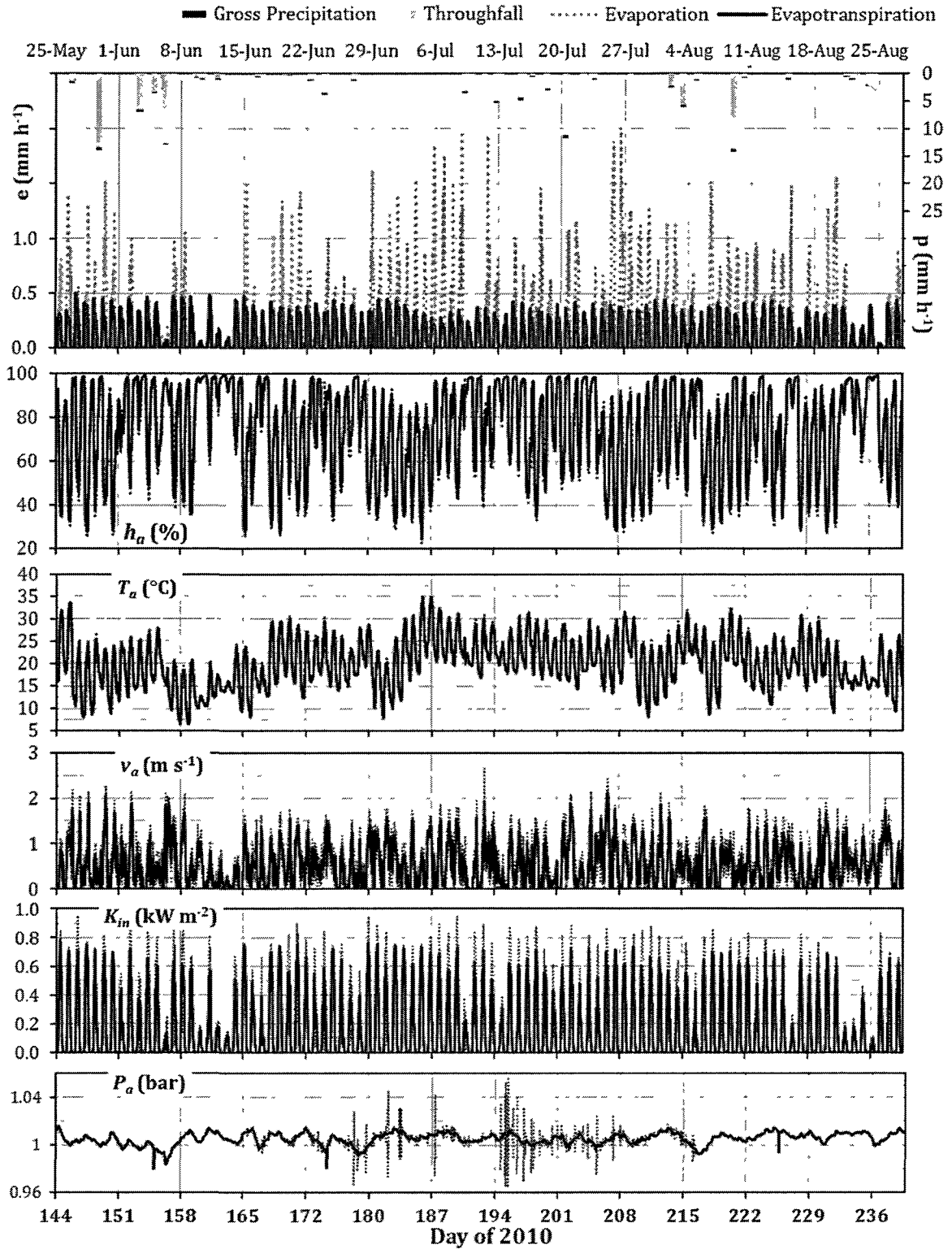
Figure 16: Meteoricalogical measurements, evapotranspiration, and throughfall timeseries. Bottom panels depict measurements, uncertainty (95% confidence) is depicted by stiples. Top panel shows precipitation and calcluated parameters (legend at top).

consistently smaller than estimated open-water evaporation and totaled 256 mm

for the evaluation period. The highest rate of meadow evapotranspiration was 0.49

mm hour[-1] on the morning of 27 May, and the total evapotranspiration for that day

was 3.9 mm. Average open-water evaporation and meadow evapotranspiration are

estimated at 4.7 mm day^{-1} and 2.9 mm day^{-1}.

Total precipitation for the evaluation period was 240 mm, and throughfall is

estimated at 226 mm. The maximum rate of precipitation and throughfall

throughout the period was 14.5 mm hour[-1] at noon on 25 August 2010. The

maximum hourly intercepted volume was 0.83 mm on the evening of 9 August 2010.

Normal summer rainfall in Concord, New Hampshire located 25 km west of the

NWSC for June, July, and August is 275 mm. Through the same time period, only 224

mm fell at the catchment, 75 mm of which fell in the final days of August suggesting

that rainfall was below normal through most of the summer.

Figure 17 illustrates the sensitivity of the Kohler-Parmele adaptation of the

Penman combination equation (KP-PCE) to variations in the input parameters

calculated for the Lower Wet Meadow during the evaluation period. The

parameters were varied by values that exceeded the manufacturer-reported

instrument measurement errors to assess the potential impact on differences

between meteorological conditions between the wet meadows and the tower

location. The four input measurements to the KP-PCE calculation (v_a, T_a, e_a, and K_{in}).

Hourly records of v_a, T_a, and e_a were varied by 10%, and hourly records of K_{in} were

varied by 5%. Multipliers for each input measurement are identified as X_v, X_T, X_e, and

X_K for v_a, T_a, e_a, and K_{in}, respectively. Figure 17 depicts the mean of predicted values

for total open-water evaporation throughout the evaluation period. The incoming solar radiation was less sensitive than other parameters. Average daily evaporation estimates range from 4.0 to 5.6 mm d^{-1} for variation in the measured windspeed of 10%. Varying input measurements of humidity (as water vapor pressure) and temperature by 10% result in KP-PCE estimates ranging from 4.3 to 5.4 mm d^{-1}. The maximum combined influences of the variation in these parameters result in a range in estimates of open-water evaporation from of 3.2 mm d^{-1} to 6.7 mm d^{-1}, a difference from predictions of -32 to +44%. However, windspeed is expected to vary as much throughout the wetland area as between the wetland and measurement tower, and is not expected to have a constant spatial bias due as may be expected for other parameters; therefore, the combined influence of other parameters is assessed while keeping windspeed at the measured values. The combined effect with unadjusted, measured windspeed results in a range in estimates of open-water evaporation from 3.7 to 5.8 mm d^{-1} representing differences ranging from -21 to +25%.

Plant evapotranspiration calculated by the PMCE is estimated to be less than open-water evaporation for two reasons: there is an additional stomatal resistance further impeding vertical transport, and the vertical wind-profile is altered by the presence of the vegetated canopy reducing the atmospheric conductance of water vapor. Partitioning the two fluxes within the Lower Wet Meadow is discussed in a later section; after partitioning the total estimated evaportranspiration flux is intermediate between the open-water evaporation and plant evapotranspiration fluxes.
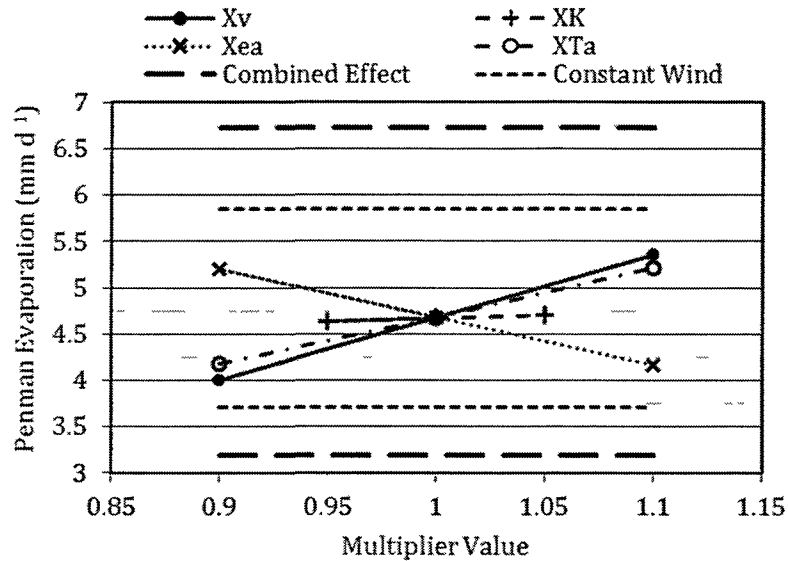
Figure 17: Sensitivity analysis of open-water evaporation to input data. The four factors represent multiplication coefficients applied to all hourly measured values for the corresponding meteorological parameter.

4.1.4 Characterization of Fractionating Conditions

The isotopic mass balance is calculated on a daily timestep. The analytical calculation approach is not suited to the observed short term fluctuations in reservoir volume or meteorological forcing data. In accordance with Gonfiantini [1986] and Horita and others [2008], the factors that describe the evaporating fractionation need to be calculated as evaporation flux-weighted averages for the period of evaluation.

The temperature of the evaporating surface is an important parameter in describing the isotopic fractionation from the water surface. Figure 18 compares the measured air temperature, the measured water temperature at s1 and s3, and the water surface temperature estimated from the Penman equation using the direct

substitution method of Tracy and others [1984]. The water temperature measured at s1 was collected at depths below the water surface ranging from 6 to 24 cm, whereas the temperature at s3 was measured about 25 cm below the surface of peat sediment. Predicted day-time surface temperatures were typically greater than temperatures measured at s1 and correspond closely to the measured air temperature from which the estimate is derived. During afternoon, evening, and morning times the estimated surface temperatures tend not to exhibit as strong of fluctuations in temperature as air temperature, but are similar to the temperature measured at s1, though the temperature at s1 was not incorporated into the estimate of the temperature or the KP-PCE. The estimated temperatures are expected to be an improvement upon using air temperature directly to estimate the temperature of the diffusive laminar layer. However, in the absence of short-wave radiation in the middle of the night or even during extreme cloud cover, the surface temperature estimate becomes unreasonably low (below freezing), and is forced to a minimum equal to the air temperature at the time period. Surface water temperatures directly from measurements at s1 are also used as input to the isotopic mass balance to estimate sensitivity to this parameter.

The hourly estimate of water surface temperature is used to calculate the normalized humidity. The surface temperature and normalized humidity are then used in the calculation of the equilibrium isotopic fractionation factor ($\alpha_{V/L}$) and kinetic isotopic enrichment factor (ε_K). In addition, measured humidity is used to estimate the molar mixing ratio (w) and specific humidity (h_s), which are required for some estimates of the atmospheric vapor composition on a daily basis. Values

for the estimated water surface temperature, molar mixing ratio, and normalized humidity are evaluated as the evaporative-flux weighted averages for each day and are depicted on Figure 19. Evaporation flux-weighted average estimates of surface temperature and molar mixing ratio indicate generally low temperatures and water content through mid-June due to low air temperatures with increasing temperatures through late June to a maximum in early July, with the exception of a three day period of low atmospheric water content at the very beginning of July. Surface temperatures and molar mixing ratio then fluctuate consistently throughout much of July and August, with several days in late July and early August showing apparent dips in atmospheric water content. Normalized humidity range from about 50% to 100%, and is generally much lower than observed humidity due to higher estimates of water surface temperature compared to air temperature. Extended periods for the lowest values of the normalized humidity correspond with the periods with the lowest molar mixing ratios (e.g. early July, and late July through early August).

4.2   Results from Tracer Analyses

A total of 137 water samples collected between June 2009 and October 2010 were analyzed for isotopic composition. These samples included 43 samples of rainfall collected between June 2009 and October 2010 (Figure 20), 50 samples of groundwater or peat water collected throughout 2010 (Figure 21), and 44 samples of surface water collected throughout the NWSC between 25 May and 12 October, 2010 (Figure 21). Table 7 summarizes the ranges of isotopic composition for
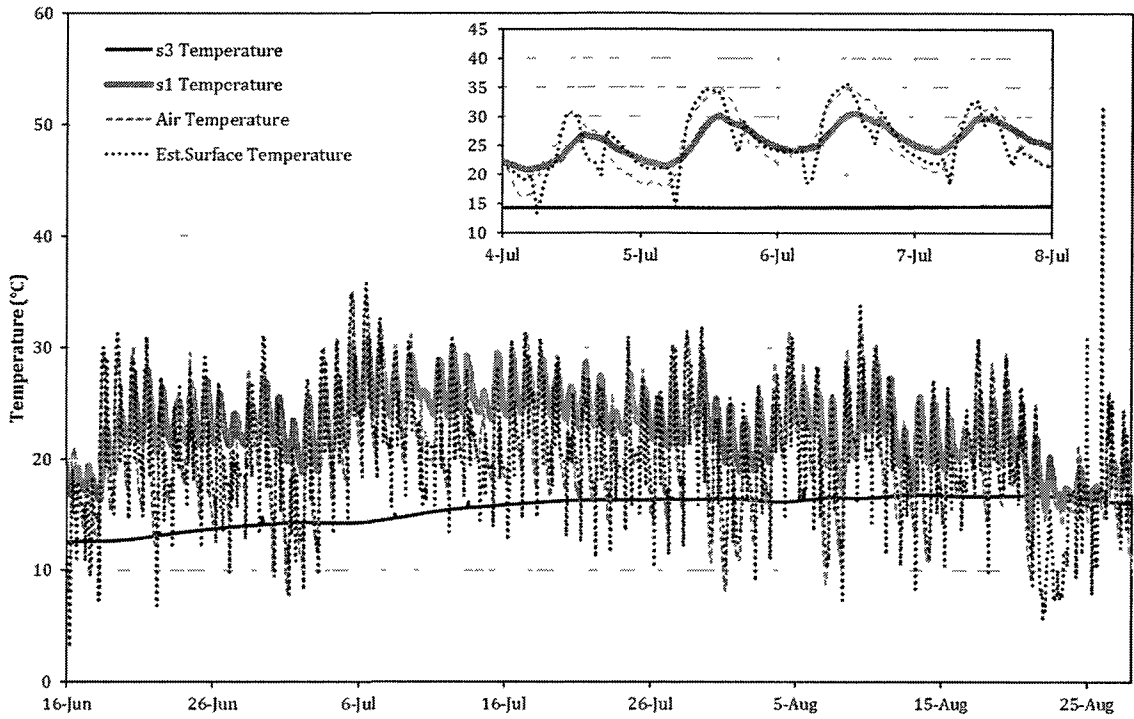
Figure 18: Comparison of estimated surface temperature to measured temperatures. Water temperature data from s1 and s3. Inset shows a four-day period in July.
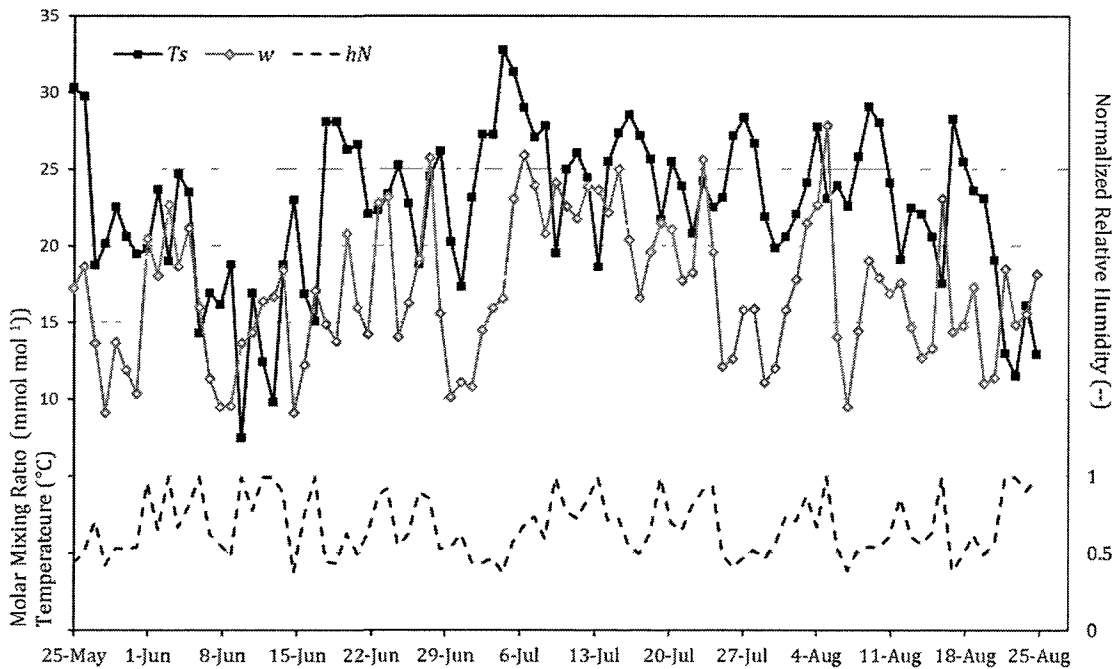
Figure 19: Daily water surface temperature, water vapor molar mixing ratio, and humidity. Water surface temperature (T_s) , water vapor molar mixing ratio (w), and normalized humidity (h_N) are calculated as daily evaporation flux-weighted averages.

114

rainfall, groundwater, peat water (collected from sediments within the Lower Wet Meadow from well g1-1), and streamflow from Lamprey Brook, Mountain Brook, s6, and the catchment outlet, and reservoir water from Meadow Lake and the wet meadows (s1, s2, and s3). Appendix A includes a complete table of analytical results. Figures 20 and 21 depict the isotopic composition of rainfall, groundwater, and surface water used in the study in relation to the local meteoric water line in δ^2H (‰)/ $\delta^{18}O$ (‰) space. Figures B1 through B8 located in Appendix B depict the isotopic composition of groundwater and surface water for individual sampling dates. Figures 21 and B1 through B8 illustrate the progressive enrichment of surface waters along an evaporative water line of an approximate slope of 4.8 throughout 2010. Regressions discussed in the following sections are used to estimate the composition of the various reservoirs daily throughout the summer. The errors of these estimates discussed in the following section are derived from the root mean square error of the predictions from the regression lines, and do not incorporate additional analytical uncertainty. In section 4.2.4, end-member mixing fractions are calculated at the outlet of the NWSC; analytical uncertainty is incorporated in these estimates in addition to the errors from the regressions.

4.2.1   Meteoric Water

Collectively, rainfall samples from the two years (Figure 20) superficially suggest consistency with the LMWL established by Frades [2008, In Prep] from precipitation samples collected between 2006 and 2007. Precipitation samples from the study were not incorporated in an attempt to adjust or improve the LMWL
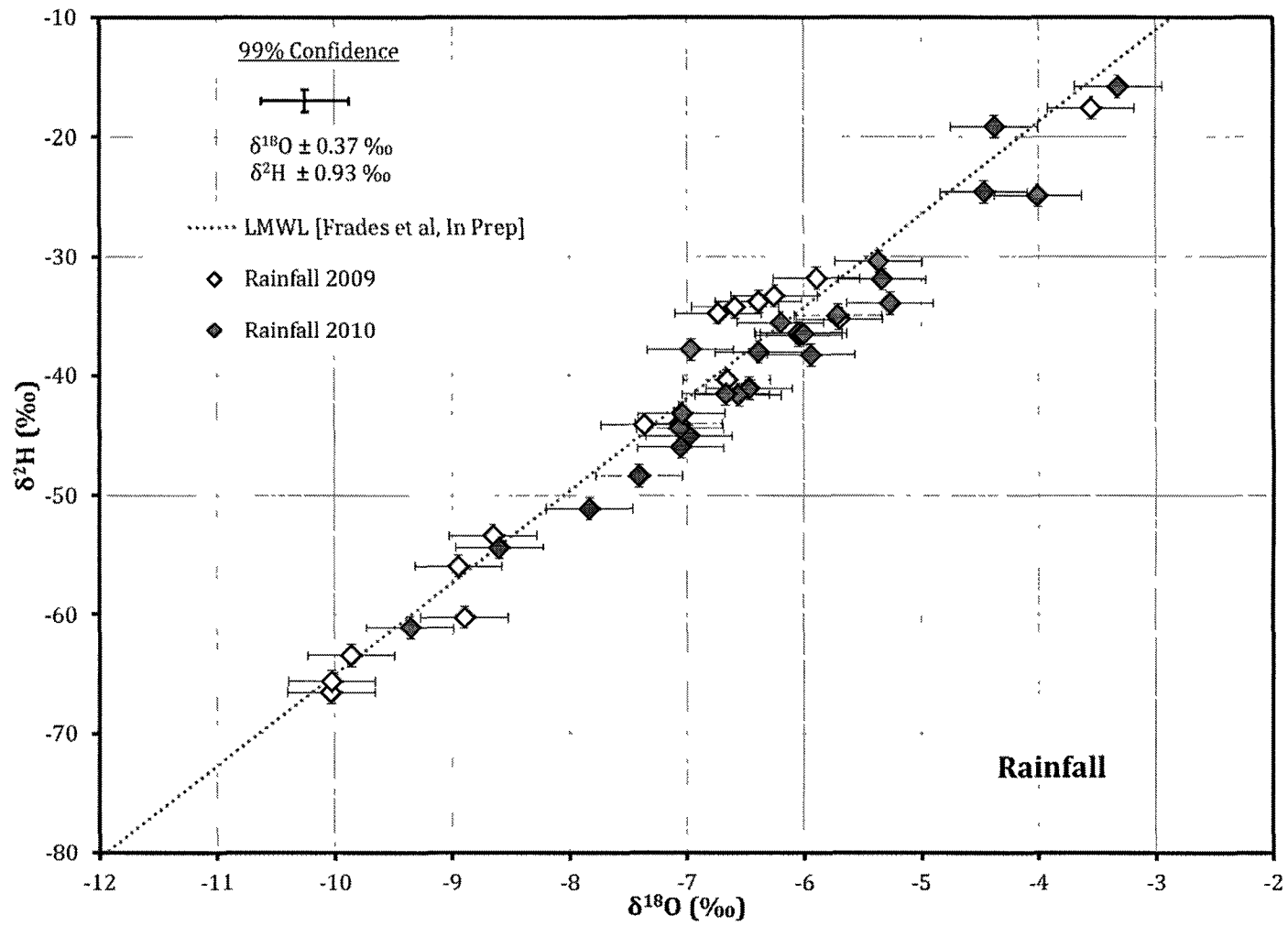
Figure 20: Stable isotopic composition of rainfall from the NWSC. Collected June - December 2009 and April - October 2010.
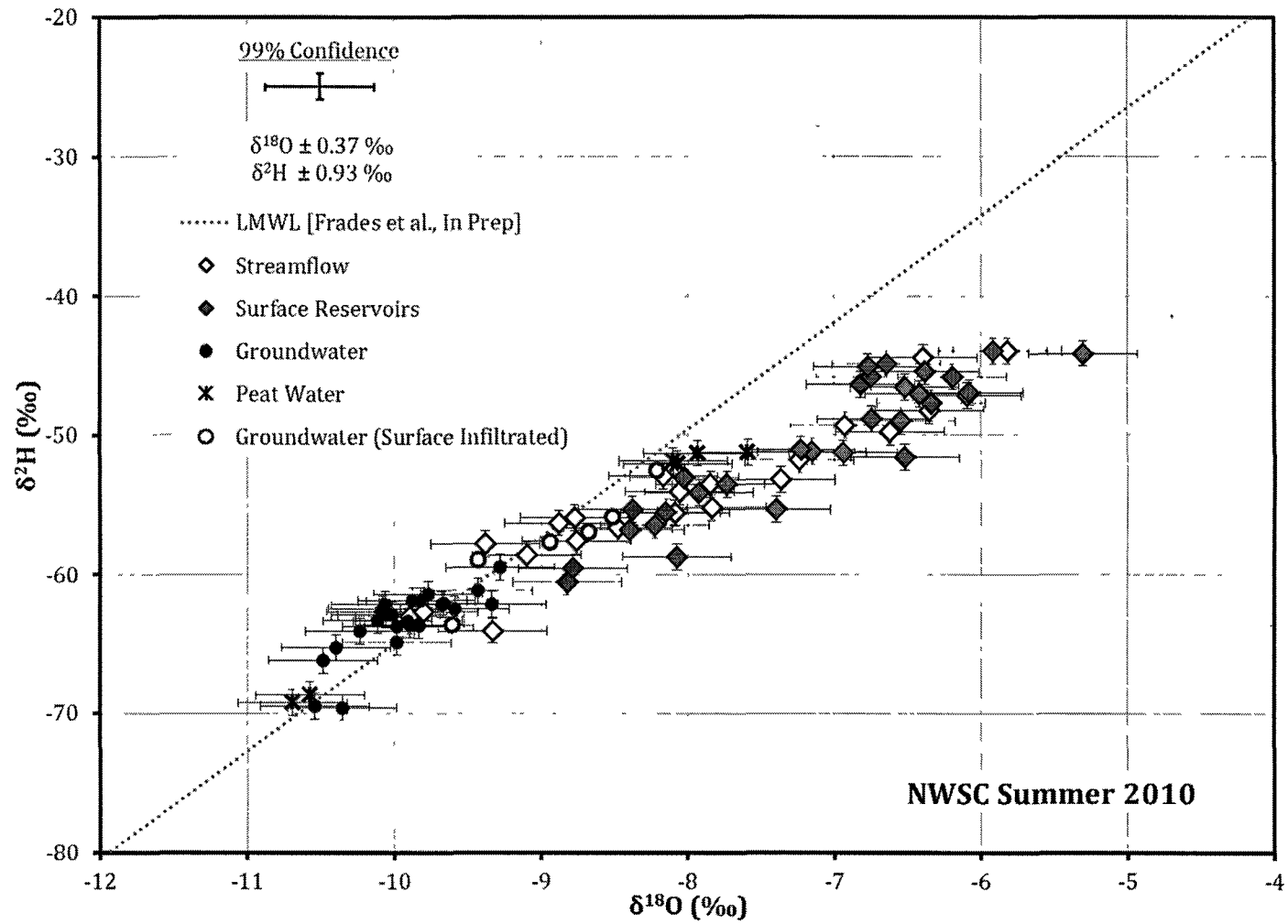
Figure 21: Stable isotopic composition of surface water and groundwater. Streamflow (sA, sC, s6, and s4), surface reservoirs (sB, s1, s2, and s3), peat water (well g1-1), groundwater (gD-1, g6-1, g4-1, and g4-3), and groundwater with apparent surface infiltration (gC-1).

Table 7: Ranges of isotopic composition of various hydrologic fluxes and stores. Collected within the Northwood Study Catchment between May and October 2010 (rainfall between June 2009 and October 2010).

Type	$\delta^{18}O$ min	$\delta^{18}O$ max	δ^2H min	δ^2H max	n
	‰		‰		
Rainfall	-9.4	-3.3	-61.1	-15.8	43
Groundwater	-11.2	-7.1	-73.9	-42.3	44
Peat Water	-10.7	-7.6	-69.3	-50.8	6
Streamflow	-9.9	-5.8	-64.1	-44.0	20
Reservoir	-8.8	-5.3	-60.5	-44.0	24

because the study of Frades appropriately sampled the entire annual range of precipitation, whereas only summer-time rainfall was analyzed in this study. Rainfall between sampling dates was attributed the average composition of precipitation over the sampling interval (Figure 22).

Isotopic composition of the atmospheric water vapor (δ_A) is calculated by the six regression estimates summarized on Table 5 (Section 3.3.2). Vapor in equilibrium with precipitation ($\delta_{V,*}$) is calculated from δ_P (Figure 22) and used in the regressions of Jacob and Sonntag [1987] and Lee and others [2006] to estimate δ_A. Other regressions used to estimate δ_A rely on evaporation flux-weighted estimates of specific humidity (h_s) or molar mixing ratio (w)[Lee et al., 2005; Lee et al., 2006; White and Gedzelman, 1984]. The results from six regressions (four for $\delta_A^{18}O$, two for δ_A^2H) are depicted in the top panel of Figure 23. The isotopic mass balance the calculation discussed in Section 4.3 requires the cumulative evaporation flux-weighted means shown in the bottom panel of Figure 23. The variance between daily regressions results are used to estimate uncertainty of the estimate of δ_A.
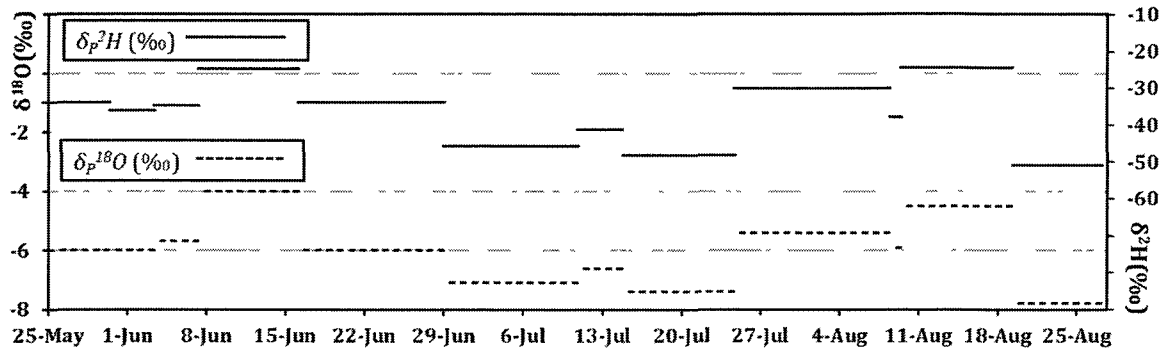
Figure 22: Time-series of the isotopic composition of rainfall (δ_P) throughout the study period. Data are used to force inputs to the isotopic mass balance, and to estimate isotopic composition of atmospheric water vapor (δ_A) (Figure 23).
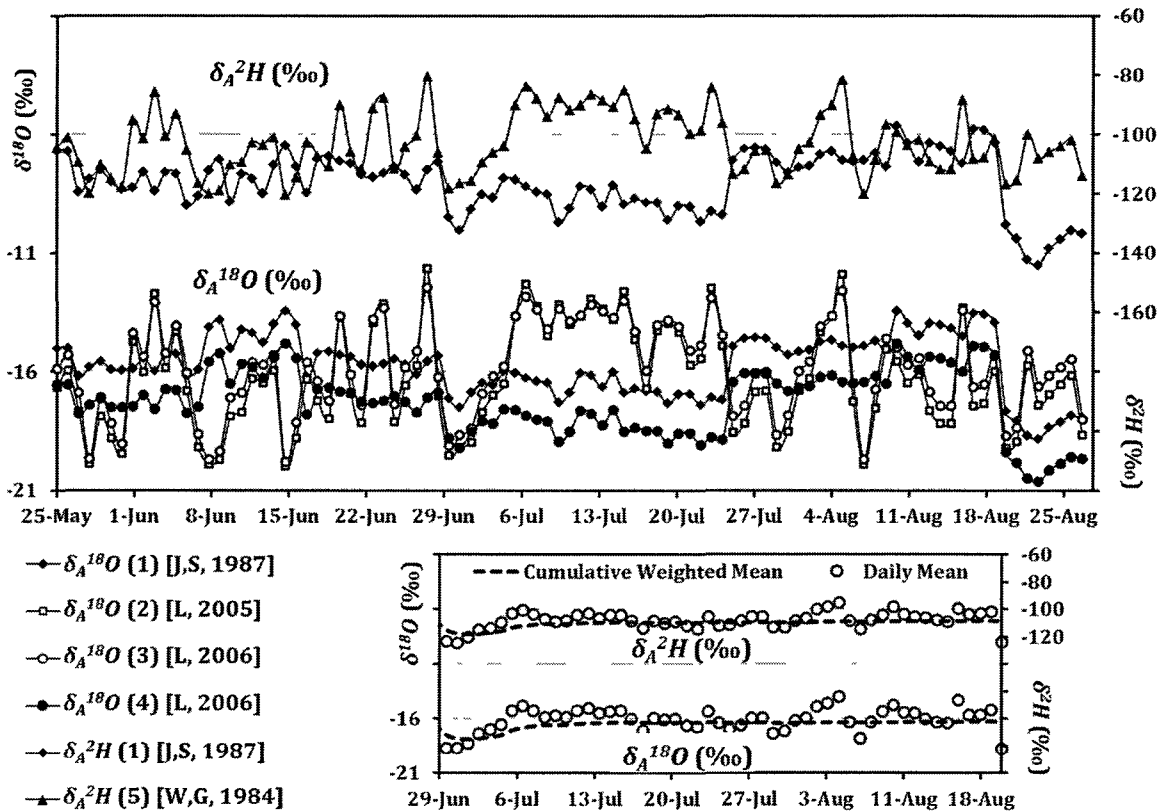
Figure 23: Estimated isotopic composition of atmospheric water vapor (δ_A). Vapor composition estimated from six different regression relations using meteorological measurements: $\delta_A{}^{18}O$ (1) and $\delta_A{}^2H$ (1) [Jacob and Sonntag, 1987, from δ_P]; $\delta_A{}^{18}O$ (2) [Lee *et al.*, 2005, from *w*]; $\delta_A{}^{18}O$ (3) [Lee *et al.*, 2006, from *w*]; $\delta_A{}^{18}O$ (4) [Lee *et al.*, 2006, from $\delta_P{}^{18}O$]; $\delta_A{}^2H$ (5) [White and Gedzelman, 1984, from h_s]. Mean compositions of $\delta_A{}^{18}O$ and $\delta_A{}^2H$ from the regression estimates (inset at bottom right for evaluation period) are calculated daily (circles) and as the cumulative evaporation flux-weighted means from the beginning of the evaluation period (dashed lines), which is used in the isotopic mass balance. The variances in estimates of δ_A from regressions characterize uncertainty in the estimate.

119

4.2.2   Riparian Groundwater

Groundwater was found to be different on average than more isotopically enriched stream and wetland water. Figure 24 depicts box plots of samples collected throughout 2010 from the monitoring well and stream networks. Means of samples from each location were tested for differences using a t-test where the Type I error cut-off value (α), defined as the acceptable probability that means are determined to be similar when they are in fact different, was set at 0.05. The tests were conducted on both sample results from $\delta^{18}O$ and $\delta^{2}H$ using JMP 8 (SAS Institute, Inc.). Sample locations that exhibit no difference in mean composition are indicated with the same letters.

$\delta^{18}O$ results distinguish clearly between riparian groundwater and surface water except for samples from sC and s6. sC and s6 have isotopic compositions that are not distinctly different from groundwater, which reflects less influence from evaporative enrichment within these catchments or greater fractions of streamflow derived directly from groundwater. $\delta^{2}H$ results do not distinguish between surface and groundwater sources as clearly; only three of eight surface sampling locations have distinct means from the groundwater samples. The clearer discrimination in $\delta^{18}O$ is expected because the greater evaporative enrichment effect is experienced by oxygen [a typical ε_K of $\delta^{18}O$ is $(1-h_N)14.2\text{\textperthousand}$ compared to $(1-h_N)12.5\text{\textperthousand}$ for $\delta^{2}H$].

On individual dates, peat water from well g1-1 was consistently more enriched than other groundwater samples at the time of sample collection, though the mean is not identified as different from other wells (Figures B1 through B8,
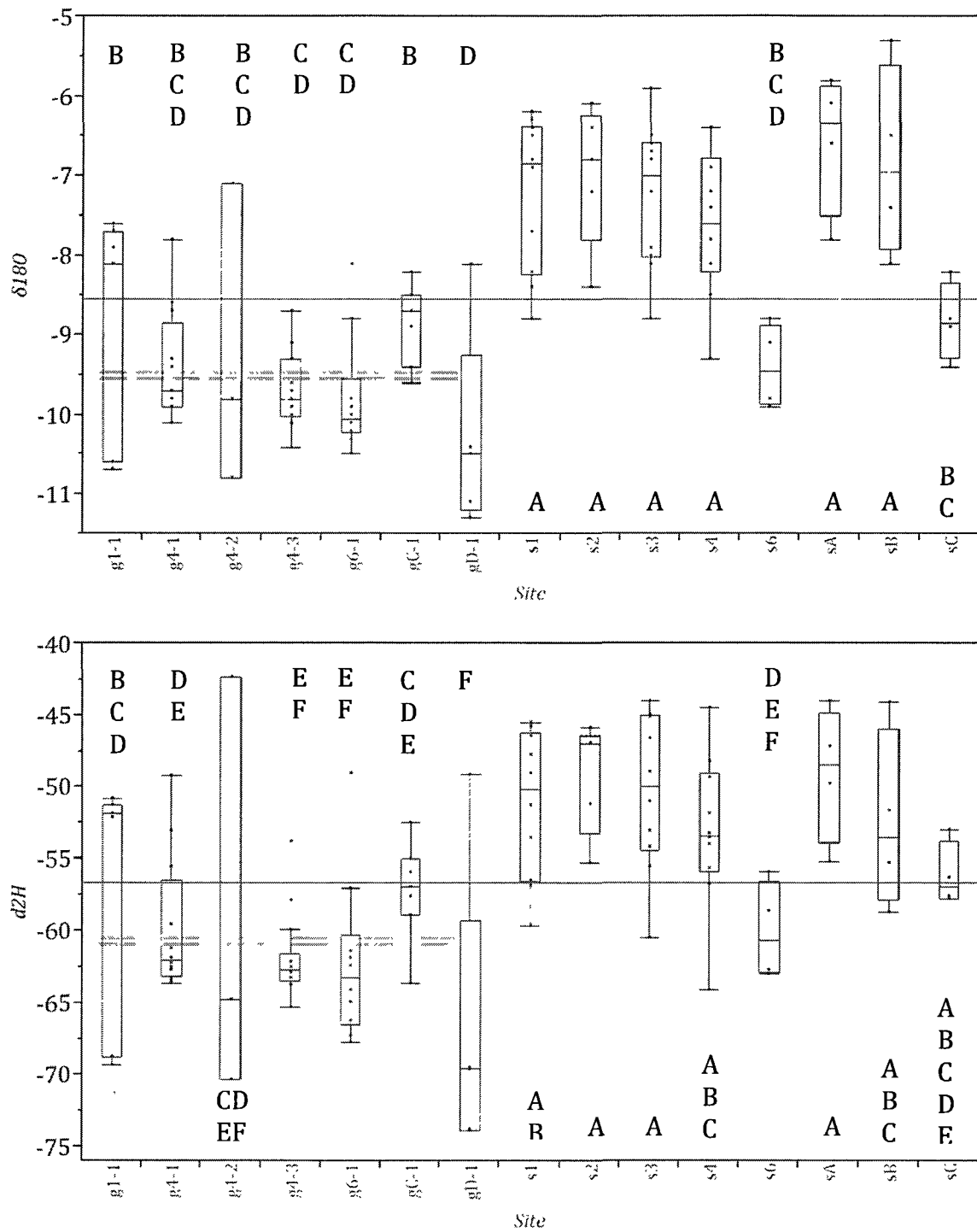
Figure 24: Comparison of mean stable isotope composition throughout 2010. Groups of sites with indistinguishable means (*t*-test, α = 0.05) share common letters. Gray dashed-lines represent the mean (with 70% confidence intervals) isotopic composition of bedrock groundwater (WT) from Frades and others [In Prep].

Appendix B). The highest δ-values of non-peat groundwater are represented by one

well (gC-1), which is identified on Figure 21 as groundwater with apparent surface

infiltration. The well is within 2 meters of an isolated pool at the edge of the

floodplain of Mountain Brook that remained saturated throughout the summer.

Infiltration from this pool is expected to have influenced the composition at gC-1

late in the summer by introducing unrepresentatively high volumes of rainwater

and evaporatively enriched water to the vicinity of the well. The pool is considered

unrepresentative of the catchment as a whole and isotopic composition measured at

this well is not considered broadly indicative of riparian groundwater composition

throughout the catchment. Wells identified by a C or D for $\delta^{18}O$ or E or F for δ^2H are

considered representative of riparian groundwater in the catchment.

Gray dashed lines in Figure 24 depict the composition of groundwater

sampled from bedrock at well WT by Frades and others [In Prep]; the separation

between the dashed lines indicates temporal variability at 70% confidence. The

mean composition of samples from several wells is similar to bedrock groundwater

composition in both $\delta^{18}O$ and δ^2H with several exceptions: g1-1 (peat water), gC-1

(influence of surface infiltration), gD-1 (appears to have a greater influence from

recharge during winter), and g4-2 (appears to reflect infiltration of direct

precipitation, and was dry and unsampled throughout the summer). It is also

evident that shallow riparian groundwater represented by the well network at

NWSC exhibits greater seasonal variability in composition than bedrock. As

hypothesized, this variability does not translate to observed composition of surface

water (Figure 24), except possibly at Mountain Brook (sC and gC-1); again, composition of sampled from gC-1 is considered influenced by surface infiltration.

Figure 25 depicts the progression in isotopic composition of riparian groundwater through the study period derived from samples collected at gD-1, g6-1, g4-1, and g4-3. Well g4-2 was dry throughout the evaluation period. Due to drying at gD-1 and g6-1, samples could not be collected at these locations on late summer sampling dates. The regression results in an estimate of the average composition of riparian groundwater on day i with an error of $\pm$ 0.7‰ and $\pm$ 5.2‰ (at 95% confidence) for $\delta_{rgw}{}^{18}O$ and $\delta_{rgw}{}^2H$, respectively, and is used to estimate the composition of groundwater entering the Lower Wet Meadow.
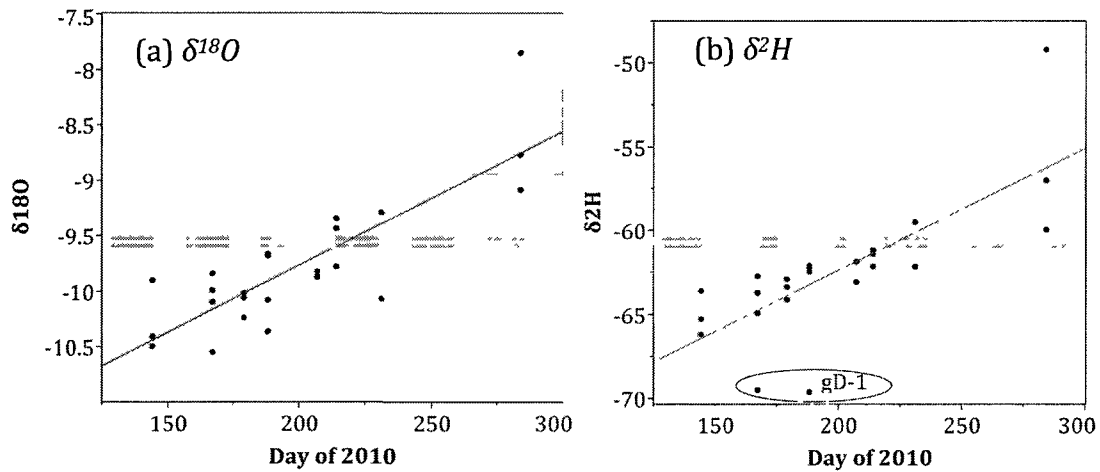
Figure 25: Trend in isotopic composition of riparian groundwater versus day of 2010. (a) $\delta^{18}O$ (r^2= 0.69, RMSE=0.36‰) and (b) δ^2H (r^2=0.58, RMSE= 2.58‰). Gray lines represent bedrock groundwater composition from Frades and others [In Prep].

4.2.3 Surface Water

The most evaporatively enriched samples of surface water were collected from Lamprey Brook (sA), which drains two nested ponds, and from Meadow Lake (sB). Throughout the summer, isotopic samples collected throughout the meadow complex (s1, s2, and s3) plotted along the observed evaporative line of a slope of approximately 4.8 in plots of δ^2H versus $\delta^{18}O$ and the isotopic compositions of the sampling points were within analytical error. On individual dates, the outlet of the NWSC (s4) was consistently represented by a composition intermediate between the evaporated wet meadow complex and groundwater; however, the mean composition at this location was not distinguished as significantly different from other surface water samples (Figure 24). Samples collected from Mountain Brook (sC) and s6 typically exhibited the least evaporative enrichment, and both had means not significantly different than groundwater.

Samples collected from sA, sB, sC, and s6 exhibit broad variability on any given sampling day, though throughout the summer, all exhibit a tendency towards evaporative enrichment. Figure 26 depicts the progression in isotopic composition of these headwater streams through the study period. The compositions of these headwater streams are used to characterize ungauged and unsampled isotopic composition the first order catchments draining to the Lower Wet Meadow (δ_u). The regression results in an estimate of the average composition of ungauged and unsampled first order catchment runoff on day i with an error of $\pm 2.8‰$ and $\pm 9.5‰$ (at 95% confidence) for $\delta_u{}^{18}O$ and $\delta_u{}^2H$.
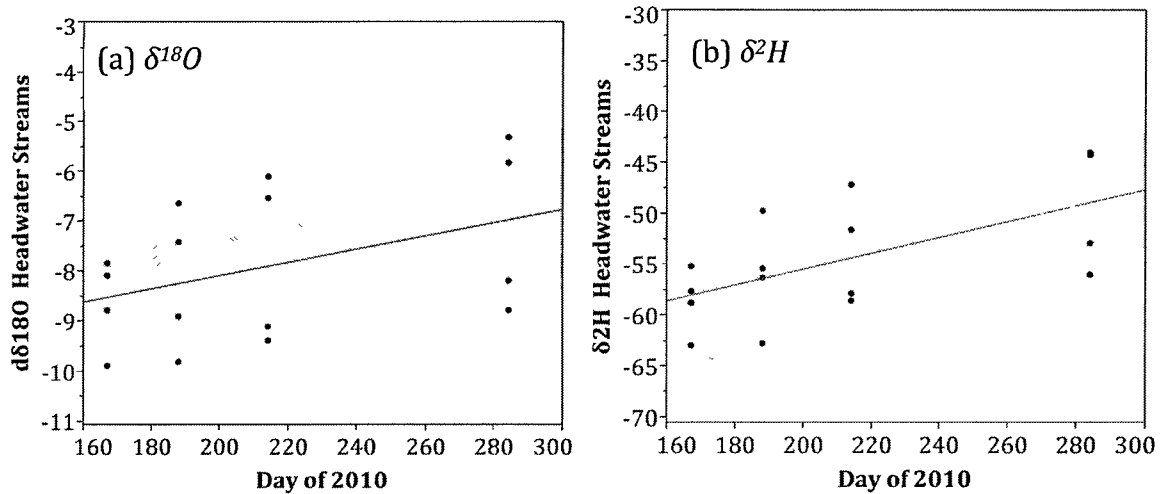
Figure 26: Trend in isotopic composition of headwater streams versus day of 2010. (a) $\delta^{18}O$ (r^2= 0.17, RMSE=1.37‰) and (b) δ^2H (r^2=0.37, RMSE= 4.78‰).

Isotopic composition of samples collected from storage with the upper (s1) and lower (s2 and s3) wet meadows and stream water at the NWSC outlet at s4 were also regressed to estimate average composition on day i throughout the study period (Figures 27, 28, and 29, respectively). The regressions provide the ability to estimate the daily proportion of discharge measured at s4 that emanated from the Lower Wet Meadow, and provides an estimate of the composition of Upper Wet Meadow discharge to the Lower Wet Meadow. The average composition of the Upper Wet Meadow (s1) is estimated with an error of ±0.6‰ and ±1.3 ‰ (at 95% confidence) for $\delta_{s1}{}^{18}O$ and $\delta_{s1}{}^2H$. The average composition of the Lower Wet Meadow on day i is estimated with an error ±0.4‰ and ±1 ‰ (at 95% confidence) for $\delta_{lwm}{}^{18}O$ and $\delta_{lwm}{}^2H$. The average composition of streamflow at the NWSC outlet on day i is estimated with an error of ±0.2‰ and ± 2.8‰ (at 95% confidence) for $\delta_{s4}{}^{18}O$ and $\delta_{s4}{}^2H$, respectively.
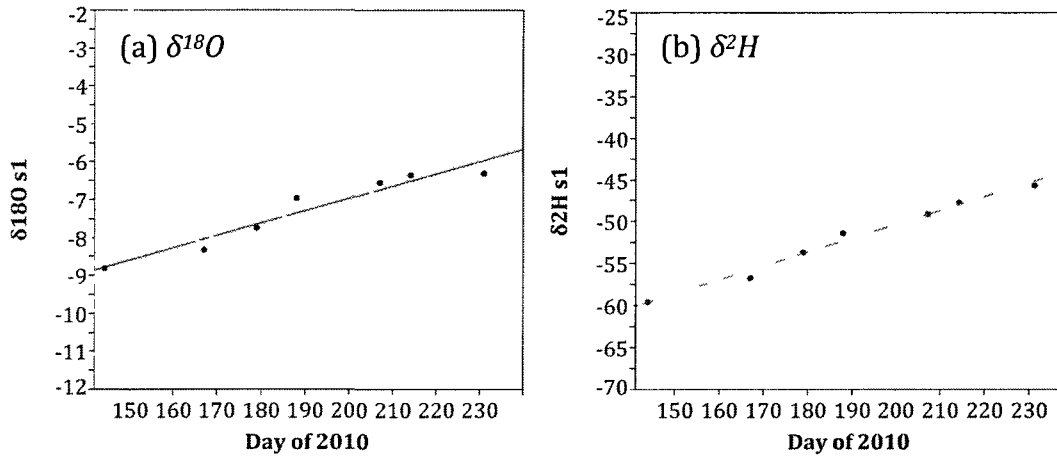
Figure 27: Trend in isotopic composition of the Upper Wet Meadow (s1) versus day of 2010. (a) $\delta^{18}O$ (r^2= 0.93, RMSE=0.29‰) and (b) δ^2H (r^2=0.99, RMSE= 0.66‰).
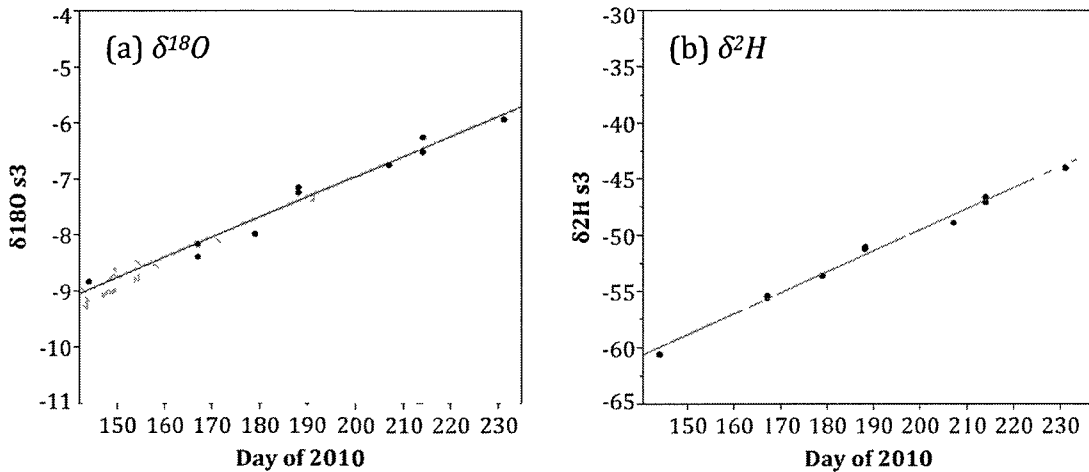
Figure 28: Trend in isotopic composition of the Lower Wet Meadow (s3 and s2) versus day of 2010. (a) $\delta^{18}O$ (r^2= 0.97, RMSE=0.19‰) and (b) δ^2H (r^2=0.99, RMSE= 0.49‰).

4.2.4   Isotopic Composition and Wetland Coverage

Wetlands and ponds were expected to result in evaporative enrichment throughout the NWSC, and subcatchments that contained a larger coverage of wetlands or ponds would be expected to exhibit relatively greater enrichment (i.e. higher δ-values). Figure 30 compares the observed δ-values for seven
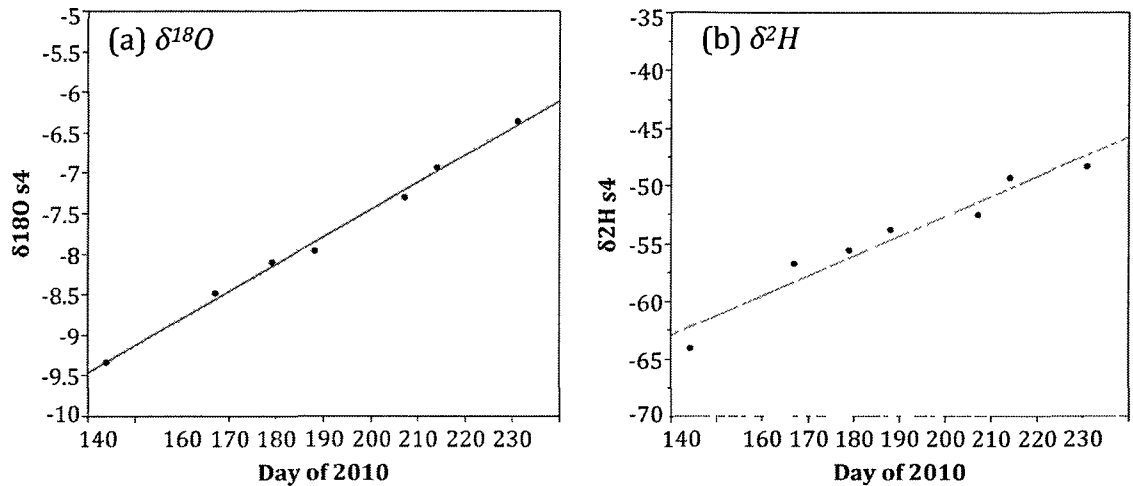
Figure 29: Trend in isotopic composition of the NWSC outlet (s4) versus day of 2010. (a) $\delta^{18}O$ (r^2= 0.99, RMSE=0.08‰) and (b) δ^2H (r^2=0.94, RMSE= 1.42‰).

subcatchments within the NWSC versus the measures of wetland or waterbody

coverage summarized in Table 6. The figures illustrate generally increasing δ-

values for increasing wetland or waterbody coverage measured by the four metrics.

Stream length within wetlands or waterbodies; however, better distinguishes

between the relative enrichment observed in the isotopic compositions between

Lamprey Brook (sA) and Mountain Brook (sC). sA exhibits greater isotopic

enrichment than sC, has a marginally lower area coverage of wetlands or

waterbodies, but has greater stream length within those wetlands. Increasing

stream length within wetlands correlates with increasing (relative enrichment)

more strongly (p 0.005) compared to either measures of wetland or waterbody area

(p = 0.017 to 0.044) for $\delta^{18}O$ using non-parametric regression (Kendall's τ).

Increasing stream length within wetlands was the only significant predictor of

increasing enrichment across the catchment at an α = 0.05 using Kendall's τ.
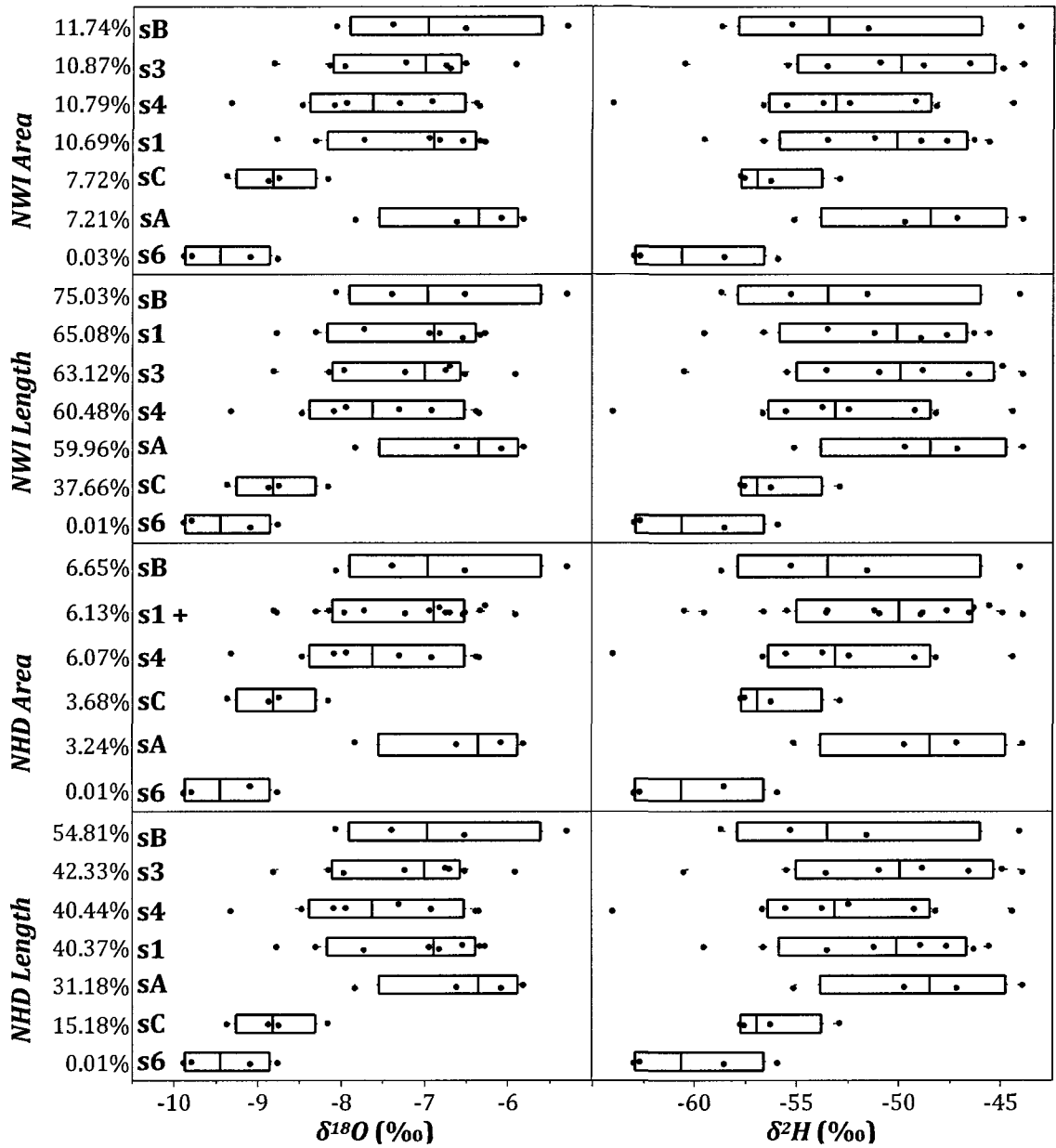
Figure 30: Effect of wetland coverage on isotopic compositions. Figure compares four metrics of wetland or waterbody coverage using wetland data from the National Wetlands Inventory (NWI), and waterbody area from the New Hampshire hydrography dataset (NHD). Metrics include fractional wetland (NWI Area) or waterbody area (NHD Area) within the catchment, and fractional catchment stream course length within wetlands (NWI Length) or waterbodies (NHD Length). Increasing δ-values indicated increasing evaporative enrichment. As expected, increasing measures of wetland or waterbody coverage broadly correlate with increasing δ-values. Increasing enrichment appears to correlate best with increasing stream length within wetlands or waterbodies.

4.2.5   Isotopic Composition at the NWSC Outlet

A binary mixing estimate of the proportional contributions of streamflow at the catchment outlet derived from storage within the Lower Wet Meadow and groundwater was calculated by equations (3.1) and (3.2) (§3.1). At a confidence greater than 95%, outflow from the NWSC is composed of less than 50% water typical of either shallow riparian groundwater or bedrock groundwater throughout much of the study period (Figures 31A and 31B). The values of f_{rgw} calculated from $\delta^{18}O$ and δ^2H result in mean suggested contributions from the riparian groundwater to catchment outflow of 15 and 20%, respectively. The values of f_{dgw} calculated from $\delta^{18}O$ and δ^2H result in mean suggested contributions from the bedrock groundwater to catchment outflow of 18 and 25%, respectively. The mean between continuous daily estimates of f_{rgw} from $\delta^{18}O$ and δ^2H using regressed estimates range from 24% to 19% during the evaluation period from day 179 to 231. The mean between continuous daily estimates of f_{dgw} from $\delta^{18}O$ and δ^2H using regressed estimates range from 30% to 18% during the evaluation period. The lower and upper bounds associated with 95% confidence result in possible values for the f_{rgw} that range from 0% to 62% at the beginning of the evaluation period, but narrow to between 0 and 40% (33% for bedrock groundwater) at the end of the evaluation period due to greater separation between the isotopic composition of the Lower Wet Meadow and groundwater. Assuming either riparian groundwater or deep bedrock groundwater discharge to the stream, only a portion of baseflow from the NWSC was accommodated directly from groundwater inputs to the stream. Moreover, the hypothesis that baseflow would be derived from greater groundwater inflows as the

summer progressed is not supported by Figures 31A and 31B. No mixtures of riparian groundwater and deep bedrock groundwater were considered.

The fraction of water contributed by discharge from the lower wet can be considered as simply the complement to values of f_{rgw} or f_{dgw} (e.g. f_{lwm} = 1–f_{rgw}, or 1–f_{dgw}). Therefore, the fraction of streamflow from the NWSC catchment derived from discharge from the Lower Wet Meadow (f_{lwm}) was between 76 and 81% (calculated assuming riparian groundwater discharge to the stream) or between 70 and 82% (calculated assuming bedrock groundwater discharge to the stream). Multiplying daily average discharge at the catchment outlet by the daily average f_{lwm} yields an estimate of daily discharge from the Lower Wet Meadow. The isotopic mass balance discussed in the next section investigates the role of groundwater in the water balance of the Lower Wet Meadow to determine to what extent surface discharge from the reservoir is accommodated by direct groundwater inflows.

4.3 Isotopic Mass Balance of the Lower Wet Meadow

To further the discussion of the relative roles that groundwater and wetlands play in maintaining baseflow from the NWSC, the following sections describe the results of the water balance and the sensitivity analysis conducted to explore the role of groundwater in sustaining surface discharge from the Lower Wet Meadow. The volumetric water balance is calibrated to ensure consistency with observed isotopic composition.
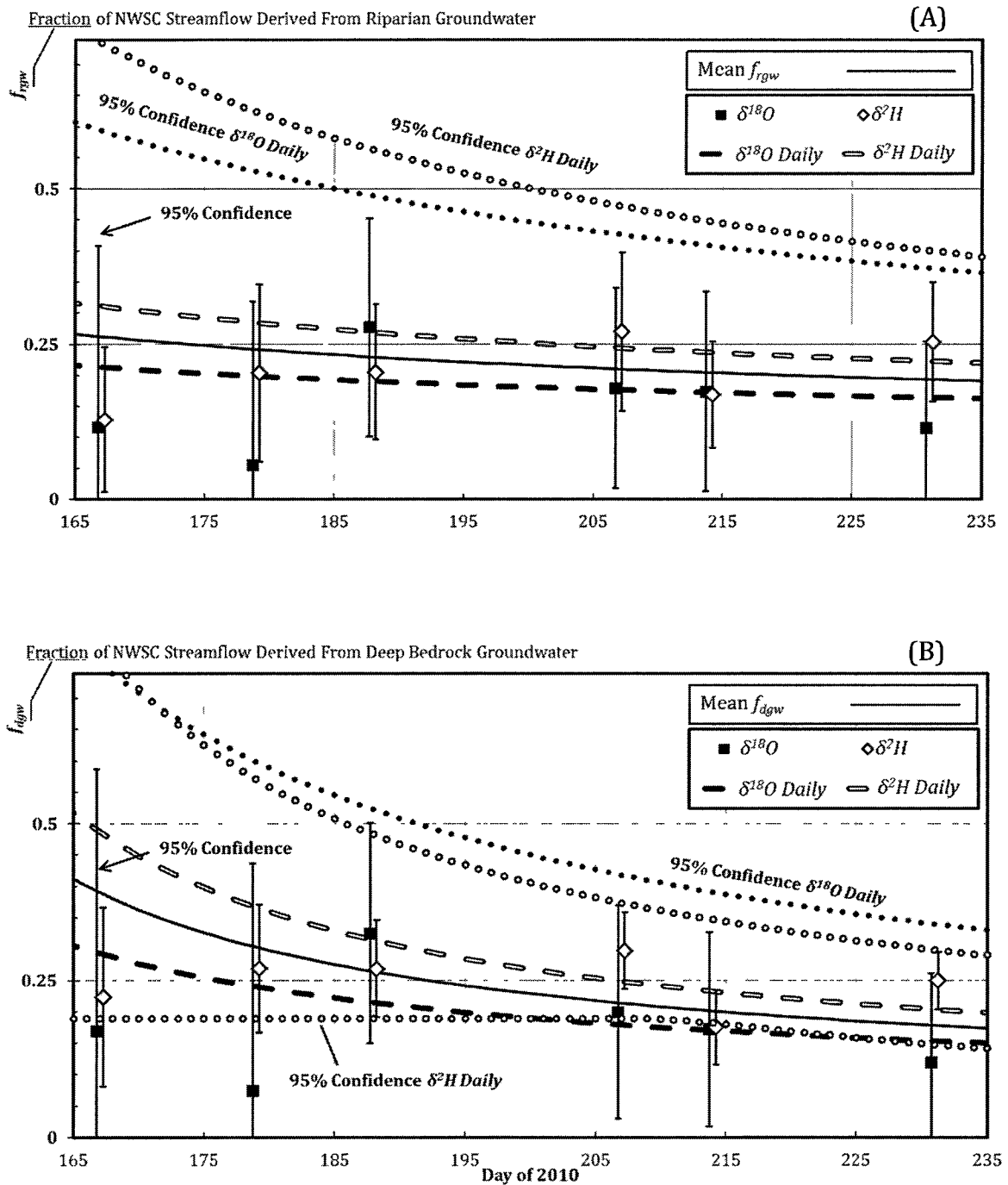
Figure 31: Fraction of groundwater in surface discharge from the NWSC. (A) f_{rgw} assumes only riparian groundwater, and (B) f_{dgw} assumes only deep bedrock groundwater in stream-flow. Mixing fraction is presented from both $\delta^{18}O$ and δ^2H sampling results as discussed. Markers with error bars and dashed lines with dotted error intervals indicate the estimate of mixing fraction and associated uncertainty on sampling dates and from daily trend regression estimates, respectively.

131

4.3.1 Model Calibration

Using expected values for precipitation, evaporation, evapotranspiration, and streamflow, their characteristic isotopic composition, and the mean estimates of the isotopic composition of atmospheric water vapor, meteorologic measurements were varied by up to 10% to calibrate the model to observed isotopic composition of the Lower Wet Meadow through the summer. For any given combination of the Lower Wet Meadow specific yield (S_{Ms} or S_{Md}) and the open-water fraction (f_w), meteorological measurements were found to predict observations as well or better than values varied from the measurements. The calibration suggests that meteorological measurements at the tower adequately describe the evaporating conditions. The fractionation effects assumed in the Craig-Gordon model are based on an ambient atmosphere. Craig and Gordon [1965] in developing the model were investigating the role of ocean evaporation and found that measurements of temperature and humidity at a height of 10 m above the evaporating water body were appropriate; this measurement height was impractical for this study. The location of the measurement tower upslope from the wet meadow, though only 2 m from the ground surface, apparently samples the ambient atmosphere accurately enough for the analytical calculation.

Three parameters (S_{Ms}, S_{Md}, and f_w) describe hypothesized system states for the Lower Wet Meadow and define the magnitude of the groundwater flux and the relative fluxes of open-water evaporation versus evapotranspiration. Values of each measure of the specific yield were varied through plausible values to assess values of the open-water fraction that result in isotopic fractionation of reservoir water

similar to observations. The parameters S_{Md} and f_w were varied through a range of physically plausible values while keeping the value of S_{Ms} constant at 0.825 (the median of its tested range). S_{Md} was varied between 0.1 and 0.6, which bound values reasonable for wetland peat sediments [Boelter, 1968]. f_w was varied between 0.0 and 0.35; higher values of f_w did not result in reasonable predictions of isotopic composition of the reservoir. Both S_{Md} and f_w were varied in 2.5% increments. Predictions of reservoir isotopic composition were calculated using the 280 parameter combinations; contours of the Nash-Sutcliffe efficiencies were plotted (Figure 32A), which depicts a region of high predictive efficiency in hashed marks that has a distinct positive correlation.

The parameters S_{Ms} and f_w were varied through a range of physically plausible values while keeping the value of S_{Md} constant at 0.25 (the median value from Boelter [1968]). S_{Ms} was varied between 0.65 and 1.0; the minimum of the range is bounded by a reasonable value for shallow wetland peat sediments [Boelter, 1968], and the high end is bounded by 1, which assumes that stage within the meadow would be moving as a free water surface. f_w was varied between 0.0 and 0.35; again, higher values of f_w did not result in reasonable predictions of isotopic composition of the reservoir. Both S_{Md} and f_w were varied in 2.5% increments. Predictions of reservoir isotopic composition were calculated using the 196 parameter combinations; contours of the Nash-Sutcliffe efficiencies were plotted (Figure 32B), which depicts regions of high predictive efficiency in hashed marks and shows that the f_w is largely insensitive to changes in S_{Ms}, due to the smaller volume represented compared to the lower portion of the meadow.

Figures 32A and 32B show many parameter combinations can represent isotopic composition of the Lower Wet Meadow well when the groundwater flux is estimated as the residual of the water balance during the evaluation period. Figures 32A and 32B were prepared assuming all groundwater inputs to the system maintained an isotopic composition of riparian groundwater. Assuming all groundwater inputs maintained an isotopic composition of bedrock groundwater yields nearly identical results, except values of f_w are decreased by about 0.02 suggesting less open-water evaporation is required to achieve the observed isotopic composition. This reflects the fact that riparian groundwater was slightly more depleted (lower δ-values) relative to bedrock groundwater throughout much of the study period. The remainder of the discussion presented assumes isotopic composition of groundwater similar to that measured from riparian wells.

Additionally, the water temperature measured at s1 may be a close measure of water surface temperature. The evaporation flux-weighted average temperature from s1 is about 1.5 °C cooler than the estimate derived from direct-substitution and re-arrangement of the KP-PCE equation. Assuming surface temperature is well described by the evaporation flux-weighted average measurement from s1 results in no discernable difference in the calculation. The estimate derived from direct-substitution and re-arrangement of the KP-PCE equation is assumed for the remainder of this discussion.
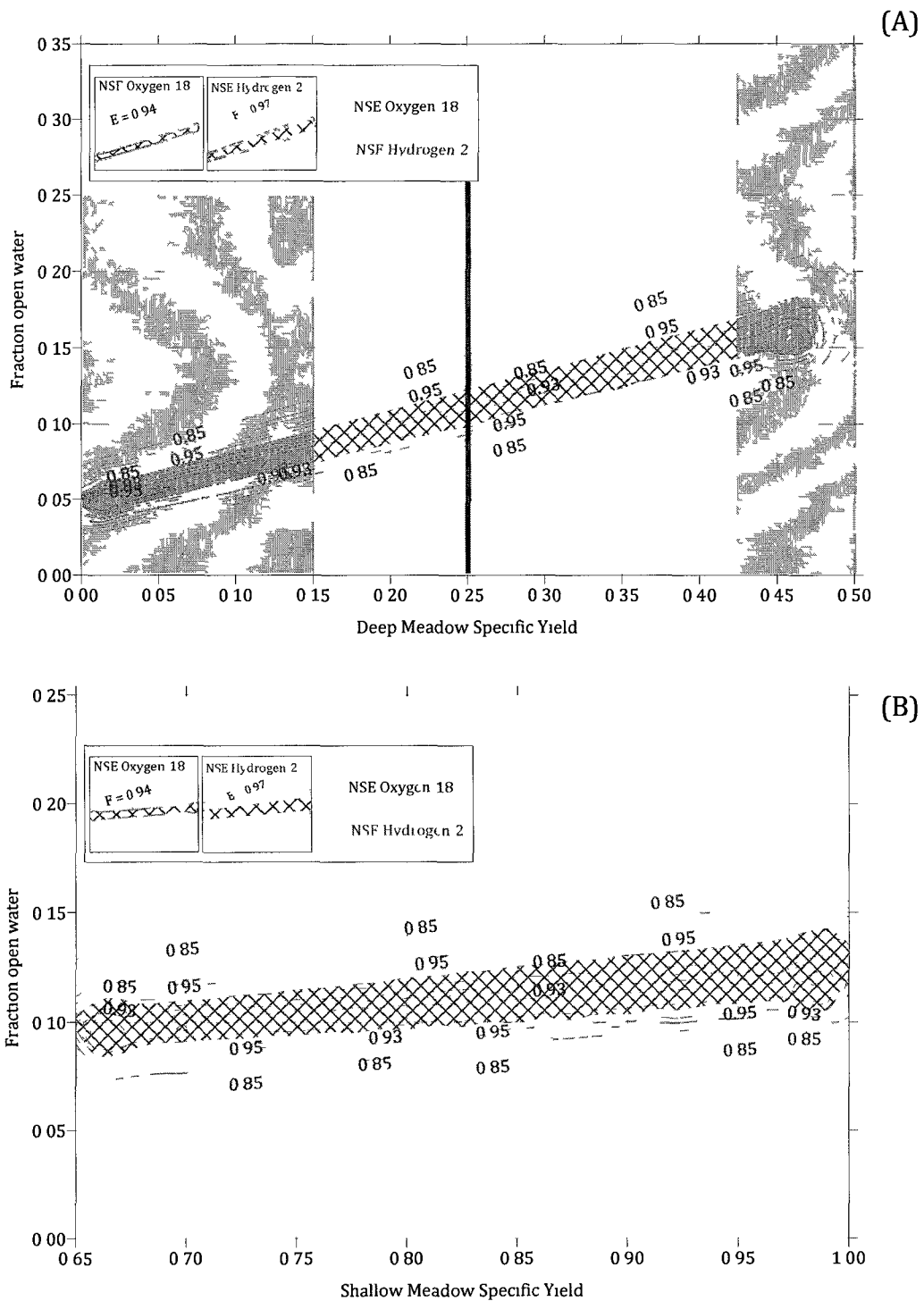
Figure 32: Contours of isotopic mass balance efficiency for various system states. The predictive efficiency (NSE) is shown as a function of (A) S_{Md} and f_w, and (B) S_{Ms} and f_w. Hatching indicates regions of highest model efficiency; high NSE values are also presented as insets with the values of the highest NSE values. Contours were generated using linear Kriging. The range and median of specific yield of deep (hemic) peat materials are identified by the unshaded region and the red vertical line [from Boelter, 1968].

4.3.2 Findings of the Mass Balance

The different values for the deep specific yield (S_{Md}) control the relative roles of fractionating evaporation versus non-fractionating evapotranspiration, which has only a minor control on the net groundwater flux. The residual of the mass balance that is attributed to the net groundwater flux; however, is controlled by the shallow specific yield of the meadow (S_{Ms}), which represents the volumetric gain or loss of water from the meadow for a given change in stage. Table 8 summarizes five parameter combinations defined by a range of values in S_{Ms}, when the values of S_{Md} and f_w were kept constant values of 0.25 and 0.10, representing the median value of peat specific yield and the corresponding value of f_w that corresponds with high efficiency models (Figure 32A). The range of values represented by Table 7 reflects values consistent with observations of the tree island wetland specific yield studied by Sumner [2007] when variation in microtopography was considered.

The role of groundwater in maintaining discharge from the outlet can be determined by the ratio of net input from groundwater to total surface outflow, defined here as the groundwater support to surface outflow (η_g) calculated as:

$$\eta_g = \frac{I_g - Q_g}{Q_S} \tag{4.1}$$

where I_g is the groundwater influx, Q_g is the groundwater outflux, and Q_S is the surface discharge leaving the Lower Wet Meadow and accommodating outflow from the catchment at s4. The groundwater support (η_g) defines the maximum fraction of surface outflow that could be contributed from the groundwater flux.

The groundwater support is defined such that an interpretation can be made regarding whether groundwater inflows may have been a primary baseflow generating mechanism that accommodated surface discharge from the Lower Wet Meadow. Table 8 summarizes values of groundwater support to Lower Wet Meadow surface discharge for the evaluation period for ranges of values of the shallow specific yield of the meadow for assumed values of S_{Md} and f_w of 0.25 and 0.10, respectively. Also included are estimates of the mean residence time (MRT) calculated as the mean estimated volume of water within the reservoir [from equation (3.12)] divided by the mean total volumetric inflows to the reservoir. Figure 33 shows a plot of predicted isotopic compositions for each of the five values of S_{Ms} from Table 8 compared to observed isotopic composition from the meadow.

As storage within the meadow decreases there is a corresponding increase in η_g. As the storage decreases, greater inflows are needed to accommodate the evapotranspiration and surface discharge fluxes from the meadow so that water balance can be maintained for the observed change in stage. Even though inflows to

Table 8: Predictive efficiency of the isotope mass balance for five values of S_{Ms}. Values of deep specific yield (S_{Md}) and open-water fraction (f_w) were kept constant at 0.25 and 0.10, respectively. Resulting values of groundwater support to outflow (η_g) and mean residence time (MRT) within the wetland are presented for each value of S_{Ms}. Values associated with the value of $S_{Ms} = 0.80$ are bolded and represent optimized model efficiencies (E > 0.95) for both $\delta_R{}^{18}O$ and $\delta_R{}^{2}H$ at values of S_{Ms} and f_w.

S_{Ms}	η_g	MRT (d)	NSE d18	NSE d2
0.6	0.27	59	0.922	0.958
0.7	0.17	63	0.942	0.978
0.8	**0.06**	**66**	**0.950**	**0.980**
0.9	-0.05	69	0.941	0.964
1.0	-0.15	72	0.910	0.935

to span the range of plausible values, the groundwater inflows to the system are at most a minor proportion of the observed discharge, or the meadow lost water to groundwater, which suggests that discharge was generated by other mechanisms.

A hydrograph of predicted component fluxes at the catchment outlet is presented in Figure 34 for the optimized value for S_{Ms}. Figure 34 suggests the role of groundwater increases throughout the summer. This is consistent with the hypothesis that groundwater would result in a larger contribution of baseflow through the summer. The finding is also suggested by analysis of NPOC and dissolved silica collected at the Lower Wet Meadow. Table 9 presents NPOC and dissolved silica results for three stations within the wet meadows, the catchment outlet, and average groundwater composition on each of the sample days from four wells (gC-1, g4-1, g4-3, and g4-6). Between 20 July and 3 August, NPOC concentrations decrease within the meadow and at the catchment outlet towards concentrations more similar to groundwater, whereas silica concentrations increase towards concentrations more similar to groundwater at the downstream sampling point of the Lower Wet Meadow and at the catchment outlet.
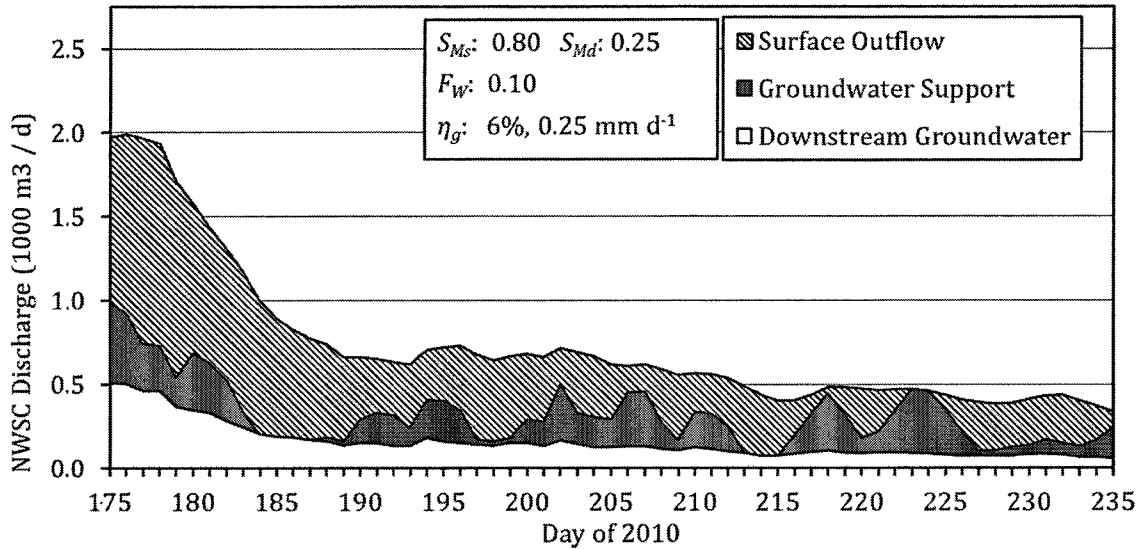
Figure 34: Discharge hydrograph of component outflow from the NWSC. Outlet discharge is estimated from the rating curve at the outlet, surface outflow from the meadow is estimated as a fraction of the catchment outflow using the isotopically derived fraction of Lower Wet Meadow (f_{lwm}), and groundwater support is calculated from the water balance as the ratio of the net groundwater flux (residual) to surface outflow from the meadow, and is presented as the 3-day moving average assuming an optimized value of S_{Ms} = 0.80.

Table 8: NPOC and dissolved silica results for the wet meadow and groundwater. The wet meadow complex was sampled at three sampling sites (s1 through s3). Samples also include the catchment outlet (s4), and mean representative groundwater (wells g4-1, g4-2, and g6-1).

	Date	s1	s2	s3	s4	GW
NPOC (mg C L^{-1})	20-Jul	6.56	7.36	8.59	9.19	1.96
NPOC (mg C L^{-1})	3-Aug	6.06	7.00	7.34	7.51	1.09
SiO$_2$ (mg SiO$_2$ L^{-1})	20-Jul	6.99	6.76	5.48	6.34	7.55
SiO$_2$ (mg SiO$_2$ L^{-1})	3-Aug	6.91	2.48	7.35	7.43	8.92

5. Discussion and Conclusions

The validity of the common assumption that baseflow is generated solely from groundwater discharge was investigated in the Northwood Study Catchment during eight weeks of baseflow recession in the summer months of 2010. The study aimed to investigate whether shallow riparian groundwater could be distinguished from evaporated sources isotopically, and whether streamflow during the baseflow recession was an apparent mixture of these sources. The isotopic composition of streamflow in any subcatchment was expected to be related to the proportion of wetlands or ponds. The relative proportion of streamflow derived from groundwater was expected to increase throughout the summer. An isotopic mass balance was developed to assess the role of groundwater inflows as support to surface discharge from an upstream wetland reservoir.

5.1 Streamflow Generation throughout the NWSC

Streamflow responses varied considerably throughout the NWSC, both in isotopic composition and magnitude, particularly run-off. It is suggested that wetlands and ponds within the catchments explain much of the variability observed, and that increasing wetland or waterbody coverage, and specifically the length of streams within these bodies result in increased run-off and the increased evaporative enrichment.

5.1.1 Isotopic Composition of Shallow Groundwater

Shallow riparian groundwater was distinguished from surface water sources (except Mountain Brook and s6) based on comparison of the mean $\delta^{18}O$ composition

of samples collected throughout the study period. The mean of shallow riparian groundwater samples appear to be similar to that observed by Frades [2008] from groundwater collected from a well set within bedrock 5 km south of the NWSC. However, shallow riparian groundwater showed more variability than bedrock groundwater due to greater influence from seasonal precipitation. At the beginning and end of the study period, the influence of depleted winter precipitation, and enriched late summer and early fall precipitation was noted throughout many of the wells. However, the observed isotopic composition of shallow riparian groundwater was not consistent with observed isotopic enrichment found in streamflow at the catchment outlet. Therefore, though shallow riparian groundwater does exhibit seasonal variation compared to bedrock groundwater, enrichment observed within inter-storm streamflow is imparted directly by storage within surface water bodies.

5.1.2   Isotopic Composition of Streamflow

The isotopic composition of streamflow varied throughout the catchment and exhibited isotopic enrichment throughout the study period. At Mountain Brook (sC) and s6, isotopic composition was not identified as distinct from groundwater at $\alpha = 0.05$. These streams have the least stream length identified within surface reservoirs though the area of the sC catchment covered by wetland or waterbody is consistent with other catchments. The headwater pond from which Mountain Brook emanates is one of the few ponds nearly absent of vegetation, a condition that is expected to impart greater potential for isotopic fractionation, such as that observed at sB. The catchment of s6 is the smallest sampled and collects hillslope drainage from Saddleback Mountain in a sphagnum covered fen located

immediately upstream of the sampling point. After 3 August, flow from the fen

ceased; however, samples collected from stagnant pools retained isotopic

composition more similar to groundwater than other surface waters. Groundwater

is considered the primary source of water from both s6 and Mountain Brook. At

both locations, streamflow ceased or nearly so (flow velocity was un-measureable

after late July in Mountain Brook) suggesting that these groundwater fed

catchments were contributing little to downstream discharge late in the summer.

Only streamflow samples from the Lamprey River at the NWSC outlet

consistently exhibited mixtures of groundwater and evaporated surface sources,

whereas this observation was expected at both Lamprey and Mountain Brooks. The

mixture between the groundwater and evaporated surface sources was exploited to

quantitatively estimate their contributing fractions; between 15 and 25% of

streamflow was estimated to be groundwater throughout the recession period. The

results of the analysis were only marginally different if a primarily riparian

groundwater source or a primarily deep bedrock groundwater source were

assumed. Actual groundwater inputs would be a combination of the two sources,

but without additional tracers that distinguish between riparian and bedrock

groundwater, it is not possible to definitively characterize a three-component

mixture in streamflow. The outlet and catchment outlet are separated by a stream

course distance of 250 m, and an additional 7 ha (0.95% of the watershed area)

drains to the outlet. The seemingly large contribution from groundwater is

considered reasonable for the specific terrain. The stream reaches downstream of

the meadow are deeply incised within gneissic schists and phyllite overlain by a

hummocky glacial deposits and significant groundwater discharge to the stream in the area is reasonable.

The confidence intervals associated with the end-member mixing fraction estimate are broad. Attributing only analytical uncertainty to each component in the mixing analysis, and disregarding known uncertainty in the spatial characterization of the components changes the estimate of f_{lwm} and its associated uncertainty little. Therefore, the majority of the uncertainty is attributed to insufficient separation between isotopic compositions of streamflow and the upstream surface reservoir.

The end-member mixing analysis makes several assumptions in evaluating the system as a binary mixture of two sources. First, it is assumed that the water within the meadow is well mixed and the isotopic composition of the wet meadow is well represented at s3 and s2, approximately 800 m and 1,100 m from the meadow outlet, respectively. The similarity in composition of samples from the meadow at s2 and s3 throughout the summer suggest homogeneity in composition throughout a large section of the meadow (Figure 28). Though sampling techniques likely yielded representation of meadow water composition to a depth of approximately 0.5 m, composition below that depth is less well represented. Gonfiantini [1986] summarized results of numerous lakes that indicate shallow lake systems typically exhibit greater mixing vertically than they do horizontally, so the observation that the Lower Wet Meadow composition is consistent at s2 and s3 may support the assumption of sufficient vertical mixing for this analysis. An additional assumption of the analysis is that there is no additional fractionation between the meadow

outlet and s4, which is reasonable considering the comparatively swift current and significant shading imparted by the channel incision and well established hemlock stand over the channel.

The conceptualization that streamflow can be isolated to two characteristic end-members is decidedly simplistic. Streamflow will contain additional sources such as drainage from unsaturated soil storage [Hewlett and Hibbert, 1963] though recent evidence suggests that in some cases, soil water may be retained in reservoirs separate from those generating baseflow [Brooks *et al.*, 2009]. An unsaturated soil source to baseflow is not characterized in this study, and would likely be represented by an isotopic composition on a continuum between antecedent evaporated surface water sources and groundwater [Barnes and Allison, 1983]. Similarly, a hyporheic drainage source would be expected to maintain an isotopic composition that reflects a mixture of groundwater and surface water sources. An additional concern in the study catchment is the possibility of discharge through or beneath the beaver dam from a deep stratified layer near the outlet of the Lower Wet Meadow that maintains a composition representing a mixture of annual precipitation (i.e. similar to groundwater). This concern can be investigated by direct sampling of deep water at the outlet and at the base of the dam; such samples have been collected but not analyzed to date. As discussed above, the groundwater end-member should be composed of a mixture of bedrock and shallow riparian groundwater discharge.

In this assessment of the groundwater-only assumption of baseflow discharge, distinguishing between groundwater components does not affect the

final interpretations. The possibility of hyporheic input to streamflow does not materially affect the interpretations either; hyporheic water is expected to reflect the relative contributions of streamflow and groundwater from which is exactly the binary mixture of interest. The possibility of soil water drainage imparting an enriched isotopic composition, or hypolimnic discharge imparting a depleted isotopic composition to streamflow could confuse the interpretation of these results. The influence of these possible effects, though they merit further consideration, is expected to be within the uncertainty already inherent in the estimate.

It was hypothesized that groundwater would represent a larger contribution to streamflow late in the summer. At the catchment outlet, a decrease in the contributing fraction from groundwater storage was suggested by the end-member mixing analysis. The decrease is not, however, resolved distinctly by the broad 95% confidence intervals, nor does it include the apparent increase in support from groundwater inflows late in the summer from the upstream Lower Wet Meadow.

Isotopic composition at Lamprey Brook and from Meadow Lake exhibited the greatest evaporative enrichment observed throughout the catchment. These catchments represent the next to the least (sA) and most (sB) coverage by wetlands or waterbodies (Table 6). However, the length of stream course through wetlands in the Lamprey Brook catchment is comparable to other catchments. The length of stream course through wetlands was found to be the best metric for describing the observed isotopic enrichment across catchments. Stream course through wetlands or waterbodies as a metric should identify only those surface reservoirs that are

connected directly to the drainage network and are more likely to contribute flow during a recession period. Upland or disconnected wetlands or waterbodies would only be expected to contribute discharge directly to the stream network during rainfall-runoff events, or by influencing the isotopic composition of shallow groundwater if the systems recharge groundwater.

5.1.3   Wetland Influences on Baseflow

Stream course through a wetland body, also appears to be an improved metric to describe the differences in subcatchment runoff. It is apparent from the hydrographs (Figures 13 and 14) that Lamprey Brook, though not logged continuously, maintained consistently high runoff throughout the study period. The consistent discharge throughout the summer suggests a stable source of baseflow generation. Groundwater inflows may provide such a source, and the greater stream course length at wetlands may indicate that these areas are locations of enhanced groundwater discharge points within the catchment, a fairly common assumption [Mitsch and Gosselink, 2000; Bullock and Acreman, 2003]. Though the Lower Wet Meadow may be unique within the catchment, groundwater inflows were not found to support a majority of discharge from the reservoir. Alternatively, the metric may reflect a nested reservoir effect where multiple surface reservoirs on the stream course act to dampen the overall recession at the outlet [Huggins, 1982]. The stream courses for Lamprey Brook and for the Lamprey River at the catchment outlet seem to exhibit such an effect, both stream segments have multiple surface reservoirs in succession (Figure 4).

Though wetlands may explain differences in runoff between subcatchments, there does not appear to be an effect on the recession rate. Recession rates for the three catchments with continuous records of discharge (sC, s1, and s4) exhibited similar changes in daily area-average runoff with respect to time throughout the study period. The three catchments had different coverage of wetlands or waterbodies and different apparent mechanisms generating baseflow. Streamflow at sC appears to have been generated primarily from groundwater discharge, whereas streamflow at the catchment outlet may have been primarily supported from upstream surface water drainage. The similarity in recessions between catchments by the derivative runoff plot (Figure 15) suggests that hydrographs from wetland-rich catchments are not distinct in form from catchments exhibiting primarily groundwater discharge. The derivative runoff plot also suggests that wetlands, and in particular the Lower Wet Meadow, may be dampening runoff response downstream. Dampened storm response was observed downstream of the Lower Wet Meadow; however, storm response at the outfall of the Upper Wet Meadow was similar to that of Mountain Brook. The Mountain Brook and Upper Wet Meadow catchments have fairly different catchment coverage; therefore it is unclear why these two catchments should respond more similar to rainfall than the Upper Wet Meadow and catchment outlet catchments.

Four possible mechanisms are suggested of how the Lower Wet Meadow may be controlling the dampening of storm-event runoff at the catchment outlet. First, the observed dampening at the outlet is a consequence of its location further down the catchment, suggesting that incremental dampening between the upper

and Lower Wet Meadows is observable, whereas incremental dampening imparted by surface reservoirs in the Mountain Brook and Upper Wet Meadow catchments is not. Secondly, the Lower Wet Meadow may have a unique and particularly high specific yield compared to other systems reservoirs within the catchment. Thirdly, ungauged catchments draining the Lower Wet Meadow below the Upper Wet Meadow outfall exhibit more dampened responses than other headwater catchments discharging to Mountain Brook or the Upper Wet Meadow. Finally, if there was a net loss to groundwater from the Lower Wet Meadow, water introduced from upstream may have promoted enhanced discharge to the aquifers resulting in a dampened stage fluctuation and surface discharge during storm events.

In summary, streamflow during interstorm periods throughout the NWSC appears to be controlled both volumetrically and isotopically by the presence of wetlands or other waterbodies. The presence of wetlands, and in particular the stream length within wetlands, appears to correlate with increased baseflow runoff from a given catchment either due to enhanced groundwater discharge or due to a nested catchment effect. A similar nested catchment effect may explain dampening of runoff during rainfall events. Isotopic enrichment from a catchment outlet also appears to correspond most closely to stream length within wetlands or waterbodies likely because this metric is a more direct measure of the role of surface reservoirs within the stream network.

5.2   Meteorologic Conditions

Meteorologic measurements used to derive evaporation estimates were

collected in the Mountain Brook catchment approximately 500 m east of the outlet

of the Upper Wet Meadow. Due to its central location and mid-slope elevation, the

tower is well suited to characterizing conditions across the catchment, and is

considered to provide a suitable estimate of conditions of the ambient atmosphere

not affected by an evaporating water body required by the assumptions of the Craig-

Gordon model of evaporative enrichment. The placement of the tower therefore

requires extrapolation of the dataset to conditions above the Lower Wet Meadow

assumed by the implementation of the Kohler-Parmele adaptation of the Penman

combination equation (KP-PCE) to estimate the evapotranspirative flux.

The investigation lacked data to directly estimate the total

evapotranspiration rate by a method such as the Bowen ratio energy balance

(BREB) or eddy covariance (EC), which is a requirement for confidence in any

wetland evapotranspiration study [Drexler *et al.*, 2004]. Further, it is unlikely that

the fetch of the Lower Wet Meadow is sufficient for reliable measurements with

either technique. Without some assessment of the spatial variability of

meteorological conditions across the meadow surface the estimate derived from the

weighted KP-PCE and associated error is expected to be incomplete [Wessel and

Rouse, 1994]. Wessel and Rouse compared three versions of the combination

equation to BREB measurements and found RMSE values of the latent heat flux (λE)

ranging from 40 to 150 W m^{-2} which correspond to errors in the evaporation rates

comparable to less than 0.1 mm h^{-1} when using instrumentation at the wetland

surface (as opposed to on an adjacent hillslope as in done in this study). The RMSE estimated under those ideal conditions was comparable to the evaporation flux estimated using data from the NWSC for early morning or late afternoon hours throughout much of the study period, and relates to a daily estimate of error of about 1.44 mm, an error of 30% of the daily average estimate at 70% confidence.

To assess the degree of sensitivity of the formulation of the KP-PCE the four primary field data (windspeed, solar radiation, air temperature, and water vapor pressure) were varied by up to 10%. For the dataset, windspeed was found to be most sensitive, and is expected to vary spatially within the Lower Wet Meadow as much as between the Lower Wet Meadow and the measurement point; therefore sensitivity was tested for a total combined effect as well as for a combined effect with constant (measured) windspeed. Deviations of -20 to +25% from measured values were predicted for total evaporation over the evaluation period. These values are expected to bound the true estimate of the thin film open-water PCE estimate experienced at the meadow surface; however, they still neglect the water stored energy. The isotopic mass balance model discussed in more detail below predicts the observed isotopic compositions well at measured values.

The humidity realized at the water surface within the meadow is controlled by the transport of water vapor from the surface, which is related to the atmospheric conductance in the PCE. The formulation of the atmospheric conductance employed in the PCE focuses on turbulent conditions above the canopy, and is described the Prandtl-von Karman Universal Velocity Distribution [Dingman, 2002] and therefore assumes zero conductance below the canopy at the water

surface. Furthermore, the formulation also neglects filtering of incoming radiation to the surface. A more complete description of evaporation at the meadow surface would describe an atmospheric conductance greater than zero at the meadow surface and explicitly treat the filtration of radiation in accordance with Beer's Law through vegetation; both processes could be improved by a treatment similar to that of Shuttleworth and Wallace [1985] or Herbst and Kappen [1999].

Incorporation of sub-canopy turbulence and radiation filtering effects is expected to decrease the overall surface area experiencing open-water evaporation required to maintain the water balance while respecting observed isotopic composition. Lower temperatures would likely be realized at the evaporating surface thereby increasing the equilibrium fractionation factor and imparting more fractionation for a lesser amount of evaporation. Further improvements to the characterization of fractionation at the evaporating surface would include incorporation of water stored energy flux into the surface energy balance approximation of surface temperature, or direct measurement of the surface temperature. Finally, improvements to the kinetic enrichment factor may be realized by explicit evaluation of the flow regime at the evaporating surface [Merlivat and Jouzel, 1979, Brutsaert, 1975a,b]. Assumptions of the appropriate exponent n in the theoretical development of the kinetic enrichment factor presented as equation (1.23, §1.3.4) were developed generally from work in marine and large lake environments, and may not be applicable for highly vegetated pools where a smooth horizontal surface is punctuated by emergent vegetation.

Though direct precipitation to the meadow was comparatively small during the evaluation period (75 mm gross), the precipitation flux was still significant to the meadow surface (8,000 m^3). Therefore, the effect of interception on the water balance within the meadow may be important. The formulation of the Liu [1997, 2001] model of interception, with the simplification to the evaporation treatment, has not been explicitly verified on an existing dataset of measured throughfall, and literature sources typically focus on total event rainfall making direct comparisons of error and validity of the continuous interception formulation used herein impossible at present. While the formulation has not been tested against field observations it is still preferred to other methods because it has been shown to be efficient compared to alternative methods in describing the interception process in total storm formulations and requires fewer assumptions of parameter values [Liu, 2001; Carlyle-Moses and Price, 2007; Carlyle-Moses *et al.*, 2010].

5.3   Implications of the Water Balance

Net groundwater inflow as the residual was estimated to be a relatively minor contribution (<27 %) of wetland surface discharge throughout the range of tested parameter values. For values of S_{Ms} equal to or greater than 0.90, the volumetric water balance predicted a net recharge to the groundwater system from meadow. Considering the meadow is dammed, it is considered possible that groundwater head adjacent to the meadow dropped below the wetland stage during the dry summer of 2010 and that a leaking reservoir is possible. For a range of plausible values for specific yield of the meadow surface, no more than 45% of

discharge at the NWSC outlet is expected to be derived from groundwater influx to the wet meadow or downstream reaches, suggesting a groundwater-only assumption to baseflow generation for the summer 2010 at NWSC would be unfounded. The remainder of possible sources includes delayed release of intermittent precipitation, upstream surface flow (early in the evaluation period), or a release from storage. Quantitative evaluation of other baseflow generation mechanisms was not conducted as part of this investigation.

5.3.1 *Specific Yield of the Meadow and Open Water Fraction*

Investigation of the mechanisms generating surface outflow from the Lower Wet Meadow, which is estimated to represent about 75% of outflow from the catchment, is explored using an isotopic mass balance estimate. The role of groundwater in supporting outflow from the Lower Wet Meadow was estimated by 1) closing a water balance calculation assuming the residual is attributed to the net groundwater flux, 2) using approximated isotopic compositions of the component fluxes to compute the isotopic composition of the Lower Wet Meadow, and 3) evaluating the groundwater flux for parameter combinations that honor the observed isotope composition.

The water balance calculation was non-unique for a range of parameters that control the available volume for water within the meadow peats and hollows (S_{Md}) and at the surface (S_{Ms}) and the fraction of the meadow surface area experiencing open-water evaporation (f_w) as opposed to non-fractionating transpiration. Areas of highest model efficiency are associated with parameter combinations between S_{Md} or S_{Ms} and f_w that exhibit positive correlation. The positive correlation arises from

the fact that additional evaporative enrichment, achieved through increases in the surface area experiencing evaporative fractionation (f_w), is required to offset greater reservoir volume implied by greater yield (S_{Ms} or S_{Md}). Parameter sets that adequately predict isotopic composition result in different volumetric water balances and component fluxes. Further characterization of either the specific yield at the surface (S_{Ms}) or vegetative cover of the open water surface (to estimate f_w) will significantly improve the estimate of groundwater inflow support to the overall flux out of the meadow.

The parameter combinations that provide the best isotopic predictions are those that optimize the NSE for both $\delta_R^{18}O$ and δ_R^2H above NSE values of 0.95. Optimization corresponds with a surface specific yield of the meadow at about 0.8 when the fraction of open water is set to about 0.10 and the deep yield of the meadow is set to 0.25, the median value for specific yield of similar peat material [Boelter, 1967]. Measurements or assumptions of surface specific yield are generally close to unity in studies of surface flow wetlands [Mitsch and Gosselink, 2000, Kadlec and Knight, 1996; Krasnostein and Oldham, 2004; Hunt et al., 1996]. The value of S_{Ms} was expected to be less than unity in the Lower Wet Meadow due to variable microtopography and the presence of hummocks or mounds at the water surface. To date, no rigorous field survey has been conducted to assess the microtopography of the Lower Wet Meadow. A value of S_{Ms} = 0.80 is well represented in a study of wetland specific yield in Florida that did incorporate the effects of microtopography [Sumner, 2007].

The physical meaning of f_w is more difficult to observe readily, as the factor accounts for more than just the spatial coverage by vegetation. The fraction of area experiencing open-water evaporation will also account for impeded fractionating open-water evaporation due to plants filtering radiation at the water surface and buffering wind and physical conductance of water vapor at the water surface. Vegetation cover is significant throughout the meadow and a value of f_w close to 10% seems appropriate. Again no rigorous field survey of plant cover that f_w can be compared to has been conducted to date. Few studies have exhaustively investigated the fraction of open-water in wetland environments; Wessel and Rouse [1994] found that open water fraction varied from 0 to 60% of the total surface area in a sub-arctic tundra wetland, which may correspond with the values of f_w observed for the Lower Wet Meadow. Krasnostein and Oldham [2004] used a similar partitioning of the evapotranspirative flux between transpiration and open water evaporation in a lumped parameter bucket model of a wetland system, though they do not report their fraction of cover occupied by macrophytes. The U.S. Fish and Wildlife Service suggest that the forested, shrub, and emergent palustrine wetlands that constitute the wet meadow complex are *dominated* by vegetation [Tiner, 2010]. Other wetland types with proportional less vegetative cover are indicated as having less than 30% vegetation cover.

5.3.2   Comparison to Other Studies

The net groundwater flux with the wet meadow ranged from an average loss of 0.6 mm d^{-1} from the meadow to a gain of 1.1 mm d^{-1}; for the optimized value of S_{Ms} of 0.8 the volumetric balance suggests a net inflow from groundwater of 0.25 mm d^{-}

1. Several studies have evaluated the inflow of water to wetlands from which we can infer their support of surface outflow. Hunt and others [1996] estimated groundwater influx between 2 and 8 mm d^{-1} for four riparian (one constructed) wetlands adjacent to the Kickapoo River in southwestern Wisconsin using four different methods (Darcy's law, stable isotope mass balance, temperature profiling, and numerical groundwater modeling). Roulet [1990] estimated that 45 mm d^{-1} of groundwater entered a series of wetlands in southern Ontario, and the rate varied little seasonally. O'Brien [1977 and 1980] estimated that between 93% and 96% of annual discharge from two small low-relief catchments dominated by the presence of wetlands in eastern Massachusetts was derived from groundwater inflows to the wetlands.

The difference between average groundwater inflow rates during the evaluation period and those reported by Hunt and others [1996] and Roulet [1990], may reflect the isolated season of this investigation. In the NWSC, groundwater depth declined steadily through the summer. Only two wells are set immediately adjacent to the wet meadow complex (gD-1 and g6-1), and neither was surveyed to a consistent datum with the stilling well set within the Lower Wet Meadow (s3). Groundwater depth was likely similar to water stage in the meadow through much of the summer; however, because both wells dried late in the season, it would not be possible to determine whether the stage and water table differences suggested a losing or gaining flux between the groundwater and Lower Wet Meadow. Because the groundwater elevation within riparian wells was observed to drop 30 cm through the summer, the groundwater influx to the meadow, at least from riparian

groundwater storage, and the estimate of -0.6 to 1.1 mm d^{-1} may be an annual low. It is not clear whether such a seasonal decline in water table, and corresponding decrease in expected flux, should be anticipated for any bedrock groundwater flux.

5.3.3   Errors Associated with Water Balance

Direct uncertainty associated with the groundwater component of the water balance has not been quantified. As discussed in §3.2, the dataset does not include spatial variability of the atmospheric conditions at the Lower Wet Meadow, or direct estimates of two sensitive parameters, specific yield and open-water area. The water balance calculation utilizes several sources of data that have error approaching 100% associated with their estimate (discharge at in-flowing and out-flowing gaging points, isotopically derived mixing fraction utilized to estimate outflow from the Lower Wet Meadow, daily estimated isotopic composition of several input fluxes), and other data that have un-quantified error (discharge from ungauged catchments, isotopic composition of the atmosphere, water surface temperature, evaporation and transpiration rates). The Kohler-Parmele adaptation of the Penman Combination Equation (KP-PCE) requires assignment of several terms and local representative measurements are not available. Furthermore, groundwater was calculated as the residual in the water balance and a summary by Winter [1981] for lakes suggests that this can result in errors of 100%.

Stable isotopic mass balance studies of surface reservoirs cite several complications in the method derived from variability of meteorologic conditions over the reservoir surface. Previous investigations have suggested that with spatially variable humidity over a lake surface and the isotopic composition of

atmospheric water vapor (δ_A) over a water body are the most sensitive parameters in isotopic mass balance studies of lakes (see Gonfiantini [1986] for summary). Furthermore, it has also been observed that the evaporative flux itself may present a significant fraction of the water vapor over the lake [Benson and White, 1994] making measurements of δ_A difficult even when the resources to do so are available. The isotopic composition of atmospheric water vapor (δ_A) was not measured in the context of this study. Improvements to predictions of isotopic water vapor may be achieved by including information regarding the historic trajectories of weather patterns [e.g. Sjostrom and Welker, 2009], but is not considered herein and is only related to average precipitation falling between sampling dates and observed atmospheric humidity.

Further work should include characterization of the spatial distribution of humidity, temperature, and mixtures of lake evaporate to the atmospheric composition of the atmosphere in the approximation of the fractionating enrichment of the Lower Wet Meadow. The spatial distribution of humidity and temperature should be of critical importance to any assessment that attempts to estimate the error associated with the evaporation or evapotranspiration flux calculated by the KP-PCE.

From 29 June to 27 July inflow from s1 (Upper Wet Meadow) was equal or up to eight times greater than estimated inflow from ungauged catchments; however, after 27 July, outflow from s1 dropped precipitously and ungauged catchment discharge estimates were greater. During the evaluation period, stage within the upper meadow dropped below the earthen dam that forms Old Mountain Road, a

historic logging road that forms the impoundment between the two meadows. Throughout much of the evaluation period, stage at this point was too low to permit accurate discharge measurements and discharge estimates are based on extrapolation of the rating curve (Figure 11, Section 2.4.3). Interflow was still evident through macropores beneath the earthen dam, justifying continuous non-zero estimates of discharge between the meadows. The quality of extrapolation of runoff estimates from sC to ungauged catchments is unclear; however, extrapolation of the rating curve below measured values was less prevalent (23% of evaluation period) than at s1 (63% of evaluation period).

To investigate the relative importance of some of the above sources of error to the isotopic mass balance of the Lower Wet Meadow, a Monte-Carlo simulation was run testing the effect of introducing observed error to the predictions of the Lower Wet Meadow composition. All errors were assumed to be normally distributed and random values falling on the standard normal distribution were calculated using the Box-Muller method [Box and Muller, 1958]. Errors associated with the isotopic composition of inflows (daily values) were varied from expected values assuming that the error associated with the flux was well characterized by the RMSE of the regression trend estimate. Errors associated with the estimate of δ_A from the regression estimates were assumed to be well represented by the standard deviation of the results of the individual estimates; uncertainty between δ_A prediction models appears greater than that observed within individual studies [White and Gedzelman, 1984; Jacob and Sonntag, 1991; Lee *et al.*, 2005; Lee *et al.*, 2006]. Uncertainty in daily discharge was estimated as the daily sum of uncertainty

on hourly discharge data. Errors associated with Lower Wet Meadow drainage included both the error on discharge at s4, and uncertainty on f_{lwm}. To reiterate a previous point, these measures of uncertainty in the mass balance estimate do not include the spatial variability of parameters describing the evaporation estimate or the conditions at the water surface that describe the evaporative fractionation, so only measure a portion of the real uncertainty in the estimate.

The simulations were run assuming a base scenario of the median value for S_{Md} of 0.25, the f_w that results in minimum error (0.10) at S_{Md} = 0.25, and the value of S_{Ms} that optimizes the NSE in $\delta^{18}O$ and δ^2H (0.80). The four expected sources of error were varied individually according to their normal estimates of error to assess how the different sources of error contribute to the overall error in the estimate. For each error source, the water balance was calculated 1,000 times and the resulting predicted composition of the Lower Wet Meadow on four sampling dates were recorded (Figure 35). The simulations were repeated assuming groundwater inputs were derived from riparian groundwater and from bedrock, and also assuming surface temperature could be adequately represented by measurement of water temperature at s1. No differences in predictions were discerned between the assumption of groundwater source or surface temperature estimate. Only results of simulations that assumed riparian groundwater input and surface temperature calculated from the KP-PCE are presented in Figure 35.

Uncertainty in streamflow estimates and in surface discharge from the Lower Wet Meadow result in the largest predictive errors of the four sources tested. The range of the prediction clouds for both of these sources of error appear comparable
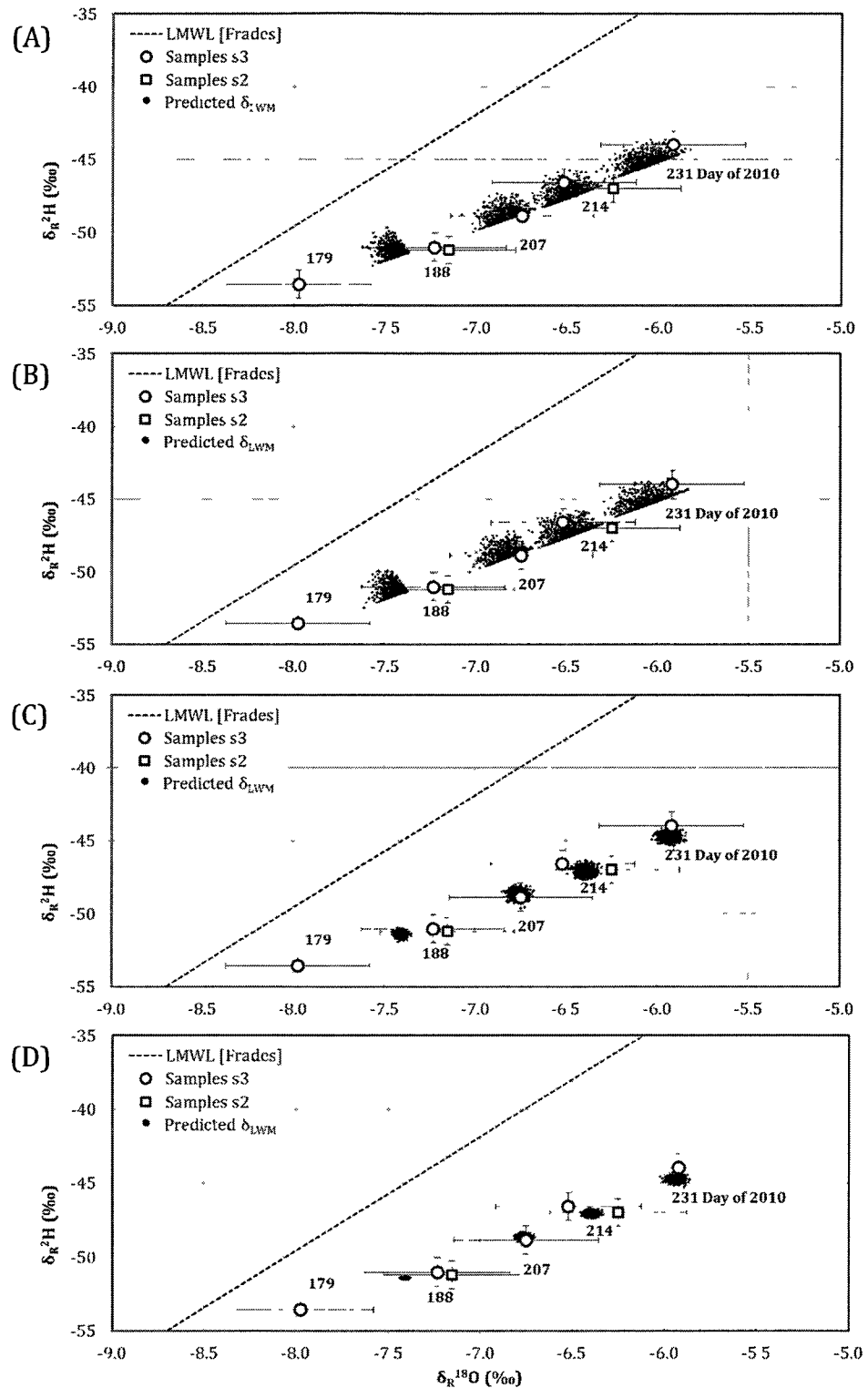
Figure 35: Effect of data uncertainty on mass balance. Effects of data uncertainty shown for: (A) surface discharge at sC, s1, and s4, (B) surface discharge from the Lower Wet Meadow, (C) isotopic composition of atmospheric water vapor, (D) isotopic composition of input fluxes. Each plot represents 1,000 calculations.

in magnitude to analytical error of the observations. The range of the prediction cloud for the isotopic composition of the atmospheric water vapor is comparable in magnitude to the analytical uncertainty for δ^2H observations; however, the cloud is within analytical uncertainty for $\delta^{18}O$ observations. Prediction errors associated with the uncertainty in the isotopic composition of input fluxes, though only loosely constrained by the trend regressions, are less than analytical uncertainty of the measurements to which they are compared. Figure 35 illustrates that the effect of uncertainty in volumetric measurements in the isotopic mass balance are comparable to analytical uncertainty for stable isotopic composition of any individual water sample. To refine the estimate of the net residual (groundwater) flux with the Lower Wet Meadow, most predictive improvement would be achieved by significant improvements to discharge measurements.

The total investigated prediction uncertainty includes the four sources of error discussed above, as well as the analytical uncertainty associated with the sample representing the initial condition of the Lower Wet Meadow. The total investigated prediction error is depicted in Figure 36 for 1,000 simulations assuming the base scenario used above. Figure 36 investigates the effect of lack of constraint in the estimates of S_{Ms} and S_{Md} in addition to total investigated prediction uncertainty. Variability in either specific yield was taken from a uniform distribution bounded by upper and lower values of specific yield for representative peat materials (S_{Md}), or the lower bound of representative peat materials and an upper bound of 1 (S_{Ms}). The value of f_w was kept constant at 0.1 throughout the simulations. Variability in the values of S_{Ms} alone has little additional effect on the
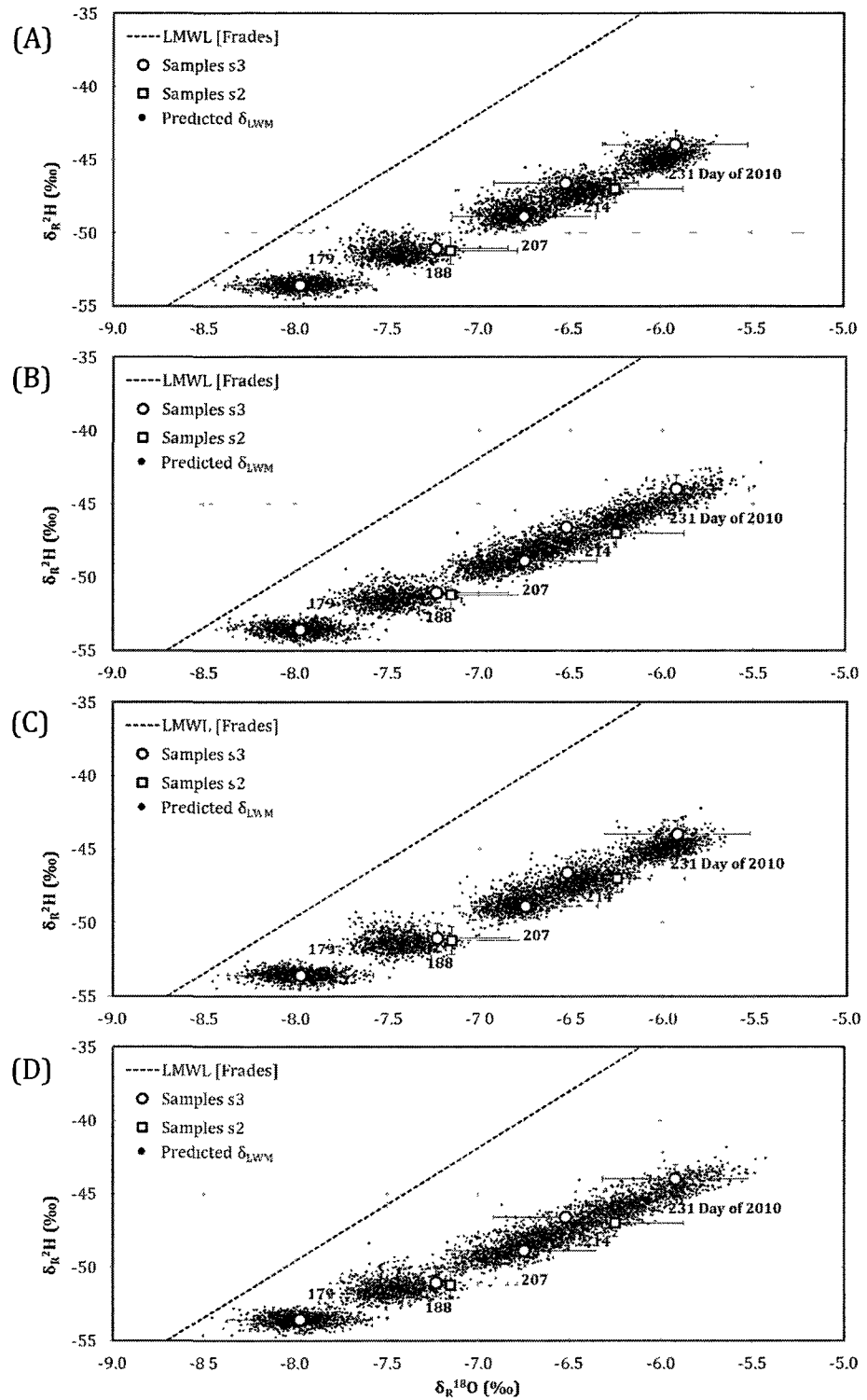
Figure 36: Effect of data uncertainty and lack of constraint of specific yield on mass balance. Each plot represents 1,000 randomized inputs from a Gaussian. (A) S_{Ms} = 0.825, S_{Md} = 0.25 (B) S_{Ms} = 0.825, 0.15 ≤ S_{Md} ≤ 0.45 (C) 0.65 ≤ S_{Ms} ≤ 1.0, S_{Md} = 0.25 (D) 0.65 ≤ S_{Ms} ≤ 1.0, 0.15 ≤ S_{Md} ≤ 0.45. Randomized values of S_{Ms} and S_{Md} taken from a uniform distribution.

predictive uncertainty of the isotopic composition of the reservoir, though the residual (groundwater) flux is entirely dependent on this parameter. In contrast, S_{Md} has little effect on the prediction of the groundwater flux but a greater effect on the predictive efficiency of the average isotopic composition of the reservoir experiencing evaporative enrichment.

The total uncertainty in the predictions from the isotopic mass balance estimate is roughly comparable to the analytical uncertainty in the measurement of the isotopic composition of the Lower Wet Meadow. The lack of constraint on S_{Md} adds more variability to the prediction than S_{Ms}, but in the formulation of the mass balance, changes in value of S_{Md} could be accommodated by relatively small changes in f_w such that predictions remain more consistent with observed values. Lack of constraint on S_{Ms} introduces little additional variability to the overall estimate of the mass balance though relatively small changes in the value of this parameter result in a net loss to groundwater transitioning to a net inflow of groundwater. The uncertainty investigated results in an uncertainty comparable to that reported by Winter [1981] regarding the volumetric water balance of lakes. Stable isotopes are therefore not considered to substantially improve the magnitude of the groundwater flux component or specific yield parameters for the lower wet meadow during the dry summer of 2010 over purely volumetric balance when the residual flux was small. The isotopic mass balance method would be better suited to evaluating the magnitude of greater flux rates, where the differences in isotopic compositions of reservoirs will have greater influence on the overall mass balance.

5.4   Summary

The assumption of baseflow generation from primarily groundwater sources was investigated within the Northwood Study Catchment (NWSC), a 740 ha temperate headwater catchment with a significant area covered by wetlands or ponds. The study used isotopic mass balance to investigate whether baseflow could be accommodated by inflows to the stream from groundwater. The stable isotopic composition of riparian groundwater varied throughout the summer in parallel with summer precipitation; however, the departure in isotopic composition of groundwater from an apparent annual average was less than the enrichment observed in streamflow at the catchment outlet. Stable isotopes distinguished between surface and groundwater sources. Surface water samples from subcatchments of the NWSC exhibited evaporative enrichment, and increasing evaporative enrichment correlates with increased wetland coverage, particularly with increases in the fraction of catchment stream course within wetlands. Moreover, area-average runoff increased with the increasing stream course within wetlands suggesting that wetlands may be either acting as groundwater discharge locations, or the progressive nested nature of these surface reservoirs within these catchments prolong the baseflow recession. Catchments with greater wetland coverage (s1 and s4) and characteristic isotopic enrichment of surface detention did not appear to exhibit consistent differences in the derivative of the runoff hydrograph from the sC catchment, which exhibited consistent groundwater inputs through the summer. This suggests that volumetric measurements alone may be insufficient to distinguish between recession characteristics resulting from the

drainage of surface or groundwater reservoirs. Considerations of similar wetland systems as baseflow generating stores should be considered in the performance of baseflow recession analyses.

Binary-mixing suggests that at the catchment outlet, less than half, and likely only about 20 – 30% was derived directly from groundwater input. The fraction of groundwater inputs to the catchment outlet did not increase through the summer as expected. The remainder of catchment discharge is assumed to be from a beaver-dammed wet meadow located about 250 m upstream of the catchment outlet. Discharge from the meadow, and from the catchment, exhibited an isotopically enriched composition attained through prolonged detention within the meadow complex. An isotopic mass balance of the meadow was developed and for a range of values of the surface specific yield of the meadow, bounded by representative values for specific yield of peat materials and by a free water surface, groundwater inflows were estimated to be no more than 27% of observed discharge from the meadow. Therefore, groundwater is not considered to have accommodated all baseflow discharge from the NWSC during the summer 2010. Groundwater inflows may have increased through the summer as evidenced by the isotopic mass balance, and results of dissolved silica and non-particulate organic carbon samples.

The isotopic mass balance was forced by estimates of the magnitude and composition of the associated hydrologic fluxes. Four potential sources of error to the water balance were investigated using a Monte-Carlo simulation. Predictive uncertainty in characterizing the isotopic composition of an evaporating reservoir

was comparable to the analytical uncertainty of any individual sample of the reservoir, even when the errors on input data were as high as 100%. Estimates of streamflow were found to be the biggest source of error in the water balance estimate, and improvements to its estimation would propagate to much greater certainty in the mass balance predictions. The lack of constraint on values of the surface specific yield of the meadow introduced negligible uncertainty to the predictions.

The mass balance predicts that the water balance of the Lower Wet Meadow was largely balanced without a net groundwater component. The predicted groundwater flux ranged from a net average loss of 0.6 mm d^{-1} to a net average gain of 1.1 mm d^{-1}, much lower than similar investigations. The low or absent groundwater inflows may reflect the dry seasonal nature of the investigation or the impoundment of the meadow. The impoundment may retard surface discharge such that stage is sustained above average head surrounding the meadow, implying a lower conductance through the dam than through aquifer materials. Groundwater leakage from the meadow may also explain the significant dampening of small storm events downstream of the Lower Wet Meadow at the catchment outlet.

The above analysis provides an example of baseflow generation emanating from a detained surface water source during drier than normal summer conditions for a near-coast temperate watershed. The water balance estimate suggests that groundwater inflows were a significant, but not the exclusive, source of streamflow

leaving the meadow during the summer of 2010. Additional work should focus on other baseflow generating mechanisms responsible for the streamflow observed.

For values of the deep and shallow specific yields at the high ends of the ranges considered plausible (S_{Md} = 0.6 and S_{Ms} = 0.95) mean residence times may be as high as 110 days within the meadow. Such residence times imply that outflow from the meadow observed throughout the summer may have still been supported by storage from significant rain and snowmelt observed in March 2010. At lower values of specific yield, mean residence times within the meadow are no less than 60 days. For the dry study period, these residence times are slightly greater than those estimated by Frades [2008] for the evaporatively enriched component of baseflow. The wet meadow complex within the NWSC may be an ideal study area to investigate the attenuation of atmospheric pollutants in New England. The linear series of wet meadows with significant summer residence time, significant plant coverage, and a large surface area for the relative shallow depth, should present ample opportunity for attenuation of atmospheric nitrogen or mercury inputs.

It is important to consider wetland systems within the Lamprey River, and possibly other near-coast temperate watersheds with extensive wetland complexes, in planning our water resource needs in a changing climate. If snowmelt continues to be pushed earlier in the year [Hodgkins and Dudley, 2007], or precipitation in the northeast becomes more seasonal [Hayhoe et al., 2006], understanding where late summer streamflow is derived will become increasingly important. The importance of understanding the role of surface storage in baseflow generation is particularly

important considering these reservoirs experience significantly greater evaporative loss than the groundwater sources typically assumed to generate baseflow.

For the range of values of the specific yield of the meadow used in calculations, isotopic enrichment consistent with observations could be imparted by only between 10 to 20% of the meadow area experiencing fractionating open-water evaporation. The isotopic mass balance method employed herein may be an effective tool in determining the relative fluxes of open-water evaporation and plant transpiration on the total evapotranspiration flux in similar emergent wetland environments.

References

Abbott, M.D., Lini, A., Bierman, P.R., 2000. $\delta^{18}O$, δD, and ^3H measurements constrain groundwater recharge patterns in an upland fractured aquifer, Vermont, USA. Journal of Hydrology, 228, 101-112.

Allen, R.G., Pereira, L.S., Raes, D., Smith, M., others, 1998. Crop evapotranspiration-Guidelines for computing crop water requirements-FAO Irrigation and drainage paper 56. FAO, Rome, 300pp.

Arnold, J.G., Allen, P.M., 1999. Automated methods for estimating baseflow and ground water recharge from streamflow records. Journal of the American Water Resources Association, 35, 411-424.

Baillie, M.N., 2005. Quantifying baseflow inputs to the San Pedro River: A geochemical approach. Thesis, University of Arizona.

Barnes, C., Allison, G., 1983. The distribution of deuterium and 18O in dry soils 1. Theory. Journal of Hydrology, 60, 141-156.

Benson, L.V., White, J.W.C., 1994. Stable isotopes of oxygen and hydrogen in the Truckee River-Pyramid Lake surface-water system. 3. Source of water vapor overlying Pyramid Lake. Limnology and Oceanography, 39, 1945–1958.

Boelter, R.M., 1968. Important Physical Properties of Peat Materials. *in* Proceedings of the Third International Peat Congress. International Peat Congress, Quebec, Canada, pp. 150-154.

Bond, B.J., Jones, J.A., Moore, G., Phillips, N., Post, D., McDonnell, J.J., 2002. The zone of vegetation influence on baseflow revealed by diel patterns of streamflow and vegetation water use in a headwater basin. Hydrological Processes, 16, 1671-1677.

Box, G.E.P., Muller, M.E., 1958. A Note on the Generation of Random Normal Deviates. Annals of Mathematical Statistics, 29, 610-611.

Bristow, KL, 1987. On solving the surface energy balance equation for surface temperature. Agricultural and Forest Meteorology, 39, 49-54.

Brooks, R.J., Barnard, H.R., Coulombe, R., McDonnell, J.J., 2009. Ecohydrologic separation of water between trees and streams in a Mediterranean climate. Nature Geosciences, 3, 100-104.

Brutsaert, W, 1975a, A theory for local evaporation (or heat transfer) from rough and smooth surfaces at ground level. Water Resources Research, 11(4), 543-550.

Brutsaert, W, 1975b, The roughness length for water vapor, sensible heat, and other scalars. Journal of the Atmospheric Sciences, 32, 2028-2031.

Brutsaert, W., Nieber, J.L., 1977. Regionalized drought flow hydrographs from a mature glaciated plateau. Water Resources Research, 13, 637-643.

Brutsaert, W., Lopez, J.P., 1998. Basin-scale geohydrologic drought flow features of riparian aquifers in the Southern Great Plains. Water Resources Research, 34, 233.

Buchanan, T.J., Somers, W.P., 1969, Discharge Measurements at Gaging Stations, Chapter A8, Techniques of Water-Resources Investigations of the United States Geological Survey, Book 3, Applications of Hydraulics. United States Geological Survey, Washington, D.C., USA.

Bullock, A., Acreman, M., 2003. The role of wetlands in the hydrological cycle. Hydrology Earth Systems Science, 7, 358-389.

Burnett, A.W., Mullins, H.T., Patterson, W.P., 2004. Relationships between atmospheric circulation and winter precipitation in $\delta^{18}O$ in central New York. Geophysical Research Letters, 31: L22209.

Burns, D.A., McDonnell, J.J., Hooper, R.P., Peters, N.E., Freer, J.E., Kendall, C., Beven, K., 2001. Quantifying contributions to storm runoff through end-member mixing analysis and hydrologic measurements at the Panola Mountain Research Watershed (Georgia, USA). Hydrological Processes, 15, 1903-1924.

Burtt, ME, 2010. History and Remembrances of The Northwood Meadows State Park, Northwood, Rockingham County, New Hampshire, Including the history of the area in colonial times, pictures, aerial photos, maps and points of interest. Also the daily record of the construction work as well as personal experiences. Published Privately, May, 1994, Fourth printing, April, 2010.

Buttle, J., 1994. Isotope hydrograph separations and rapid delivery of pre-event water from drainage basins. Progress in Physical Geography, 18, 16-41.

Buttle, J.M., Peters, D.L., 1997. Inferring hydrological processes in a temperate basin using isotopic and geochemical hydrograph separation: a re-evaluation. Hydrological Processes, 11, 557-573.

Cappa, C.D., Hendricks, M.B., DePaolo, D.J., Cohen, R.C., 2003. Isotopic fractionation of water during evaporation. Journal of Geophysical Research, 108, 4525.

Carlyle-Moses, D.E., Price, A.G., 2007. Modelling canopy interception loss from a Madrean pine-oak stand, northeastern Mexico. Hydrological Processes, 21, 2572-2580.

Carlyle-Moses, D.E., Park, A.D., Cameron, J.L., 2010. Modelling rainfall interception loss in forest restoration trials in Panama. Ecohydrology, 3, 272-283.

Chow, V.T., 1959, Open-Channel Hydraulics, The Blackburn Press, New Jersey, USA.

Coplen, T.B., 1996. New guidelines for reporting stable hydrogen, carbon, and oxygen isotope-ratio data. Geochimica et Cosmochimica Acta, 60, 3359-3360.

Cowardin, L.M., Carter, V., Golet, F.C., LaRoe, E.T., 1979. Classification of Wetlands & Deepwater Habitats of the US. U.S. Department of the Interior, Fish and Wildlife Service, Washington, D.C.

Criss, R.E., 1999. Principles of Stable Isotope Distribution. Oxford University Press, New York, New York.

Craig, H., 1961. Isotopic Variations in Meteoric Waters. Science, 133, 1702-1703.

Craig, H., Gordon, L., Horibe, Y., 1963. Isotopic exchange effects in the evaporation of water. Journal of Geophysical Research, 68, 5079-5087.

Craig, H., Gordon, L.I., 1965. Isotopic Oceanography: Deuterium and Oxygen 18 variations in the ocean and marine atmosphere. Marine Geochemistry, 3, 277-374.

Daley, M, J Potter, E Difranco, WH McDowell, 2010. Nitrogen assessment for the Lamprey River Watershed. New Hampshire Water Resources Research Center, Department of Natural Resources, University of New Hampshire. prepared for the New Hampshire Department of Environmental Services.

Dansgaard, W., 1964. Stable isotopes in precipitation. Tellus, 16, 436-468.

Dawson, T.E., Ehleringher, J.R., 1998. Plants, Isotopes, and Water Use: A Catchment-Scale Perspective. in Isotope Tracers in Catchment Hydrology, eds. C Kendall and JJ McDonnell, Elsevier, Amsterdam.

Dinçer, T., 1968. The Use of Oxygen 18 and Deuterium Concentrations in the Water Balance of Lakes. Water Resources Research, 4, 1289.

Dingman, S.L., 2002, Physical Hydrology, Second Edition, Waveland Press, Illinois, USA.

Drexler, J.Z., Snyder, R.L., Spano, D., Paw U, K.T., 2004. A review of models and micrometeorological methods used to estimate wetland evapotranspiration. Hydrological Processes, 18, 2071-2101.

Ehalt, D., Knott, K., 1965. Kinetische Isotopentrennung bei der Verdampfung von Wasser. Tellus B, 17, 389-397.

Flanagan, L.B., Ehleringer, J.R., 1991. Stable isotope composition of stem and leaf water: applications to the study of plant water use. Functional Ecology, 5, 270–277.

Flint, S.A., 2007. Impacts of palustrine wetlands on surface water quality in the Lamprey River Watershed, NH. Thesis, University of New Hampshire.

Flynn, R., Tasker, G., 2004. Generalized estimates from streamflow data of annual and seasonal ground-water-recharge rates for drainage basins in New Hampshire. Scientific Investigations Report 2004-5019, U.S. Geological Survey, Pembroke, New Hampshire, USA. 67pp.

Frades, M.C., 2008. Hydrologic analysis of the headwaters lamprey river watershed using water isotopes. Thesis, University of New Hampshire.

Frades, M.C., Davis, J.M., Bryce, J.G., McDowell, W.H, In Prep. Isotopic characterization of (baseflow in the) Headwaters Lamprey River Watershed, New Hampshire USA.

Freeze, R.A., Cherry, J.A., 1979. Groundwater, Prentice-Hall, Inc., Englewood Cliffs, New Jersey, USA.

Garratt, J.R., Segal, M., 1988. On the contribution of atmospheric moisture to dew formation. Boundary-Layer Meteorology, 45, 209-236.

Gat, J.R., 1980. The isotopes of hydrogen and oxygen in precipitation. in Handbook of Environmental Isotope Geochemistry, eds. Fritz, P., and Fontes, J-Ch., Volume 1, pp. 24-48, Elsevier, New York, USA.

Gat, J., Mook, W., Meijer, H., 2000. Atmospheric Water (Section II). *in* Environmental Isotopes in the Hydrological Cycles: Principles and Applications. UNESCO, Paris.

Genereux, D., 1998. Quantifying uncertainty in tracer-based hydrograph separations. Water Resources Research, 34, 915-919.

Genereux, D.P., and Hooper, R.P., 1998. Oxygen and Hydrogen Isotopes in Rainfall-Runoff Studies. *in* Isotope Tracers in Catchment Hydrology, *eds.* Kendall, C., McDonnell, J.J., Elsevier, Amsterdam.

Genereux, D., Wood, S., Pringle, C., 2002. Chemical tracing of interbasin groundwater transfer in the lowland rainforest of Costa Rica. Journal of Hydrology, 258, 163-178.

Gibson, J.J., Edwards, T.W.D., Bursey, G.G., Prowse, T.D., 1993. Estimating Evaporation Using Stable Isotopes: Quantitative Results and Sensitivity Analysis for. Nordic Hydrology, 24, 79–94.

Gibson, J.J., Edwards, T.W.D., Prowse, T.D., 1996. Development and validation of an isotopic method for estimating lake evaporation. Hydrological Processes, 10, 1369–1382.

Gibson, J.J., Edwards, T.W.D., Prowse, T.D., 1999. Pan-derived isotopic composition of atmospheric water vapour and its variability in northern Canada. Journal of Hydrology, 217, 55-74.

Gibson, J.J., Prepas, E., McEachern, P., 2002. Quantitative comparison of lake throughflow, residency, and catchment runoff using stable isotopes: modelling and results from a regional survey of Boreal lakes. Journal of Hydrology, 262, 128-144.

Gonfiantini, R., 1986. Environmental Isotopes in Lake Studies. *in* Handbook of Environmental Isotope Geochemistry, Volume 2, The Terrestrial Environment, B, *eds.* P. Fritz and J.C. Fontes, Elsevier, Amsterdam, The Netherlands.

Gonfiantini, R., Fröhlich, Araguás-Araguás, L., Rozanski, K., 1998. Isotopes in Groundwater Hydrology. *in* Isotope Tracers in Catchment Hydrology, *eds.* Kendall, C., McDonnell, J.J., Elsevier, Amsterdam.

Goulden, M., Litvak, M., Miller, S., 2007. Factors that control Typha marsh evapotranspiration. Aquatic Botany, 86, 97-106.

Gonzales, A., Nonner, J., Heijkers, J., Uhlenbrook, S., 2009. Comparison of different base flow separation methods in a lowland catchment. Hydrology and Earth System Sciences Discussions, 6, 3483-3515.

Hayashi, M., Quinton, W.L., Pietroniro, A., Gibson, J.J., 2004. Hydrologic functions of wetlands in a discontinuous permafrost basin indicated by isotopic and chemical signatures. Journal of Hydrology, 296, 81–97.

Hayhoe, K., Wake, C.P., Huntington, T.G., Luo, L., Schwartz, M.D., Sheffield, J., Wood, E., Anderson, B., Bradbury, J., DeGaetano, A., Troy, T.J., Wolfe, D., 2006. Past and future changes in climate and hydrological indicators in the US Northeast. Climate Dynamics, 28, 381-407.

Herbst, M., Kappen, L., 1999. The ratio of transpiration versus evaporation in a reed belt as influenced by weather conditions. Aquatic botany, 63, 113–125.

Hewlett, J.D., Hibbert, A.R., 1963. Moisture and Energy Conditions within a Sloping Soil Mass during Drainage. Journal of Geophysical Research, 68, 1081-1087.

Hodgkins, G.A., Dudley, R.W., 2006. Changes in the timing of winter–spring streamflows in eastern North America, 1913–2002. Geophysical Research Letters, 33, L06402.

Horita, J., Rozanski, K., Cohen, S., 2008. Isotope effects in the evaporation of water: a status report of the Craig-Gordon model. Isotopes in Environmental and Health Studies, 44, 23-49.

Horita, J., Wesolowski, D., 1994. Liquid-vapor fractionation of oxygen and hydrogen isotopes of water from the freezing to the critical temperature. Geochimica et Cosmochimica Acta, 58, 3425-3437.

Hostetler, S., Benson, L.V., 1994. Stable isotopes of oxygen and hydrogen in the Truckee River-Pyramid Lake surface-water system. 2. A predictive model of ^{18}O and ^{2}H in Pyramid Lake. Limnology and Oceanography, 39, 356-364.

Huggins, L.F., 1982. Surface Runoff, Storage, and Routing. *in* Hydrologic Modeling of Small Watersheds. *eds.* Haan, C.T., Johnson, H.P., Brakensiek, D.L, Monograph 5, American Society of Agricultural Engineers, Michigan, USA.

Hunt, R.J., Krabbenhoft, D.P., Hunt, M.P., 1996. Groundwater inflow measurements in wetland systems. Water Resources Research 32, 495-507.

Ingraham, N.L., 1998. Isotopic Variations in Precipitation. *in* Isotope Tracers in Catchment Hydrology, *eds.* C Kendall and JJ McDonnell, Elsevier, Amsterdam.

Jacob, H., Sonntag, C., 1991. An 8-year record of the seasonal variation of ^2H and ^{18}O in atmospheric water vapour and precipitation at Heidelberg, Germany. Tellus B, 43, 291-300.

Joerin, C., Beven, K., Iorgulescu, I., Musy, A., 2002. Uncertainty in hydrograph separations based on geochemical mixing models. Journal of Hydrology, 255, 90-106.

Kadlec, R.H., Knight, R.L, 1996. Treatment Wetlands. CRC Press, Florida, USA.

Kendall, C., and Caldwell, E.A., 1998. Fundamentals of Isotope Geochemistry. *In* Isotope Tracers in Catchment Hydrology, *eds.* C Kendall and JJ McDonnell, Elsevier, Amsterdam.

Kohler, M.A., Parmele, L.H., 1967. Generalized estimates of free-water evaporation. Water Resources Research, 3, 997-1005.

Krasnostein, A.L., Oldham, C.E., 2004. Predicting wetland water storage. Water Resources Research, 40, W10203.

Kværner, J., Kløve, B., 2006. Tracing sources of summer streamflow in boreal headwaters using isotopic signatures and water geochemical components. Journal of Hydrology, 331, 186-204.

Kværner, J., Kløve, B., 2008. Generation and regulation of summer runoff in a boreal flat fen. Journal of Hydrology, 360, 15–30.

LANDSAT, Complex Systems Research Center, 2001. NH Land Cover Assessment 2001. *available from* Complex Systems Research Center, University of New Hampshire.

Lee, X., Sargent, S., Smith, R., Tanner, B., 2005. In situ measurement of the water vapor $^{18}O/^{16}O$ isotope ratio for atmospheric and ecological applications. Journal of Atmospheric and Oceanic Technology, 22, 555–565.

Lee, X., Smith, R., Williams, J., 2006. Water vapour $^{18}O/^{16}O$ isotope ratio in surface air in New England, USA. Tellus B, 58, 293-304.

Letts, M.G., Roulet, N.T., Comer, N.T., Skarupa, M.R., Verseghy, D.L., 2000. Parameterization of Peatland Hydraulic Properties for the Canadian Land Surface Scheme. Atmosphere-Ocean, 38, 141-160.

Lis, G, LI Wassenaar, MJ Hendry, 2007. High-precision laser spectroscopy D/H and $^{18}O/^{16}O$ measurements of microliter natural water samples, Analytical Chemistry, AC701716Q.

Liu, S., 1997. A new model for the prediction of rainfall interception in forest canopies. Ecological Modelling, 99, 151–159.

Liu, S., 2001. Evaluation of the Liu model for predicting rainfall interception in forests world-wide. Hydrological Processes, 15, 2341-2360.

Luz, B., Barkan, E., Yam, R., Shemesh, A., 2009. Fractionation of oxygen and hydrogen isotopes in evaporating water. Geochimica et Cosmochimica Acta, 73, 6697-6703.

Majoube, M., 1971. Fractionation in O-18 between ice and water vapor. Journal de Chimie Physique et de Physico-Chimie Biologique, 68, 625–636.

Mann, C.J., Wetzel, R.G., 2000. Hydrology of an impounded lotic wetland—subsurface hydrology. Wetlands, 20, 33–47.

Mau, D.P., Winter, T.C., 1997. Estimating ground-water recharge from streamflow hydrographs for a small mountain watershed in a temperate humid climate, New Hampshire, USA. Ground Water, 35, 291-304.

McDonnell, J.J., 1990. A rationale for old water discharge through macropores in a steep, humid catchment. Water Resources Research, 26, 2821-2832.

McHale, M.R., Cirmo, C.P., Mitchell, M.J., McDonnell, J.J., 2004. Wetland nitrogen dynamics in an Adirondack forested watershed. Hydrological Processes, 18, 1853-1870.

Merlivat, L., Jouzel, J., 1979. Global climatic interpretation of the deuterium-oxygen 18 relationship for precipitation. Journal of Geophysical Research, 84(C8), 5029-5033.

Merlivat, L., 1978. Molecular Diffusivities of $H_2{}^{16}O$, $HD^{16}O$, and $H_2{}^{18}O$ in gases. Journal of Chemical Physics, 69, 2864-2871.

Mitsch, W.J., Gosselink, J.G., 2000, Wetlands, Third Edition, John Wiley & Sons, New York, USA.

Monteith, J., Evaporation and environment: the state and movement of water in living organisms. Symposium of the Society for Experimental Biology, 19, 205-234.

Mook, W.G., 2006. Introduction to Isotope Hydrology: Stable and Radioactive Isotopes of Hydrogen, Oxygen, and Carbon. Taylor & Francis, London, United Kingdom.

Moriasi, D.N., Arnold, J.G., Van Liew, M.W., Bingner, R.L., Harmel, R.D., Veith, T.L., 2007. Model evaluation guidelines for systematic quantification of accuracy in watershed simulations. Transactions of the American Society of Agricultural and Biological Engineers, 50, 885-900.

Mosley, M.P., McKerchar, A.I., 1993. Streamflow. *in* Handbook of Hydrology, *ed.* Maidment, D., McGraw-Hill, USA.

Mosner, M.S., 2002. Stream-aquifer relations and the potentiometric surface of the upper Floridian aquifer in the Lower Apalachicola Chattahoochee-Flint River basin in parts of Georgia, Florida, and Alabama, 1999-2000. Water-Resources Investigations Report 02-4244, U.S. Department of the Interior, U.S. Geological Survey, Atlanta, Georgia, USA.

Nash, J.E., Sutcliffe, J.V., 1970. River flow forecasting through conceptual models part I–A discussion of principles. Journal of Hydrology, 10, 282–290.

N.H. Department of Transportation, 2007. 2005 1-Foot Color Aerial Photos, Southeast, N.H.. *available from* Complex Systems Research Center, University of New Hampshire.

N.H. Geological Survey, 2007. New Hampshire-Maine 10 meter Digital Elevation Model. *available from* N.H. Department of Environmental Services.

O'Brien, A.L., 1977. Hydrology of two small wetland basins in eastern Massachusetts. Water Resources Bulletin, 13, 325-340.

O'Brien, A.L., 1980. The role of ground water in stream discharges from two small wetland controlled basins in eastern Massachusetts. Ground Water 18, 359-365.

Penman, H.L., 1948. Natural evaporation from open water, bare soil and grass. Proceedings of the Royal Society of London. Series A, Mathematical and Physical Sciences, 193, 120–145.

Price, K., Jackson, C.R., 2007. Effects of forest conversion on baseflows in the southern Appalachians: a cross-landscape comparison of synoptic measurements. Georgia Water Resources Institute, Proceedings of the 2007 Georgia Water Resources Conference, March 27–29, 2007, at the University of Georgia.

Roulet, N.T., 1990. Hydrology of a headwater basin wetland: groundwater discharge and wetland maintenance. Hydrological Processes, 4, 387-400.

Rutledge, A., 2000. Considerations for use of the RORA program to estimate ground-water recharge from streamflow records. Open-File Report 00-156, U.S. Department of the Interior, U.S. Geological Survey, Reston, Virginia, USA.

Rutledge, A., Mesko, T., 1996. Estimated hydrologic characteristics of shallow aquifer systems in the Valley and Ridge, the Blue Ridge, and the Piedmont physiographic provinces based on analysis of stream recession and base flow. Professional Paper 1422-B, U.S. Department of the Interior, U.S. Geological Survey, Denver, Colorado, USA.

Rutter, A.J., Kershaw, K.A., Robins, P.C., Morton, A.J., 1971. A predictive model of rainfall interception in forests, 1. Derivation of the model from observations in a plantation of Corsican pine. Agricultural Meteorology, 9, 367-384.

St. Amour, N.A., Gibson, J.J., Edwards, T.W.D., Prowse, T.D., Pietroniro, A., 2005. Isotopic time-series partitioning of streamflow components in wetland-dominated catchments, Lower Liard River basin, Northwest Territories, Canada. Hydrological Processes, 19, 3357-3381.

Santhi, C., Allen, P.M., Muttiah, R.S., Arnold, J.G., Tuppad, P., 2008. Regional estimation of base flow for the conterminous United States by hydrologic landscape regions. Journal of Hydrology, 351, 139–153.

Shuttleworth, W.J., Wallace, J.S., 1993, Evaporation from sparse crops-an energy combination theory. Quarterly Journal of the Royal Meteorological Society, 111, 839-855.

Sjostrom, D.J., Welker, J.M., 2009. The influence of air mass source on the seasonal isotopic composition of precipitation, eastern USA. Journal of Geochemical Exploration, 102, 103–112.

Sklash, M.G., Farvolden, R., Fritz, P., 1976. A conceptual model of watershed response to rainfall. Developed through the use of oxygen- 18 as a natural tracer. Canadian Journal of Earth Sciences, 13, 271-283.

Sklash, M.G., Stewart, M.K., Pearce, A.J., 1986. Storm Runoff Generation in Humid Headwater Catchments: 2. A Case Study of Hillslope and Low-Order Stream Response. Water Resources Research, 22, 1273-1282.

Sklash, M., 1990. Environmental Isotope Studies of Storm and Snowmelt Runoff Generation. *in* Process Studies in Hillslope Hydrology. Chichester, West Sussex, England.

Smakhtin, V.U., Batchelor, A.L., 2005. Evaluating wetland flow regulating functions using discharge time-series. Hydrological Processes, 19, 1293-1305.

Smith, M.A., Frades, M., Scudder, R., Bryce, J.G., Davis, J.M., 2007, Strontium isotopes and trace metals in the delineation of flow paths in the Lamprey River watershed. Geological Society of America Abstracts with Programs, 39(1), 47.

Snyder, E., 2009. An Ecological Assessment of the Northwood Area Land Management Collaborative (NALMC) Neighborhood.

Soil Survey Staff, Natural Resources Conservation Service, United States Department of Agriculture, 2011. Web Soil Survey. Available online at http://websoilsurvey.nrcs.usda.gov/. Accessed 8 April 2011.

Stewart, J., 1988. Modelling surface conductance of pine forest. Agricultural and Forest Meteorology, 43, 19-35.

Stewart, M.K., 1975. Stable isotope fractionation due to evaporation and isotopic exchange of falling waterdrops: Applications to atmospheric processes and evaporation of lakes. Journal of Geophysical Research, 80, 1133-1146.

Stewart, M.K., Mehlhorn, J., Elliott, S., 2007. Hydrometric and natural tracer (oxygen-18, silica, tritium and sulphur hexafluoride) evidence for a dominant groundwater contribution to Pukemanga Stream, New Zealand. Hydrological Processes, 21, 3340-3356.

Sumner, D.M., 2007. Effects of capillarity and microtopography on wetland specific yield. Wetlands, 27, 693-701.

Tallaksen, L.M., 1995. A review of baseflow recession analysis. Journal of Hydrology 165, 349–370.

Tetzlaff, D., Soulsby, C., 2008. Sources of baseflow in larger catchments – Using tracers to develop a holistic understanding of runoff generation. Journal of Hydrology, 359, 287-302.

Tiner, R.W., 2010. Wetlands of the Northeast: Results of the National Wetlands Inventory. U.S. Department of the Interior, U.S. Fish and Wildlife Service, Northeast Region, Hadley, MA.

Tracy, C.R., Van Berkum, F.H., Tsuji, J.S., Stevenson, R.D., Nelson, J.A., Barnes, B.M., Huey, R.B., 1984. Errors resulting from linear approximations in energy balance equations. Journal of Thermal Biology, 9(4), 261-264.

Uhlenbrook, S., Frey, M., Leibundgut, C., Maloszewski, P., 2002. Hydrograph separations in a mesoscale mountainous basin at event and seasonal timescales. Water Resources Research, 38, 1096.

U.S. Fish and Wildlife Service, 2001. National Wetlands Inventory. *available from* Complex Systems Research Center, University of New Hampshire.

U. S. Fish and Wildlife Service, 2010. WETDBA.CONUS_wet_poly. (digital update)

U.S. Geological Survey, U.S. Environmental Protection Agency, Complex Systems Research Center, and N.H. Department of Environmental Services, 2006., New Hampshire Hydrography Dataset. *available from* Complex Systems Research Center, University of New Hampshire.

Wang, X.F., Yakir, D., 2000. Using stable isotopes of water in evapotranspiration studies. Hydrological Processes, 14, 1407–1421.

Welhan, J.A., Fritz, P., 1977. Evaporation pan isotopic behavior as an index of isotopic evaporation conditions. Geochimica et Cosmochimica Acta, 41, 682–686.

Weiler, M., Scherrer, S., Naef, F., Burlando, P., 1999. Hydrograph separation of runoff components based on measuring hydraulic state variables, tracer experiments, and weighting methods. IAHS Publication No. 258, 249–256.

Wessel, D.A., Rouse, W.R., 1994. Modelling evaporation from wetland tundra. Boundary-Layer Meteorology, 68, 109–130.

White, J.W.C., Gedzelman, S.D., 1984. The isotopic composition of atmospheric water vapor and the concurrent meteorological conditions. Journal of Geophysical Research, 89, 4937-4939.

White, J.W.C., Cook, E.R., Lawrence, J.R., Wallace, S.B., 1985. The ratios of sap in trees: Implications for water sources and tree ring ratios. Geochimica et Cosmochimica Acta, 49, 237-246.

Winter, T.C., 1981. Uncertainties in estimating the water balance of lakes. Water Resources Bulletin, 17, 82-113.

Woessner, WW, 2007, Building a compact, low-cost, and portable peristaltic sampling pump, Ground Water 45(6), 795-797.

Appendix A

Table A1: Stable Isotopic Analytical Results.

Table A2: Replicate Analyses of Laboratory Standards.

Table A1: Stable isotopic analytical results from the Northwood Study Catchment.

Sample ID	Site	Date	$\delta^{18}O$	$\delta^{2}H$	Type	Laboratory
NWP-1	NWP	7/15/09	-5.70	-35.21	Precip	CPSIL
NWP-2	NWP	7/22/09	-7.36	-44.11	Precip	CPSIL
NWP-3	NWP	8/3/09	-10.03	-66.55	Precip	CPSIL
NWP-3	NWP	8/3/09	-10.02	-65.61	Precip	CPSIL
NWP-4	NWP	8/12/09	-6.66	-40.39	Precip	CPSIL
NWP-5	NWP	8/27/09	-3.55	-17.59	Precip	CPSIL
NWP-6	NWP	9/20/09	-6.59	-34.20	Precip	CPSIL
NWP-6	NWP	9/20/09	-6.73	-34.71	Precip	CPSIL
g4-2-3	g4-2	1/16/10	-7.09	-42.29	GW	CPSIL
g4-3-5	g4-3	1/16/10	-8.69	-53.83	GW	CPSIL
g6-1-5	g6-1	1/16/10	-8.14	-48.98	GW	CPSIL
gC-1-5	gC-1	1/16/10	-8.21	-52.49	SIGW	CPSIL
gD-1-5	gD-1	1/16/10	-8.10	-49.08	GW	CPSIL
g4-1-6	g4-1	3/20/10	-8.59	-53.02	GW	CPSIL
g1-1-1	g1-1	3/21/10	-10.69	-69.25	PT	CPSIL
g4-1-5	g4-1	3/21/10	-8.68	-55.47	GW	CPSIL
g4-2-4	g4-2	3/21/10	-9.77	-64.74	GW	CPSIL
g4-3-6	g4-3	3/21/10	-9.34	-57.89	GW	CPSIL
g1-1-2	g1-1	4/20/10	-10.57	-68.71	PT	CPSIL
g4-1-7	g4-1	4/20/10	-9.67	-62.51	GW	CPSIL
g4-2-5	g4-2	4/20/10	-10.78	-70.33	GW	CPSIL
g4-3-7	g4-3	4/20/10	-9.85	-62.92	GW	CPSIL
g4-3-7	g4-3	4/20/10	-9.80	-63.26	GW	CPSIL
g6-1-6	g6-1	4/20/10	-10.35	-67.66	GW	CPSIL
g6-1-6	g6-1	4/20/10	-10.14	-67.31	GW	CPSIL
gC-1-6	gC-1	4/20/10	-9.60	-63.64	SIGW	CPSIL
gD-1-6	gD-1	4/20/10	-11.06	-73.93	GW	CPSIL
gD-1-6	gD-1	4/20/10	-11.32	-73.84	GW	CPSIL
g4-1-8	g4-1	5/25/10	-9.89	-63.59	GW	CPSIL
g4-3-8	g4-3	5/25/10	-10.40	-65.27	GW	CPSIL
g6-1-7	g6-1	5/25/10	-10.48	-66.20	GW	CPSIL
s1-7	s1	5/25/10	-8.78	-59.55	RES	CPSIL
s3-6	s3	5/25/10	-8.82	-60.54	RES	CPSIL
s4-7	s4	5/25/10	-9.33	-64.05	SF	CPSIL
NWP-7	NWP	5/31/10	-6.47	-41.08	Precip	CPSIL
NWP-8	NWP	6/4/10	-6.05	-36.39	Precip	CPSIL
NWP-9	NWP	6/8/10	-5.71	-34.88	Precip	CPSIL
g1-1-5	g1-1	6/17/10	-8.10	-51.85	PT	CPSIL
g4-1-10	g4-1	6/17/10	-10.09	-62.69	GW	CPSIL
g4-3-10	g4-3	6/17/10	-9.83	-63.70	GW	CPSIL
g6-1-9	g6-1	6/17/10	-9.98	-64.90	GW	CPSIL

Table A1 (Continued): Stable isotopic analytical results.

Sample ID	Site	Date	$\delta^{18}O$	$\delta^{2}H$	Type	Laboratory
gC-1-9	gC-1	6/17/10	-9.43	-58.93	SIGW	CPSIL
gD-1-9	gD-1	6/17/10	-10.54	-69.50	GW	CPSIL
s1-9	s1	6/17/10	-8.22	-56.49	RES	CPSIL
s1-9	s1	6/17/10	-8.39	-56.82	RES	CPSIL
s2-10	s2	6/17/10	-8.38	-55.31	RES	CPSIL
s3-8	s3	6/17/10	-8.15	-55.52	RES	CPSIL
s4-9	s4	6/17/10	-8.48	-56.67	SF	CPSIL
s6-8	s6	6/17/10	-9.89	-63.01	SF	CPSIL
sA-9	sA	6/17/10	-7.84	-55.18	SF	CPSIL
sB-9	sB	6/17/10	-8.08	-58.72	RES	CPSIL
sC-10	sC	6/17/10	-8.76	-57.58	SF	CPSIL
NWP-10	NWP	6/17/10	-4.00	-24.91	Precip	CPSIL
g4-1-12	g4-1	6/29/10	-9.91	-63.35	GW	CPSIL
g4-1-12	g4-1	6/29/10	-10.11	-63.30	GW	CPSIL
g4-3-12	g4-3	6/29/10	-10.06	-62.89	GW	CPSIL
g6-1-11	g6-1	6/29/10	-10.23	-64.08	GW	CPSIL
s1-11	s1	6/29/10	-7.73	-53.54	RES	CPSIL
s3-10	s3	6/29/10	-8.03	-53.03	RES	CPSIL
s3-10	s3	6/29/10	-7.92	-54.11	RES	CPSIL
s4-11	s4	6/29/10	-8.09	-55.58	SF	CPSIL
g1-1-7	g1-1	7/8/10	-8.07	-52.07	PT	CPSIL
g1-1-7	g1-1	7/8/10	-7.59	-51.27	PT	CPSIL
g4-1-13	g4-1	7/8/10	-9.68	-62.17	GW	CPSIL
g4-3-13	g4-3	7/8/10	-9.66	-62.10	GW	CPSIL
g6-1-12	g6-1	7/8/10	-10.08	-62.45	GW	CPSIL
gC-1-12	gC-1	7/8/10	-8.94	-57.63	SIGW	CPSIL
gD-1-12	gD-1	7/8/10	-10.35	-69.60	GW	CPSIL
s1-12	s1	7/8/10	-6.94	-51.27	RES	CPSIL
s2-13	s2	7/8/10	-7.15	-51.20	RES	CPSIL
s3-11	s3	7/8/10	-7.23	-51.03	RES	CPSIL
s4-12	s4	7/8/10	-7.85	-53.52	SF	CPSIL
s4-12	s4	7/8/10	-8.06	-54.03	SF	CPSIL
s6-11	s6	7/8/10	-9.80	-62.70	SF	CPSIL
sA-12	sA	7/8/10	-6.62	-49.76	SF	CPSIL
sB-12	sB	7/8/10	-7.40	-55.32	RES	CPSIL
sC-13	sC	7/8/10	-8.88	-56.30	SF	CPSIL
NWP-11	NWP	7/12/10	-7.05	-45.98	Precip	CPSIL
NWP-12A	NWP	7/16/10	-6.56	-41.61	Precip	CPSIL
NWP-12B	NWP	7/16/10	-6.56	-41.62	Precip	CPSIL
NWP-13	NWP	7/26/10	-7.41	-48.38	Precip	CPSIL

Table A1 (Continued): Stable isotopic analytical results.

Sample ID	Site	Date	$\delta^{18}O$	δ^2H	Type	Laboratory
g4-1-16	g4-1	7/27/10	-9.82	-61.90	GW	CPSIL
g4-3-16A	g4-3	7/27/10	-10.01	-62.90	GW	CPSIL
g4-3-16B	g4-3	7/27/10	-9.98	-63.74	GW	CPSIL
g4-3-16B	g4-3	7/27/10	-9.59	-62.49	GW	CPSIL
g6-1-14	g6-1	7/27/10	-9.87	-61.87	GW	CPSIL
s1-15	s1	7/27/10	-6.55	-48.99	RES	CPSIL
s3-14	s3	7/27/10	-6.75	-48.86	RES	CPSIL
s4-15	s4	7/27/10	-7.24	-51.77	SF	CPSIL
s4-15	s4	7/27/10	-7.37	-53.19	SF	CPSIL
g1-1-11	g1-1	8/3/10	-7.93	-51.28	PT	CPSIL
g4-1-17	g4-1	8/3/10	-9.43	-61.17	GW	CPSIL
g4-3-17	g4-3	8/3/10	-9.33	-62.14	GW	CPSIL
g6-1-14	g6-1	8/3/10	-9.77	-61.38	GW	CPSIL
gC-1-16	gC-1	8/3/10	-8.68	-56.94	SIGW	CPSIL
gC-1-16	gC-1	8/3/10	-8.51	-55.88	SIGW	CPSIL
s1-16	s1	8/3/10	-6.34	-47.71	RES	CPSIL
s2-17	s2	8/3/10	-6.08	-46.94	RES	CPSIL
s2-17	s2	8/3/10	-6.42	-47.05	RES	CPSIL
s3-15	s3	8/3/10	-6.52	-46.59	RES	CPSIL
s4-16	s4	8/3/10	-6.93	-49.28	SF	CPSIL
s6-15	s6	8/3/10	-9.10	-58.57	SF	CPSIL
sA-16	sA	8/3/10	-6.09	-47.19	SF	CPSIL
sB-16	sB	8/3/10	-6.52	-51.60	RES	CPSIL
sC-17	sC	8/3/10	-9.38	-57.80	SF	CPSIL
NWP-14	NWP	8/9/10	-5.37	-30.41	Precip	CPSIL
NWP-15	NWP	8/10/10	-5.94	-38.23	Precip	CPSIL
g4-1-19	g4-1	8/20/10	-9.28	-59.46	GW	CPSIL
g4-3-19	g4-3	8/20/10	-10.06	-62.13	GW	CPSIL
s1-18	s1	8/20/10	-6.38	-45.46	RES	CPSIL
s1-18	s1	8/20/10	-6.19	-45.80	RES	CPSIL
s3-17	s3	8/20/10	-5.92	-43.99	RES	CPSIL
s4-18	s4	8/20/10	-6.35	-48.25	SF	CPSIL
NWP-16	NWP	8/20/10	-4.46	-24.63	Precip	CPSIL
NWP-17	NWP	8/30/10	-7.83	-51.12	Precip	CPSIL
NWP-18	NWP	9/15/10	-6.67	-41.55	Precip	CPSIL
NWP-19	NWP	9/17/10	-6.97	-37.82	Precip	CPSIL
NWP-20	NWP	10/7/10	-6.39	-38.02	Precip	CPSIL
g1-1-14	g1-1	10/12/10	-7.67	-50.78	PT	CPSIL
g4-1-20	g4-1	10/12/10	-7.84	-49.18	GW	CPSIL
g4-3-20	g4-3	10/12/10	-9.08	-59.93	GW	CPSIL

Table A1 (Continued): Stable isotopic analytical results.

Sample ID	Site	Date	$\delta^{18}O$	δ^2H	Type	Laboratory
g6-1-15	g6-1	10/12/10	-8.76	-56.97	GW	CPSIL
gC-1-19	gC-1	10/12/10	-8.52	-54.97	GW	CPSIL
s1-19	s1	10/12/10	-6.82	-46.36	RES	CPSIL
s2-20	s2	10/12/10	-6.75	-45.86	RES	CPSIL
s3-18	s3	10/12/10	-6.77	-45.07	RES	CPSIL
s3-18	s3	·10/12/10	-6.64	-44.91	RES	CPSIL
s4-19	s4	10/12/10	-6.39	-44.45	SF	CPSIL
s6-18	s6	10/12/10	-8.77	-55.93	SF	CPSIL
sA-19	sA	10/12/10	-5.82	-43.97	SF	CPSIL
sB-19	sB	10/12/10	-5.31	-44.13	RES	CPSIL
sC-20	sC	10/12/10	-8.17	-52.93	SF	CPSIL

Abbreviations:

GW - Groundwater

SIGW - Surface Influenced Groundwater

PT - Peat water

RES - Surface Reservoir

SF - Streamflow

CPSIL - Colorado Plateau Stable Isotope Laboratory

All results presented in permil

Table A2: Colorado Plateau Stable Isotope Laboratory replicate analyses.

Meas($\delta^{18}O$)	Exp($\delta^{18}O$)	Meas(δ^2H)	Exp(δ^2H)	Reported
2.544	2.540	7.593	7.250	May-10
2.382	2.540	7.252	7.250	May-10
2.692	2.540	6.902	7.250	May-10
2.395	2.540	7.398	7.250	May-10
2.841	2.540	7.072	7.250	May-10
2.380	2.540	7.277	7.250	May-10
-28.745	-28.610	-191.538	-191.740	May-10
-28.560	-28.610	-191.384	-191.740	May-10
-28.522	-28.610	-192.295	-191.740	May-10
-28.562	-28.610	-191.057	-191.740	May-10
-28.651	-28.610	-192.068	-191.740	May-10
-28.612	-28.610	-192.092	-191.740	May-10
-21.026	-20.990	-128.972	-128.440	May-10
-21.073	-20.990	-129.441	-128.440	May-10
-21.005	-20.990	-129.832	-128.440	May-10
-21.105	-20.990	-129.105	-128.440	May-10
-21.080	-20.990	-128.986	-128.440	May-10
-6.352	-6.120	-41.738	-41.260	May-10
-6.341	-6.120	-41.515	-41.260	May-10
-6.146	-6.120	-42.321	-41.260	May-10
-6.463	-6.120	-41.952	-41.260	May-10
-6.132	-6.120	-42.199	-41.260	May-10
-6.181	-6.120	-42.428	-41.260	May-10
-10.700	-10.570	-74.210	-73.360	May-10
-10.795	-10.570	-74.000	-73.360	May-10
-10.572	-10.570	-74.037	-73.360	May-10
-10.879	-10.570	-74.353	-73.360	May-10
-10.654	-10.570	-74.055	-73.360	May-10
-10.811	-10.570	-74.114	-73.360	May-10
-10.796	-10.570	-74.421	-73.360	May-10
-10.530	-10.570	-73.910	-73.360	May-10
-10.656	-10.570	-73.626	-73.360	May-10
-10.297	-10.570	-74.332	-73.360	May-10
-10.850	-10.570	-74.334	-73.360	May-10
-10.707	-10.570	-74.355	-73.360	May-10
-10.784	-10.570	-73.795	-73.360	May-10
-10.569	-10.570	-73.541	-73.360	May-10
-10.454	-10.570	-74.005	-73.360	May-10
-10.123	-10.570	-72.280	-73.360	May-10
-10.500	-10.570	-73.046	-73.360	May-10
-10.554	-10.570	-72.838	-73.360	May-10

Table A2: Colorado Plateau Stable Isotope Laboratory replicate analyses.

Meas(δ^{18}O)	Exp(δ^{18}O)	Meas(δ^2H)	Exp(δ^2H)	Reported
-10.585	-10.570	-73.839	-73.360	May-10
-10.869	-10.570	-74.022	-73.360	May-10
-10.678	-10.570	-73.477	-73.360	May-10
-10.695	-10.570	-74.205	-73.360	May-10
-10.513	-10.570	-72.464	-73.360	May-10
-10.264	-10.570	-73.261	-73.360	May-10
2.136	2.540	6.664	7.250	Aug-10
2.797	2.540	7.369	7.250	Aug-10
2.677	2.540	7.713	7.250	Aug-10
2.533	2.540	7.000	7.250	Aug-10
2.663	2.540	7.842	7.250	Aug-10
2.422	2.540	6.905	7.250	Aug-10
2.439	2.540	7.271	7.250	Aug-10
2.470	2.540	7.510	7.250	Aug-10
2.703	2.540	6.967	7.250	Aug-10
2.472	2.540	7.006	7.250	Aug-10
2.409	2.540	7.134	7.250	Aug-10
2.737	2.540	7.609	7.250	Aug-10
-28.806	-28.610	-191.953	-191.740	Aug-10
-28.485	-28.610	-191.529	-191.740	Aug-10
-28.529	-28.610	-191.735	-191.740	Aug-10
-28.581	-28.610	-191.745	-191.740	Aug-10
-28.534	-28.610	-191.964	-191.740	Aug-10
-28.713	-28.610	-191.508	-191.740	Aug-10
-28.943	-28.610	-192.230	-191.740	Aug-10
-28.546	-28.610	-191.562	-191.740	Aug-10
-28.333	-28.610	-191.425	-191.740	Aug-10
-28.558	-28.610	-191.747	-191.740	Aug-10
-28.613	-28.610	-191.588	-191.740	Aug-10
-28.657	-28.610	-191.883	-191.740	Aug-10
-21.271	-20.990	-128.604	-128.440	Aug-10
-20.694	-20.990	-128.215	-128.440	Aug-10
-20.712	-20.990	-127.766	-128.440	Aug-10
-20.792	-20.990	-128.059	-128.440	Aug-10
-20.955	-20.990	-128.781	-128.440	Aug-10
-21.262	-20.990	-129.520	-128.440	Aug-10
-20.624	-20.990	-128.022	-128.440	Aug-10
-20.467	-20.990	-127.912	-128.440	Aug-10
-20.407	-20.990	-127.610	-128.440	Aug-10
-21.126	-20.990	-128.614	-128.440	Aug-10
-21.243	-20.990	-128.687	-128.440	Aug-10

Table A2: Colorado Plateau Stable Isotope Laboratory replicate analyses.

Meas($\delta^{18}O$)	Exp($\delta^{18}O$)	Meas(δ^2H)	Exp(δ^2H)	Reported
-10.360	-10.570	-73.111	-73.360	Aug-10
-10.741	-10.570	-73.423	-73.360	Aug-10
-10.415	-10.570	-73.280	-73.360	Aug-10
-10.297	-10.570	-72.864	-73.360	Aug-10
-10.674	-10.570	-73.795	-73.360	Aug-10
-10.443	-10.570	-73.217	-73.360	Aug-10
-10.350	-10.570	-72.753	-73.360	Aug-10
-10.358	-10.570	-72.705	-73.360	Aug-10
-10.357	-10.570	-72.622	-73.360	Aug-10
-10.378	-10.570	-72.360	-73.360	Aug-10
-10.165	-10.570	-72.598	-73.360	Aug-10
-6.216	-6.120	-40.674	-41.260	Aug-10
-6.517	-6.120	-41.318	-41.260	Aug-10
-6.127	-6.120	-40.545	-41.260	Aug-10
-5.915	-6.120	-40.600	-41.260	Aug-10
-6.607	-6.120	-41.102	-41.260	Aug-10
-6.341	-6.120	-40.750	-41.260	Aug-10
-6.120	-6.120	-40.852	-41.260	Aug-10
-6.106	-6.120	-41.132	-41.260	Aug-10
-6.300	-6.120	-40.711	-41.260	Aug-10
-6.200	-6.120	-40.945	-41.260	Aug-10
-5.932	-6.120	-40.612	-41.260	Aug-10
-6.188	-6.120	-41.083	-41.260	Aug-10
-6.296	-6.120	-41.513	-41.260	Aug-10
-6.087	-6.120	-40.553	-41.260	Aug-10
-6.144	-6.120	-41.062	-41.260	Aug-10
-6.203	-6.120	-41.466	-41.260	Aug-10
-6.472	-6.120	-41.379	-41.260	Aug-10
-6.586	-6.120	-41.546	-41.260	Aug-10
-6.607	-6.120	-41.039	-41.260	Aug-10
-6.247	-6.120	-41.164	-41.260	Aug-10
-6.386	-6.120	-41.865	-41.260	Aug-10
-6.263	-6.120	-41.175	-41.260	Aug-10
-6.147	-6.120	-40.992	-41.260	Aug-10
-6.139	-6.120	-40.951	-41.260	Aug-10
-6.269	-6.120	-40.868	-41.260	Aug-10
-6.185	-6.120	-41.429	-41.260	Aug-10
-6.395	-6.120	-41.209	-41.260	Aug-10
-6.119	-6.120	-40.848	-41.260	Aug-10
2.659	2.540	6.868	7.250	Nov-10
2.537	2.540	7.610	7.250	Nov-10

Table A2: Colorado Plateau Stable Isotope Laboratory replicate analyses.

Meas($\delta^{18}O$)	Exp($\delta^{18}O$)	Meas(δ^2H)	Exp(δ^2H)	Reported
2.558	2.540	7.130	7.250	Nov-10
2.512	2.540	7.369	7.250	Nov-10
2.561	2.540	6.658	7.250	Nov-10
2.472	2.540	7.474	7.250	Nov-10
2.587	2.540	7.613	7.250	Nov-10
-28.665	-28.610	-192.024	-191.740	Nov-10
-28.635	-28.610	-191.855	-191.740	Nov-10
-28.529	-28.610	-191.338	-191.740	Nov-10
-28.701	-28.610	-191.887	-191.740	Nov-10
-28.685	-28.610	-191.661	-191.740	Nov-10
-28.442	-28.610	-191.672	-191.740	Nov-10
-28.608	-28.610	-191.853	-191.740	Nov-10
-28.648	-28.610	-191.168	-191.740	Nov-10
-28.574	-28.610	-192.193	-191.740	Nov-10
-20.979	-20.990	-128.721	-128.440	Nov-10
-20.838	-20.990	-128.424	-128.440	Nov-10
-20.943	-20.990	-128.589	-128.440	Nov-10
-21.145	-20.990	-128.699	-128.440	Nov-10
-21.054	-20.990	-128.678	-128.440	Nov-10
-21.077	-20.990	-128.721	-128.440	Nov-10
-20.898	-20.990	-129.580	-128.440	Nov-10
-21.177	-20.990	-128.677	-128.440	Nov-10
-21.372	-20.990	-128.571	-128.440	Nov-10
-10.508	-10.570	-73.488	-73.360	Nov-10
-10.705	-10.570	-72.985	-73.360	Nov-10
-10.476	-10.570	-73.309	-73.360	Nov-10
-10.739	-10.570	-73.695	-73.360	Nov-10
-10.633	-10.570	-73.231	-73.360	Nov-10
-10.936	-10.570	-73.241	-73.360	Nov-10
-10.948	-10.570	-73.708	-73.360	Nov-10
-10.988	-10.570	-73.566	-73.360	Nov-10
-10.941	-10.570	-73.643	-73.360	Nov-10
-6.241	-6.120	-40.933	-41.260	Nov-10
-6.012	-6.120	-40.859	-41.260	Nov-10
-6.073	-6.120	-40.495	-41.260	Nov-10
-6.230	-6.120	-40.651	-41.260	Nov-10
-6.154	-6.120	-40.882	-41.260	Nov-10
-6.323	-6.120	-41.354	-41.260	Nov-10
-6.015	-6.120	-40.974	-41.260	Nov-10
-6.259	-6.120	-41.224	-41.260	Nov-10
-6.356	-6.120	-41.447	-41.260	Nov-10

Table A2: Colorado Plateau Stable Isotope Laboratory replicate analyses.

Meas($\delta^{18}O$)	Exp($\delta^{18}O$)	Meas(δ^2H)	Exp(δ^2H)	Reported
-6.150	-6.120	-41.606	-41.260	Nov-10
-6.236	-6.120	-41.361	-41.260	Nov-10
-6.171	-6.120	-40.881	-41.260	Nov-10
-6.581	-6.120	-41.711	-41.260	Nov-10
-6.063	-6.120	-40.875	-41.260	Nov-10
-6.551	-6.120	-41.142	-41.260	Nov-10
-6.641	-6.120	-42.127	-41.260	Nov-10
-6.570	-6.120	-41.006	-41.260	Nov-10
-6.314	-6.120	-41.853	-41.260	Nov-10
-6.296	-6.120	-41.040	-41.260	Nov-10
-6.552	-6.120	-41.426	-41.260	Nov-10
-7.456	-7.590	-62.437	-62.279	Nov-10
-7.371	-7.590	-62.552	-62.279	Nov-10
-7.398	-7.590	-62.503	-62.279	Nov-10
-7.557	-7.590	-61.800	-62.279	Nov-10
-7.551	-7.590	-61.800	-62.279	Nov-10
-7.563	-7.590	-61.952	-62.279	Nov-10
-7.813	-7.590	-62.849	-62.279	Nov-10
-7.847	-7.590	-62.580	-62.279	Nov-10
-7.759	-7.590	-62.037	-62.279	Nov-10

Abbreviations:

Meas( ) - Instrument measured value

Exp( ) - Accepted value for standard

All composition data presented in permil.

Appendix B

Figure B1: Isotopic composition of surface and groundwater on 25 May

Figure B2: Isotopic composition of surface and groundwater on 17 June

Figure B3: Isotopic composition of surface and groundwater on 29 June

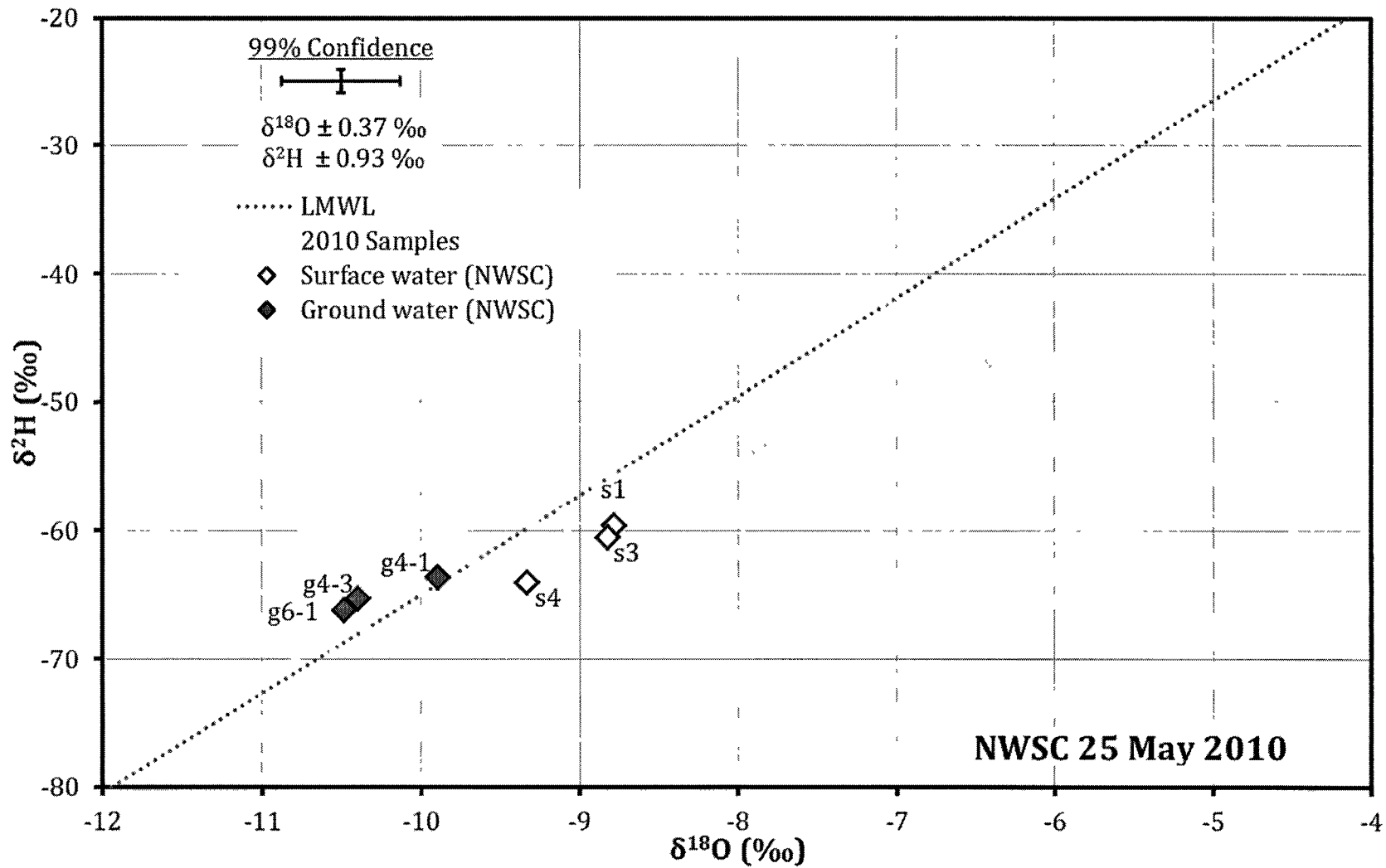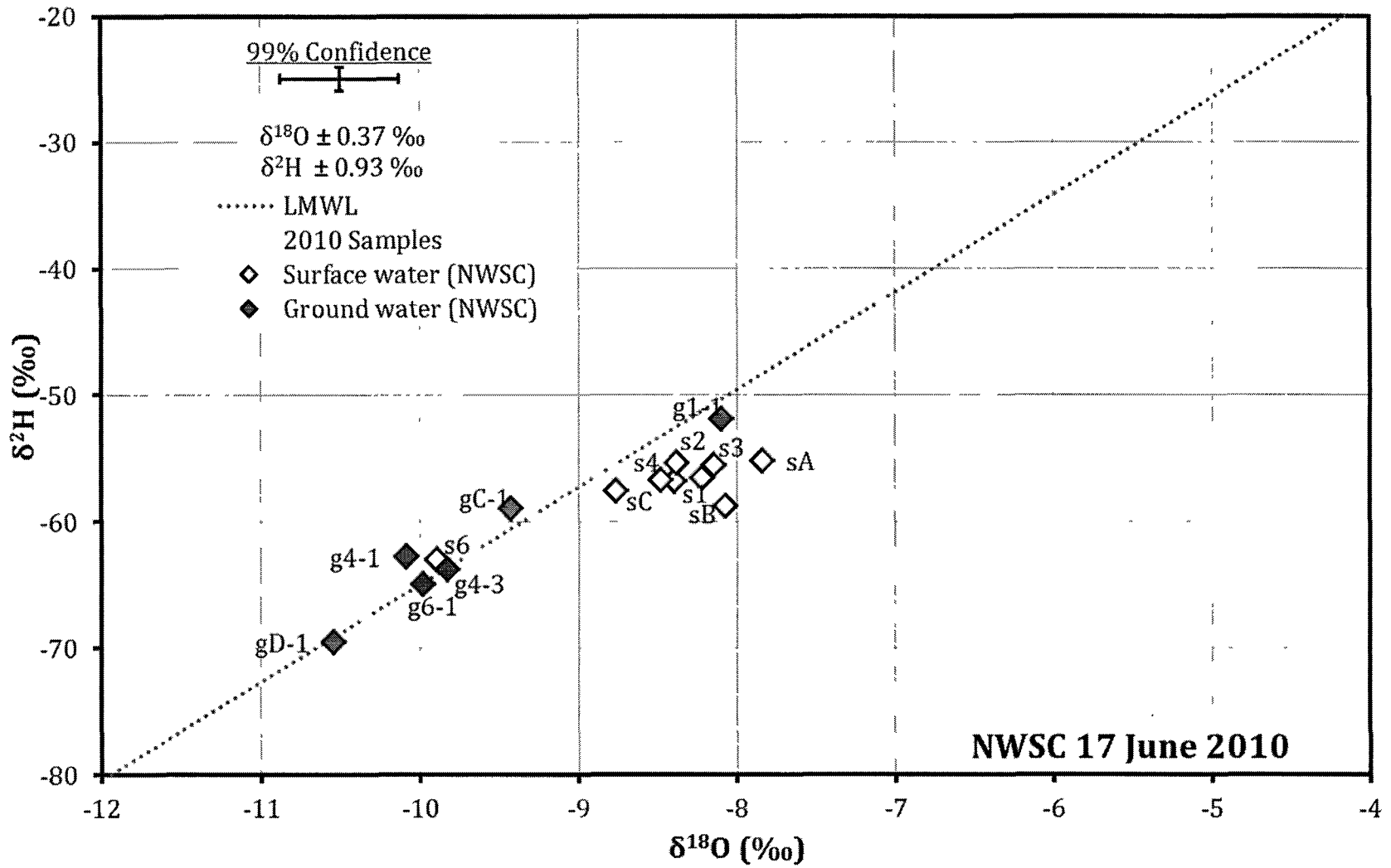*Figure B4: Isotopic composition of surface and groundwater on 8 July*

Figure B5: Isotopic composition of surface and groundwater on 27 July

Figure B6: Isotopic composition of surface and groundwater on 3 August

Figure B7: Isotopic composition of surface and groundwater on 20 August

Figure B8: Isotopic composition of surface and groundwater on 12 October

Figure B1: Isotopic composition of groundwater and streamflow on 25 May.

Figure B2: Isotopic composition of groundwater and streamflow on 17 June.
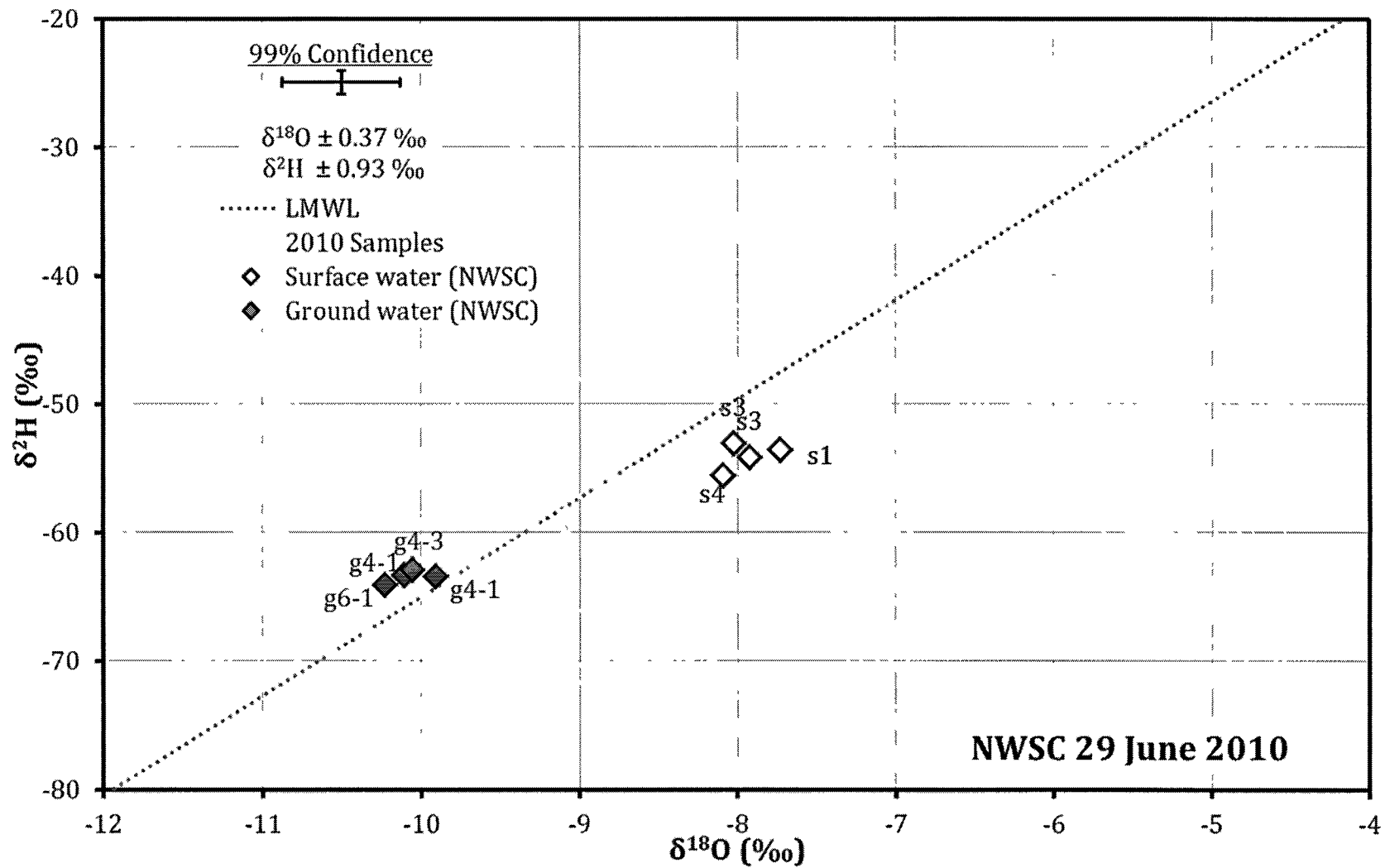
Figure B3: Isotopic composition of groundwater and streamflow on 29 June.
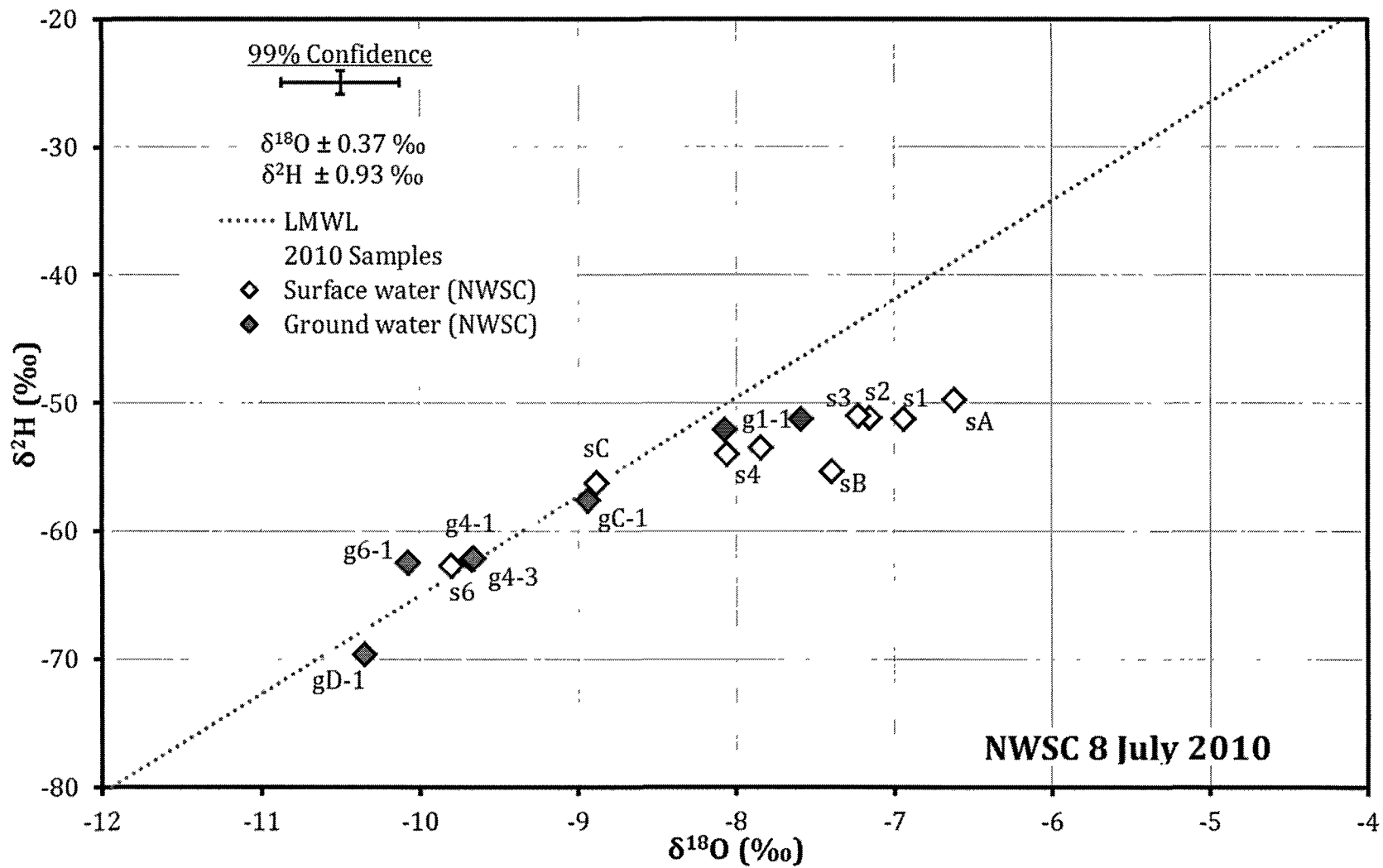
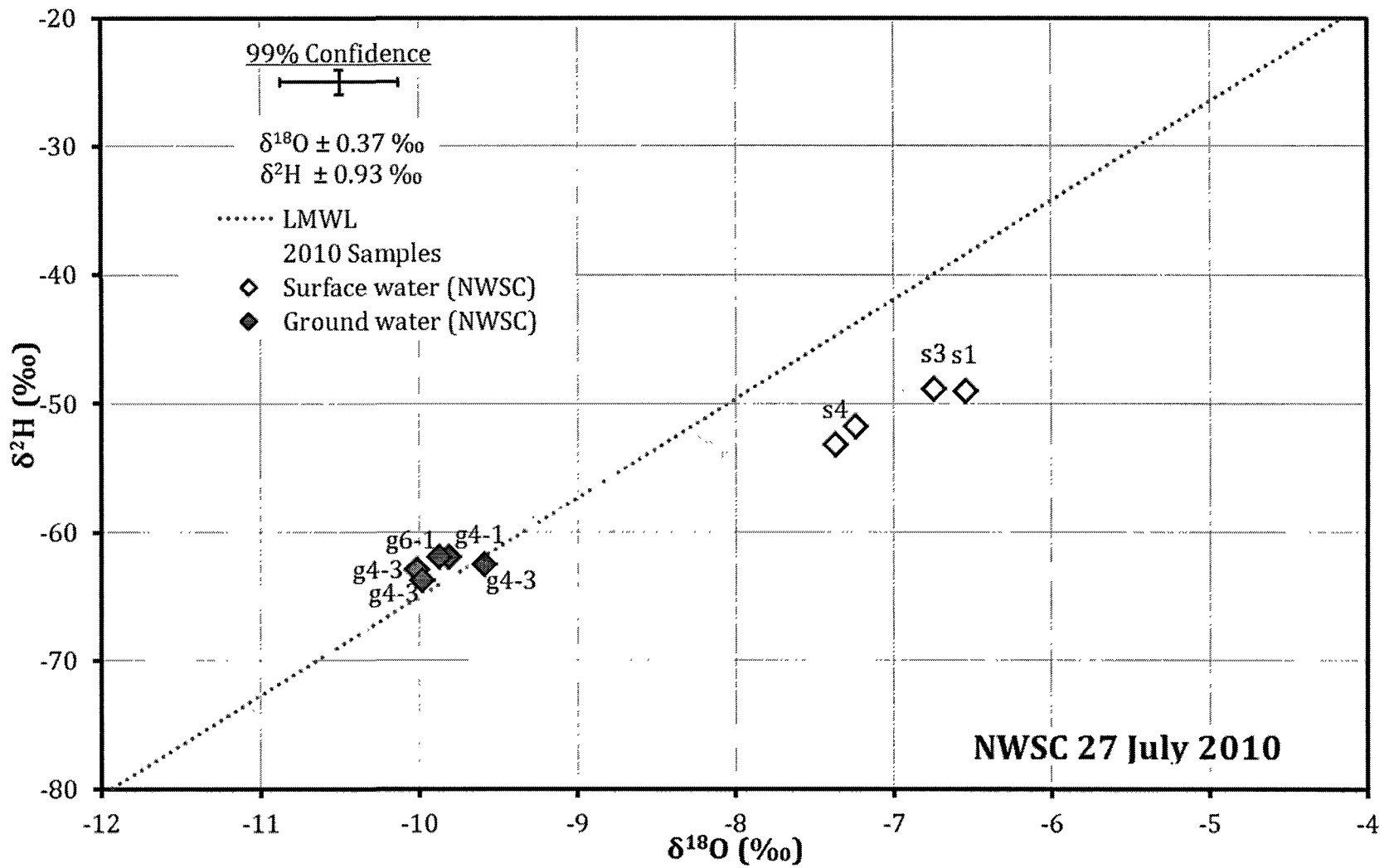*Figure B4: Isotopic composition of groundwater and streamflow on 8 July.*

Figure B5: Isotopic composition of groundwater and streamflow on 27 July.
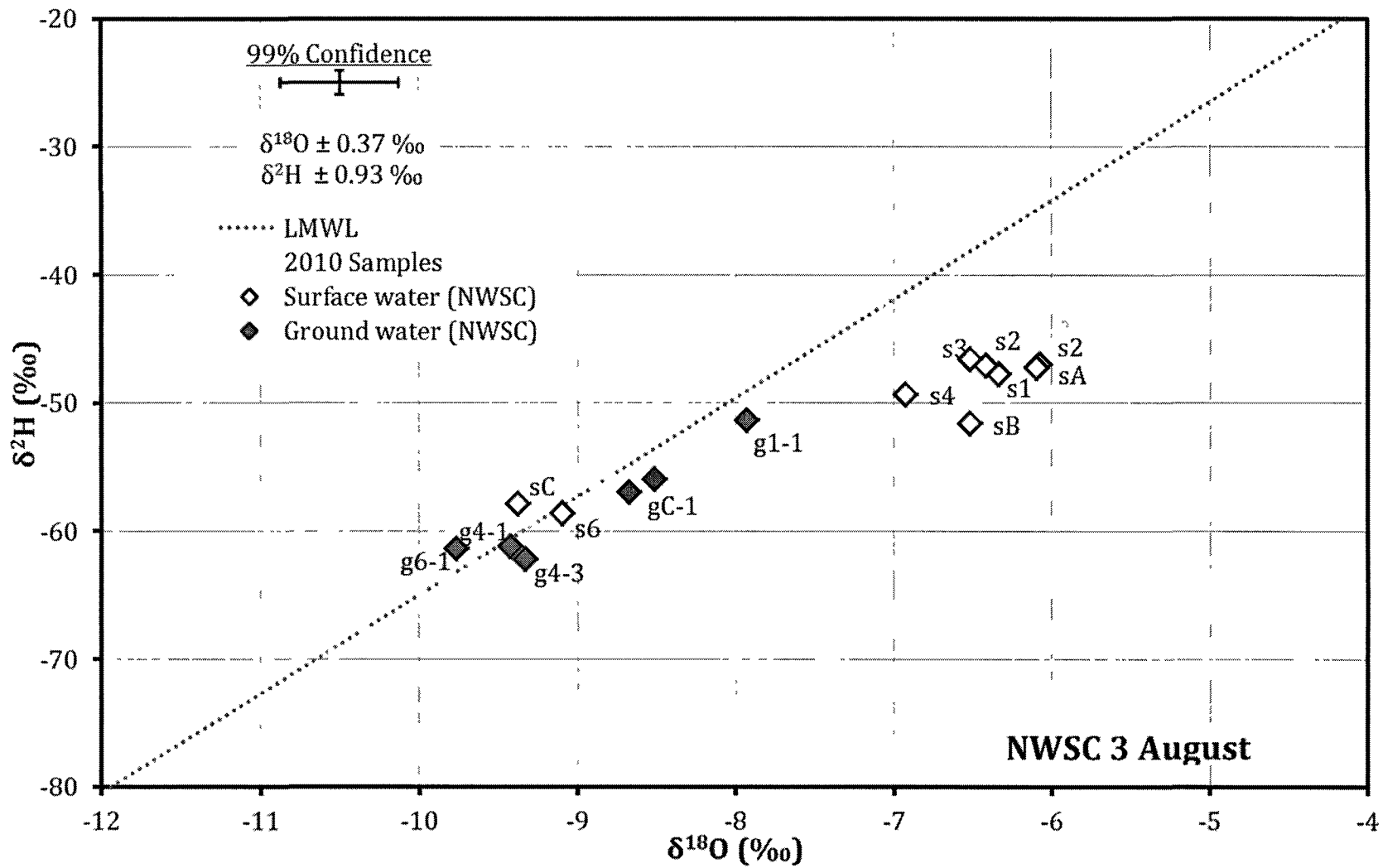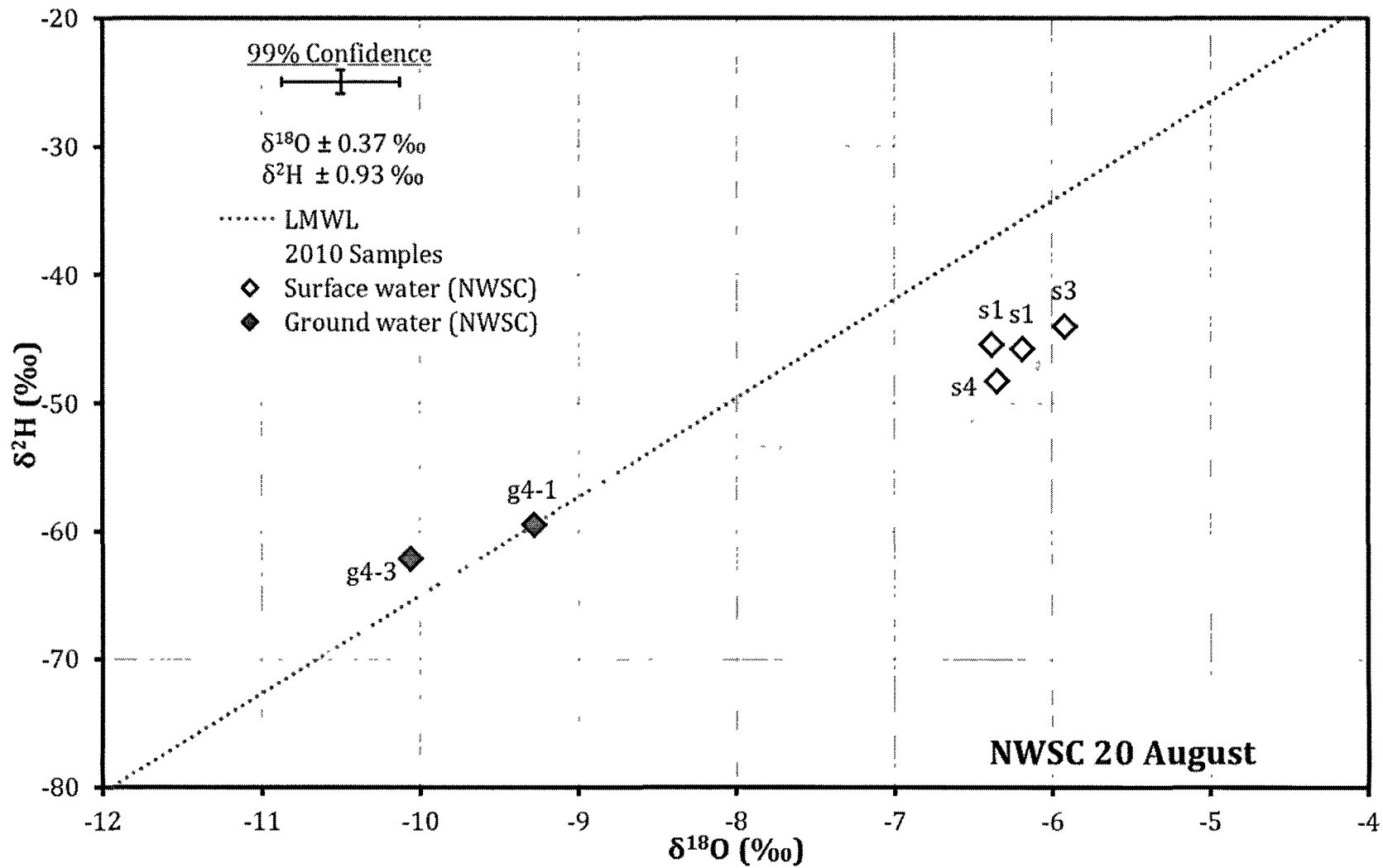
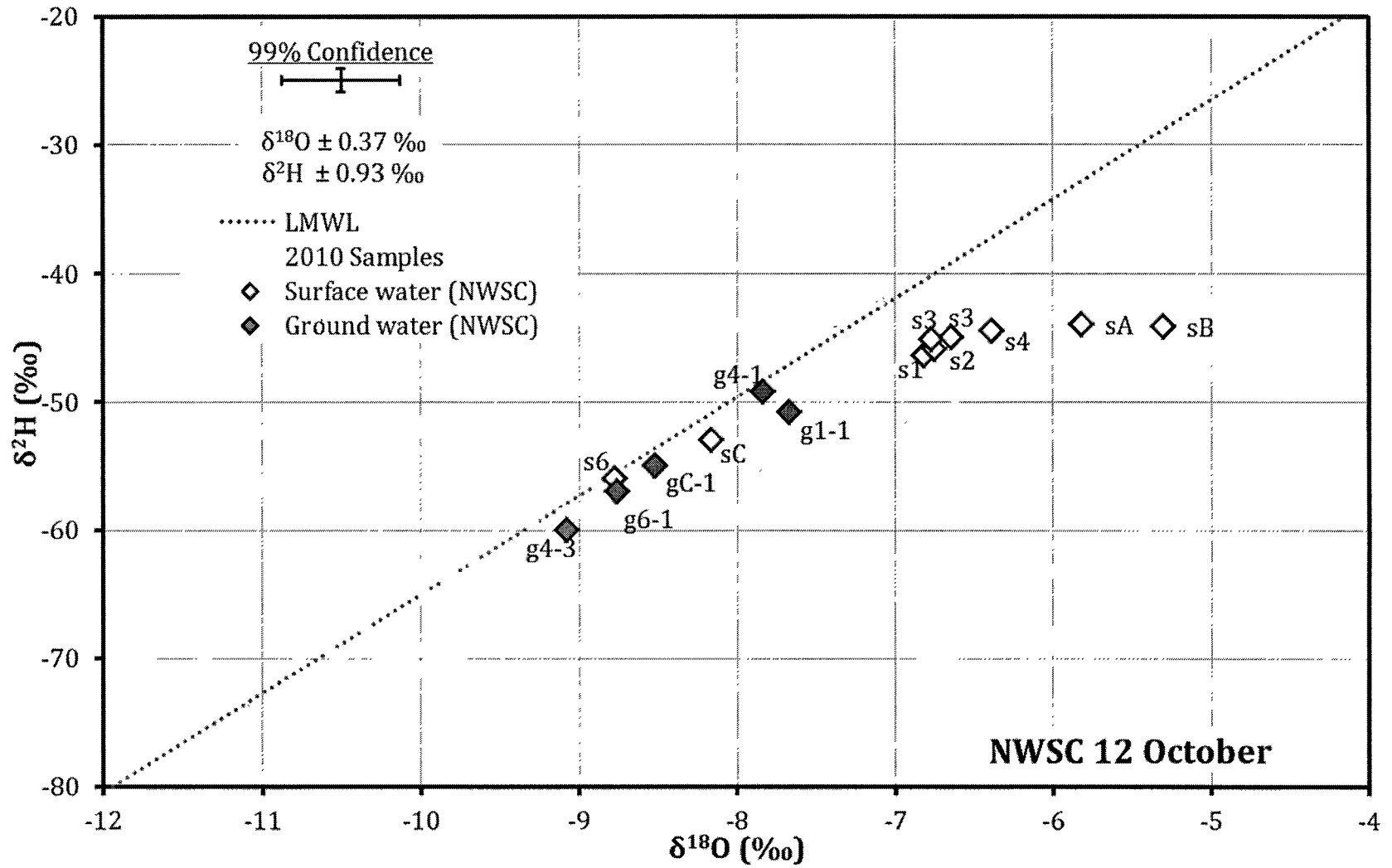Figure B6: Isotopic composition of groundwater and streamflow on 3 August.

Figure B7: Isotopic composition of groundwater and streamflow on 20 August.

Figure B8: Isotopic composition of groundwater and streamflow on 12 October.